DYNAMIC LATERAL FEEDBACK INHIBITION

IN THE RETINA

By

Evan Dean Vickers

A DISSERTATION

Presented to the Neuroscience Graduate Program, the Vollum Institute, and the

Oregon Health and Science University School of Medicine, in partial fulfillment of

the requirements for the degree of

Doctor of Philosophy

April 20th, 2012

School of Medicine

Oregon Health & Science University

CERTIFICATE OF APPROVAL

This is to certify that the Ph.D. dissertation of

EVAN VICKERS

has been approved on April 20th, 2012

Advisor, Henrique von Gersdorff, PhD

Member and Chair, Laurence Trussell, PhD

Member, Robert Duvoisin, PhD

Member, Craig Jahr, PhD

Member, Rowland Taylor, PhD

TABLE OF CONTENTS

LIST OF FIGURES

CHAPTER 1

iii

CHAPTER 2

CHAPTER 3

APPENDIX I

ACKNOWLEDGEMENTS

First, I would like to thank Dr. Henrique von Gersdorff, my PhD mentor, for all of the time, effort, resources, and inspiration that he has provided, without which this work would not have been possible. In particular, I would like to thank him for so quickly and eagerly accepting me into his lab at a somewhat advanced stage in my tenure as a PhD student at OHSU. In retrospect, things seem to have worked out quite well for both of us, and I will always remember the difficult experiments, the constant stream of new ideas and possible project directions, and his never-waivering willingness to examine and discuss new data.

Dr. von Gersdorff also helped me establish two crucial collaborations during the creation of this work, and I have benefited greatly from these relationships. First, I would like to thank Dr. Jozsef Vigh, a former post-doctoral researcher in the von Gersdorff lab, for training me on several key experimental protocols and participating in ongoing discussions concerning the interpretation of our results. I would also like to thank Dr. Daniel Calvo, our collaborator in Buenos Aires, Argentina, for the opportunity to work on a surprising, interesting project that bore much fruit.

I would also like to thank the members of my thesis advisory committee, Dr. Laurence Trussell, Dr. Craig Jahr, and Dr. W. Rowland Taylor, for their time and for all of their efforts in guiding me through the process of completing this effort. I feel lucky to have had such an excellent group of scientists take the time, over the course of several years, to discuss and critique my work. In addition, I would like to thank all the former and current members of the von Gersdorff lab that I have interacted with on a regular basis over the past five years (and the two years before that, as well), including Dr. Geng-lin Li, Dr. Mean-Hwan Kim, Dr. Soyoun Cho, Dr. Veera Balakrishnan, Dr. Geetha Srinivasan, Dr. Jun-Hee Kim, and Dr. Robert Renden. The assistance, at times

ABSTRACT

The role of inhibitory signaling in CNS microcircuits depends on the specific connectivity and frequency-dependent plasticity of synapses from interneurons onto principle cells. Feedforward, feedback, and lateral inhibition in general are thought to subserve gating, dynamic range tuning, and spatial sharpening functions, respectively, in multiple brain areas including cortex, striatum, the olfactory bulb, and the retina. In the retina, inhibition is mediated either by horizontal cells (HCs) in the OPL, or by amacrine cells (ACs) in the IPL. Both classes of cells have been shown to mediate feedback and lateral inhibition, and ACs are known to mediate feedforward inhibition onto ganglion cells (GCs), the output neurons of the retina. ACs also mediate lateral feedback inhibition at bipolar cell (BC) presynaptic terminals, although the synaptic mechanisms, timing, and frequency dependence of these inhibitory inputs in response to light stimulation had not been previously well characterized, due to the relative inaccessibility of BC presynaptic terminals to direct electrophysiological recording. Here, we recorded directly from axotomized, large presynaptic terminals of ON-type, mixed rod/cone input (Mb) bipolar cells in a slice preparation of goldfish retina. By stimulating with light, we were able to electrophysiologically isolate lateral feedback inhibition in the form of lateral inhibitory post-synaptic currents (L-IPSCs). In order to investigate the role that these L-IPSCs may play in the regulation of vesicular glutamate release from Mb terminal ribbon synapses onto ACs and GCs, we first examined their timing, light sensitivity, and pharmacology in response to single, full-field light flashes. We hypothesized that L-IPSCs, mediated by a tri-synaptic circuit from photoreceptors to BCs to ACs to BC terminals, would depend on different combinations of rod and cone inputs under different background light conditions, would rely on diverse glutamatergic signaling at BC to AC synapses, and would be mediated primarily by GABAergic signaling at Mb terminals. Furthermore, we

ix

expected that L-IPSCs would be delivered by a set of AC synaptic inputs distinct from those that mediate reciprocal inhibition at the Mb terminal, and thus constitute an independently regulated pathway for control of Mb glutamate release in response to spatiotemporal modulation of surround light stimulation.

First, we showed that L-IPSCs at the Mb terminal consist of an ON component, with an onset roughly 50 ms following the initiation of light flash, and an OFF component, occurring 100-150 ms following the offset of the light flash. We found that ON L-IPSCs were driven by a combination of rod and cone input, and that OFF L-IPSCs were driven primarily by cone inputs. Next, we showed that ON and OFF L-IPSCs are both mediated by a combination of signaling at GABA$_A$R and GABA$_C$R and rely on a combination of signaling at AMPARs and NMDARs at BC to AC synapses, although ON L-IPSCs were, unexpectedly, enhanced in the presence of the specific AMPAR antagonist, NBQX. Both ON and OFF L-IPSCs were disinhibited following application of SR-95531, a specific GABA$_A$R antagonist, consistent with the idea that serial inhibitory signaling between ACs plays a major role in regulating L-IPSC strength. Blockade of voltage-gated Na$^+$ channels with TTX markedly reduced OFF L-IPSCs but had mixed effects on ON L-IPSCs, suggesting that the AC class providing OFF inputs signals via regenerative Na$^+$ action potentials, while ON ACs may propagate lateral inhibition via analog, subthreshold depolarization. Finally, we showed that step-depolarization-evoked reciprocal inhibitory feedback and light-evoked L-IPSCs did not cross-depress, suggesting that they are mediated by distinct classes of ACs.

Next, we sought to examine the short-term plasticity (STP) of ON and OFF L-IPSC size and timing. Such plasticity would indicate a modulation of lateral feedback inhibition by surround temporal contrast, and provide a novel mechanism for adaptation or sensitization of local, feed-forward light-responses by dynamic presynaptic inhibition at BC terminals. We hypothesized that STP of strength and timing for convergent ON

and OFF L-IPSCs would provide a framework for precise regulation of both analog EPSPs and regenerative Ca^{2+} action potentials at the Mb terminal. In order to address the mechanisms that would regulate this STP, we first examined the role of diverse GABAergic signaling and background light adaptation on L-IPSC amplitude, charge transfer, and onset latency. We found that block of signaling at $GABA_A Rs$ enhanced amplitude and charge transfer and increased onset latencies. Under scotopic background conditions, ON L-IPSC exhibited an increase in amplitude and onset latency relative to mesopic background conditions, while OFF L-IPSCs showed an increase in amplitude and a decrease in onset latency. We used a paired light flash protocol to address STP, and found that ON L-IPSCs exhibited short-term depression (STD) of amplitude and charge transfer that recovered over 2 s, and showed delay (increase) of onset latency at short intervals (50 - 300 ms). OFF L-IPSCs also exhibited STD of amplitude and charge transfer, but this STD recovered over 1 s and transformed into short-term facilitation (STF) of amplitude for intervals from 1-2 s. In addition, OFF L-IPSCs showed advance (decrease) of onset latency at short intervals (300 ms). Because L-IPSC timing is likely critical for proper regulation of glutamate release from Mb terminals, we examined the role that ACs play in determining L-IPSC latencies. We found that block of voltage-gated Na^+ channels with TTX caused an increase in OFF L-IPSC onset latencies, and, with paired recordings of Mb terminals and AC somata, we showed that long L-IPSC onset latencies, as well as their sustained and asynchronous nature, are likely driven by processes intrinsic to ACs.

In order to pursue additional mechanisms that may regulate plasticity of GABAergic L-IPSCs, we examined the role of endogenous ascorbic acid (Asc) in the regulation of $GABA_A R$ and $GABA_C R$ mediated currents. We found that Asc acts as a stereospecific reducing agent at the two cysteines in the extracellular cys-loop, and at histidine 141, of heterologously expressed $GABA_C Rs$, to reversibly enhance $GABA_C R$

mediated Cl$^-$ current in a manner dependent on the concentration of both GABA and Asc. We showed that Asc applied to retinal slices reversibly enhanced standing GABA$_C$R mediated leak current, puff-evoked GABA$_C$R mediated currents, and GABA$_A$ mIPSC amplitudes, and that intracellular Asc prevented run-down of puff-evoked GABA$_C$ currents over a period of 15 minutes in axotomized Mb terminals. The presence of high endogenous concentrations of Asc in the retina (~0.2 mM), along with studies that show glutamate-evoked release of Asc and the retinal expression of SVCT2, a Na$^+$ / Asc cotransporter, suggest that Asc may play a role in activity dependent regulation of STP of L-IPSCs at BC presynaptic terminals.

BACKGROUND AND INTRODUCTION

The retina is a useful model system for the study of general central nervous system (CNS) function for several reasons. First, as a peripheral sensory transduction organ it is easily isolated experimentally and can be directly probed with its physiological stimulus, light. Second, the retina has a clear laminar organization, and is populated by six distinct, easily identified cell classes (photoreceptor (PR), bipolar cell (BC), ganglion cell (GC), horizontal cell (HC), amacrine cell (AC), and Mueller glial cell) that form canonical circuits that transmit information from the photoreceptor input layer to the ganglion cell output layer (Dowling, 1970; Werblin, 2011). Third, and most importantly for this work, the heterogeneity of synaptic organization and cellular diversity in the inner plexiform layer (IPL) of the retina (Witkovsky and Dowling, 1969) makes it an excellent system in which to study the general issue of inhibitory signaling and plasticity in the CNS.

Neural processing in the retina dynamically filters the incoming visual stimulus so that novel, unpredictable inputs are efficiently encoded in GC spike trains (Srinivasan et al., 1982; Hosoya et al., 2005), which transmit information primarily to the lateral geniculate nucleus (LGN) of the thalamus (Guido, 2008) and on to higher visual cortical structures (Lund, 1988). Feedback and lateral inhibition in the outer retina, mediated by horizontal cell inhibition of photoreceptor Ca^{2+} channels and bipolar cell dendrites, significantly contributes to the formation of bipolar cell center-surround receptive fields (Naka, 1971; Kaneko, 1973; Fahrenfort et al., 2005 & 2009; Zhang and Wu, 2009). However, in addition to refinement of the GC center-surround, many higher-order properties of GC receptive fields likely require synaptic short-term plasticity (STP) in the IPL at inhibitory GABAergic and glycinergic synapses from diverse classes of AC onto BC presynaptic terminals, GC dendrites, or other ACs (Hosoya et al., 2005). In order to explore the role that this STP plays in shaping GC stimulus representations, we have

1

recorded from a large BC presynaptic terminal in the goldfish retina (the ON, mixed rod/cone input bipolar cell, or "Mb"). When the Mb terminal is separated from its soma and dendrites by fortuitous severing of its axon during the retinal slicing procedure (Palmer et al., 2003), it is possible to stimulate the *in vitro* slice preparation with light and record pure lateral inhibitory post-synaptic currents (L-IPSCs). In order to understand the role that STP of L-IPSCs may play in retinal processing in general, it is necessary, first, to review the overall anatomical and functional structure of the retina and the pre- and post- synaptic mechanisms thought to be generally involved in STP at CNS synapses.

Structure and Function of the Retina

Light enters the eye through the pupil and is focused onto the PR surface (scleral) of the retina, which it reaches after traveling though the GC layer (vitreal) and the inner nuclear layer (INL), which contains the cell bodies of BCs and ACs (Dowling, 1970). At the PR level, light stimuli are initially separated into channels based on intensity and wavelength; in carp retina, rods respond optimally to dim light (peak response at 525 nm), while cones respond to bright light and express photopigment, or opsins, that are preferentially sensitive to short- (440 nm), medium- (530 nm), or long- wavelength (610 nm) light (Witkovsky et al., 1973). Rod and cone PRs, which are depolarized and release glutamate onto HC and BC dendrites in the dark, transduce light via photoisomerization of rhodopsin in their outer segments, which initiates a molecular signaling cascade that results in membrane hyperpolarization, the closing of presynaptic L-type Ca^{2+} channels, and cessation of glutamate release (Cervetto and Piccolino, 1982; Baylor, 1987; McNaughton, 1990). In the outer plexiform layer (OPL), this results in HC hyperpolarization, which provides negative feedback by alleviating H^+ mediated and/or ephaptic inhibition of PR Ca^{2+} channels (Wu, 1992; Kamermans and Spekreijse, 1999; Kamermans and Fahrenfort, 2004; Fahrenfort et al., 2005 & 2009). PR hyperpolarization

has more complex effects at the level of BC dendrites, where information about the polarity, or sign of the light stimulus is separated into two channels, "ON" and "OFF" (Familglietti and Kolb, 1976; Schiller, 1992; Connaughton, 2001; Slaughter and Awatramani, 2002). In ON BCs, which project to ACs and GC dendrites in the inner IPL ("sublamina b"), decreased glutamate release from PRs at light onset leads to decreased activation of dendritic mGluR6 receptors, which in turn leads to the opening of TRPM1 cation channels and BC depolarization (Shen et al., 2009; Morgans et al., 2009). In some lower vertebrates, including goldfish, sign-inversion at ON BC dendrites following light onset is also mediated by cessation of glutamate binding to EAAT5 glutamate transporters (primarily at cone inputs; Wong et al, 2005), which reduces transporter-coupled outward Cl^- currents and causes BC depolarization. In OFF BCs, which project to ACs and GC dendrites in the outer IPL ("sublamina a"), increased glutamate release at light offset causes activation of AMPA and kainate receptors, which mediate a depolarizing mixed cation conductance (Kim and Miller, 1993; Sasaki and Kaneko, 1996).

Once ON and OFF signals are directed into separate BC pathways, they pass through a sign preserving, glutamatergic (AMPAR and NMDAR mediated) synapse onto the dendrites of GCs (Yang, 2004; Shen et al., 2006; Palmer, 2010). GCs then integrate these inputs and produce Na^+ action potentials that propagate along their axons, leave the retina, and terminate at the LGN of the thalamus. However, BCs also release glutamate onto ACs, which depolarize and exhibit either passive/analog or active/digital signal propagation (Taylor, 1999), and release either inhibitory GABA or glycine onto BC axon terminals (reciprocal or lateral feedback inhibition), ACs (serial inhibition), or GC dendrites (feedforward inhibition) (Lukasiewicz, 2005; Eggers and Lukasiewicz, 2011). While the separation of ON and OFF visual streams is largely maintained at the level of GCs, there are a few notable exceptions. For instance, some classes of GCs are known

to exhibit "ON/OFF" response characteristics, stratify in both sublamina "a" and "b", and receive corresponding excitatory inputs from both OFF and ON type BCs (Barlow and Hill, 1963; Sivyer et al., 2011).

The responses of these GCs, as well as those of purely ON or OFF GCs, can be further classified according to the duration of stimulus evoked spiking (i.e. transient vs. sustained; Kuffler, 1953; Wunk and Werblin, 1979; Awatramani and Slaughter, 2000). Although intrinsic membrane properties of GCs likely account for some of these differences in excitability, feedforward and reciprocal/lateral feedback inhibition from ACs onto GCs and BC terminals, respectively, are also thought to significantly regulate the onset latency of the initial spike in a GC response, as well as the spike frequency and response duration (i.e. offset latency; Dong and Werblin, 1998; Arai et al., 2011). These properties of GC responses likely encode diverse information about the visual stimulus that is later "decoded" downstream, either at the level of the LGN or visual cortex (Field and Chichilnisky, 2007).

Another exception to the general segregation of ON and OFF information in the retina is the existence of "crossover" inhibition in the IPL (Hsueh at al., 2008), mediated by ACs that receive excitatory inputs from ON BCs and release glycine or GABA onto OFF BCs (or OFF GCs), or vice versa. In mammals, this crossover inhibition is primarily mediated by narrow-field, glycinergic ACs, and is thought to act primarily to rectify or linearize either ON or OFF signals, which would otherwise exhibit distortions due to the nonlinearity imposed by the steep Ca^{2+} dependence of glutamate release at BC terminals (Molnar et al., 2009; Werblin, 2010). Transient decreases in crossover inhibition from ACs onto GC dendrites or BC axon terminals has also been shown, in some cases, to directly drive GC excitatory responses via disinhibition (Venkataramani and Taylor, 2010; Manu and Baccus, 2011).

The traditional model of neural transmission in the retina holds that signals are propagated by analog, subthreshold depolarizations (EPSPs) in PRs, HCs, BCs, and ACs, and that the conversion of information into the form of active, regenerative potentials (i.e. Na^+ action potentials, or "spikes") occurs for the first time at the level of GCs. It has been argued that this scheme allows for maintenance of high signal-to-noise and temporal bandwidth of signaling in the outer retina and IPL, while minimizing the high metabolic cost associated with high frequency Na^+ spikes (Sterling and Freed, 2007). However, notable exceptions to this view have been recently discovered. In particular, certain classes of ACs, including those that make large, wide-field projections that span the retina (Bloomfield, 1996), have been shown to exhibit Na^+ spikes. In addition, there is evidence suggesting that Ca^{2+} and/or Na^+ spikes may occur in BCs under certain conditions of background light adaptation (Protti et al., 2000; Arai et al., 2010) and BC resting membrane potential (Dreosti et al., 2011; Baden et al., 2011).

Despite these exceptions, the presynaptic terminals of PRs and BCs primarily experience graded changes in membrane potential, are characterized by specialized "ribbon" structures, consisting primarily of the protein RIBEYE, that tether neurotransmitter containing vesicles close to the L-type Ca^{2+} channels known to mediate the Ca^{2+} influx that triggers rapid, analog release of glutamate onto BCs and HCs, and GCs and ACs, respectively (Sterling and Matthews, 2005; Heidelberger et al., 2005). These ribbon synapses appear to be particularly well suited to enable exocytosis to closely follow continuously modulated, subthreshold depolarizations at PR and BC presynaptic terminals. Recent evidence shows that ribbons are required for the rapid replenishment of vesicles to enable sustained release at these synapses (Snellman et al., 2011). Furthermore, the relatively hyperpolarized activation voltage range (roughly -60 to -50 mV; Singer and Diamond, 2003) and slow rate of inactivation of these L-type Ca^{2+} channels allow release to be highly sensitive to small fluctuations in resting

5

membrane potential over multiple timescales. For these reasons, glutamate release from BC terminals can be strongly modulated by relatively small reciprocal and lateral IPSCs originating from ACs (Oltedal et al., 2009; Eggers and Lukasiewicz, 2011; Sagdullaev et al., 2011). Furthermore, recent studies have shown that phasic and sustained components of release from rod BCs (RBCs) onto AII ACs in mouse efficiently compute the temporal contrast (i.e. variance) and mean luminance of the visual stimulus, respectively (Oesch and Diamond, 2011), and that adaptation in these representations can be due to either Ca^{2+} channel inactivation or vesicle depletion (Jarsky et al., 2011). Importantly for the work presented in this dissertation, the timing of inhibition arriving at BC terminals (Oltedal et al., 2009, Manu and Baccus, 2011) will therefore determine its ability to shape representations of either temporal contrast or mean luminance before this information reaches the level of GC dendrites.

Diversity Among Vertebrate Retinas

Although the goldfish Mb BC is the direct counterpart of the mammalian RBC, which is the key element in the retinal circuit that processes dim light stimuli under dark, or "scotopic" conditions, several key differences in the synaptic transmission and circuitries involved in these two systems have been well characterized (Joselevitch and Kamermans, 2009). However, several recent findings show the existence of more similarities between the retinal structure and function of teleosts, such as goldfish, and mammals than were previously thought (Pang et al., 2010). In order to highlight these issues in a way that will inform the understanding and interpretation of the present work, I will first give an overview of the well-studied RBC to AII AC pathway in mammalian retina. Then, I will give an outline of specific comparisons with the Mb pathway in goldfish.

Mammalian rod PRs exhibit a peak wavelength sensitivity of around 498 nm, are able to detect the flux of a single photon at their outer segments under scotopic background conditions, and are, in the case of old world primates, excluded from the fovea, a central area of the retina specializing in high acuity vision that has a diameter of roughly 1 mm in humans. Around 20-50 rods provide convergent glutamatergic input (via ribbon synapses) onto the dendritic arbor of a single RBC (Taylor and Smith, 2004), which exhibits a depolarizing response to the onset of a light stimulus (i.e. removal of glutamatergic input). A single RBC, in turn, makes glutamatergic ribbon synapses on 5-9 AII ACs, which are a specialized class of bistratified ON-OFF AC that make sign-preserving gap junctional contacts onto ON cone BCs and sign-inverting glycinergic synapses onto OFF cone BCs and OFF GCs (Strettoi et al., 1992). Each RBC ribbon synapse forms a dyad (Raviola and Dacheux, 1987), with the second output directed to the dendritic bouton of an A17 AC, which has been shown to mediate local, reciprocal GABAergic signaling onto the RBC terminal (Chavez et al., 2006). Because RBCs have not been observed to make direct synaptic contacts onto GCs (Kolb, 1979), the AII effectively allows scotopic information from the rod pathway to "piggyback" onto the cone pathway at the level of the IPL (Oesch and Diamond, 2009). Interestingly, recent studies have shown that photopic, ON information is also able to invade the AII via the gap junctional contacts from ON cone BCs and elicit crossover inhibition of OFF cone BCs via glycine release (Munch et al., 2009). Furthermore, AIIs from multiple species have been to shown to contact most, if not all, classes of ON and OFF cone BC, suggesting that the signals from the rod pathway may be effectively distributed across the entire BC array that normally encodes photopic (cone) information (Familglietti and Kolb, 1975; Petrides and Trexler, 2008).

In the teleost (e.g. goldfish) retina, the Mb BC receives inputs from both rods and cones (Stell, 1978; Joselevitch and Kamermans, 2007). So, although the RBC and Mb

both receive rod inputs and are "ON" type, the Mb receives additional cone inputs under mesopic (dim background; Krizaj, 2000) and photopic (bright background) conditions that allow it to respond over a larger dynamic range of background and stimulus light intensities. In the goldfish, a corresponding mixed-input BC has been described in the OFF pathway (the "Ma" BC; Stell, 1978; Marc and Liu, 2000). Interestingly, recent studies have shown that many classes of mammalian BC may also receive a combination of rod and cone inputs, although these inputs may be much more asymmetric that those received by the Mb or Ma (Pang et al., 2010). While the degree of PR convergence onto the Mb appears to be similar (for rods) to that of the RBC, divergence from the Mb onto ACs and GCs is much greater than from the RBC onto AII and A17 ACs (Strettoi et al., 1992; Marc and Liu, 2000). Electron microscope (EM) and immunocytochemistry showed that each individual Mb terminal makes roughly 350 synapses with ACs, of which around 50% are reciprocal, and 50% are lateral/unidirectional (Witkovsky and Dowling, 1969; Marc and Liu, 2000). Mb contacts onto GC dendrites were observed at a much lower frequency (~16%), but the functionality of these synapses has been directly shown with paired recordings (Palmer, 2010; Arai et al., 2010). Overall, these findings suggest that the Mb may, like the RBC, distribute rod signals to an array of cone pathways (and, possibly, the Ma pathway), but in addition is able to pass signals directly to a class of ON GC.

Reciprocal and Lateral Inhibition at BC terminals

At the mammalian RBC, reciprocal GABAergic inhibition appears to be mediated entirely by the A17 AC, which releases GABA onto both $GABA_A$ and $GABA_C$ receptors on the RBC following glutamate binding to Ca^{2+} permeable AMPA receptors (Chavez et al., 2006). This rapid feedback is thought to shorten the duration of the glutamate transient experienced by the AII (Dong and Hare, 2003), and likely expands the dynamic range of

RBC to AII signaling during high frequency stimulation (Chavez et al., 2006; Li et al.,

2007). In contrast, lateral feedback inhibition at the mammalian RBC terminal, evoked by

either electrical stimulation / glutamate puffing in the IPL or by puffing CPPG (an

mGluR6 antagonist) or kainate in the OPL, is mediated primarily by signaling at non-

reciprocal synapses containing $GABA_CRs$ following binding of glutamate to Ca^{2+}

permeable and non-permeable AMPARs on ACs that exhibit active signal propagation

dependent on activation of voltage-gated Na^+ channels (Chavez et al., 2010). This

lateral inhibition likely contributes to center-surround receptive field refinement,

regulation of the offset of RBC glutamate release, and/or suppression of Ca^{2+} spike

initiation at the RBC terminal (Chavez et al., 2010). An *in vivo* study of ON GCs in a

transgenic mouse line that lacks $GABA_CRs$ showed enhanced spontaneous firing rates

and prolonged light responses (Sagdullaev et al., 2006). The role of reciprocal and

lateral $GABA_CR$ mediated inhibition has also been examined at mouse ON cone BCs *in

vitro* during either electrical stimulation of the IPL or OPL, or center- or full-field light

stimulation (Sagdullaev et al., 2011). Recordings from post-synaptic ON GCs showed

that this TPMPA sensitive inhibition acts to prevent short-term depression (STD) of GC

light responses at interstimulus intervals (ISIs) < 1 s. Despite these many key findings

from the mammalian retina, the small size of RBCs generally prevents routine direct

recordings of their presynaptic terminal (with some exceptions: see Oltedal et al., 2007;

Oltedal et al., 2009; Morkve and Hartveit, 2009; Oltedal and Hartveit, 2010). Electrotonic

filtering of IPSCs arriving at the terminal during somatic recordings likely distorts their

amplitude and kinetics (Oltedal et al., 2009), and makes quantification of precise onset

and offset latencies difficult. Furthermore, it is often difficult experimentally to completely

isolate the lateral and reciprocal components of feedback inhibition, especially under

conditions of physiological light stimulation.

Previous studies of the synaptic mechanisms and short-term plasticity (STP) of reciprocal feedback inhibition at the goldfish Mb BC have utilized the technique of direct patch-clamp recording of axotomized terminals in an acute retinal slice preparation (Palmer et al., 2003; Li et al., 2007). It has been shown that this inhibition consists of a combination of $GABA_AR$ and $GABA_CR$ mediated signaling (Matthews et al., 1994), and that the $GABA_A$ component is desensitizing (Hull et al., 2006a) and driven largely by AMPAR activation on AC terminals, while the $GABA_C$ component is non-desensitizing (Matthews et al., 1994) and dependent on activation of AC NMDARs (Vigh and von Gersdorff, 2005). Also, strong depolarization of the Mb terminal is able to evoke long-lasting (~10 min) potentiation of reciprocal feedback that is dependent on activation of mGluR1 on AC boutons (Vigh et al., 2005). Furthermore, recording of reciprocal GABAergic currents in whole-cell and outside-out patch configurations revealed that STD due to AC vesicle depletion recovers with a time-constant (τ) of roughly 12 s, and that desensitization of Mb $GABA_ARs$ in response to evoked, synaptic GABA transients (estimated at 1 mM over ~5 ms) likely recovers completely within ~ 2 s (Li et al., 2007). However, estimates of the rate of $GABA_AR$ recovery from desensitization in cultured hippocampal neurons following preconditioning in 1 μM GABA for 20 s were much slower, with a τ = 8 s (Overstreet et al., 2000). The presence of a $GABA_CR$ mediated standing leak current at the Mb terminal, which has been shown to be regulated by GAT-1 GABA transporter activity and can exert significant influence over Ca^{2+} spike initiation (Hull et al., 2006a), suggests that levels of tonic extracellular GABA at the Mb terminal, which recent evidence suggests are regulated by release of GABA from DIDS sensitive anion channels (Jones and Palmer, 2011) may contribute to the entry of $GABA_ARs$ into a prolonged desensitized state under certain conditions. However, the exact concentration range of tonic background GABA in the IPL *in vivo* is unknown.

The current work is the first to characterize the synaptic mechanisms and sensitivity **(Chapter 1)**, and STP **(Chapter 2)** of light-evoked lateral feedback inhibition at the Mb terminal. In addition, we present a mechanism and regulatory scheme for the action of ascorbic acid, an endogenous allosteric modulator of $GABA_ARs$ and $GABA_CRs$, at Mb terminals **(Chapter 3)**. Although we do not directly show light-evoked modulation of extracellular ascorbic acid levels on the timescale relevant for paired-pulse plasticity (i.e. < 2 s), this finding represents a novel mechanism that may exert a strong influence over inhibitory signaling in the IPL. In order to interpret the findings presented in this work, both in terms of potential presynaptic AC (or upstream BC, HC, or PR) and postsynaptic Mb mechanisms that may underlie STP of lateral feedback inhibition, it is first necessary to review the general role and mechanisms of STP in the CNS.

Synaptic Mechanisms of Short-term Plasticity

The strength of excitatory and inhibitory synapses can be modified via various processes that vary in mechanism and timescale of both induction and decay. Classical, Hebbian long-term potentiation (LTP), thought to be involved in processes such as memory formation and learning, requires temporally coordinated pre- and post-synaptic action potentials or depolarization, and is typically mediated by increases in post-synaptic Ca^{2+} and subsequent modifications of the post-synaptic density and/or architecture of dendritic spines that persist, at least, over minutes or hours (Abbott and Nelson, 2000; Bi and Poo, 2001). Long-term depression (LTD) can often be induced by slight modification of the frequency or relative pre- and post-synaptic timing of stimulation used in LTP induction protocols, and is usually associated with smaller and/or slower spatiotemporal profiles of post-synaptic Ca^{2+} transients (Artola and Singer, 1993). Homeostatic plasticity, also known as synaptic scaling, is another form of plasticity, operating over the period of hours to days, wherein the relative strength of

excitatory and inhibitory inputs is modified to compensate for changes in tonic

depolarization or hyperpolarizing drive to a particular neuron, or a circuit (Turrigiano,

1999). Although Ca^{2+} influx and retrograde messengers such as nitric oxide (NO; Le

Roux et al., 2009; Steinert et al., 2011) and brain-derived neurotrophic factor (BDNF;

Rutherford et al., 1998) are likely involved in multiple forms of synaptic scaling, the

mechanisms for this form of long-term plasticity appear to be more diverse than those

that mediate LTP and LTD.

Short-term plasticity (STP), in stark contrast to these two main forms of long-term

plasticity, is a change in the size or timing of the post-synaptic response (either

excitatory post-synaptic current (EPSC) or inhibitory post-synaptic current (IPSC)) that

typically operates over timescales ranging from tens of milliseconds to tens of seconds,

and is generally thought to be involved in processes such as dynamic gain regulation

and temporal frequency tuning (von Gersdorff and Borst, 2002; Zucker and Regehr,

2002). Despite these differences, some forms of STP share with LTP, LTD, and

homeostatic scaling a strong mechanistic dependence of induction on highly regulated

spatiotemporal Ca^{2+} transients. However, in the case of STP, these Ca^{2+} transients, or

"residual Ca^{2+}", are typically presynaptic and act on various molecular targets (e.g.

CaMKII, synapsin, Doc2α, RIM, CAPS, PKC, munc18, munc13, and rabphilin; Zucker

and Regehr, 2002; Wierda et al., 2007) to regulate vesicular release probability, number

of release sites, and/or the size of the readily releasable (RRP) pool (Zucker and

Regehr, 2002). Similarly to LTP and LTD, STP induction is highly dependent on the

range of stimulation frequency used to drive the presynaptic neuron (Muller et al., 2010).

The main forms of short-term synaptic enhancement, known as facilitation,

augmentation, and post-tetanic potentiation, are induced and decay over timescales of

tens to hundreds of milliseconds, seconds to tens of seconds, and tens of seconds to

minutes, respectively (Zucker and Regehr, 2002).

Short-term depression (STD), in contrast to short-term enhancement, is typically thought to be mediated either by the depletion of release-competent vesicles in the RRP (Schneggenburger et al., 2002), presynaptically, or receptor desensitization (i.e. especially in the case of AMPARs or GABA$_A$Rs), post-synaptically (Zucker and Regehr, 2002; Papke et al., 2011). These pre- and post-synaptic mechanisms, which, like in short-term facilitation (STF), typically develop in response to high frequency stimulation (although some forms of STD are initiated by low frequency stimulation), operate over timescales ranging from tens of milliseconds to seconds (Zucker and Regehr, 2002). Alternate forms of STD include presynaptic activation of metabotropic receptors (e.g. GABA$_B$Rs; Buonomano and Merzenich, 1998) that mediate changes in voltage-gated ion channels (e.g. Ca^{2+} channels; Delaney et al., 2009) and/or vesicle release probability (Mapelli et al., 2009), negative allosteric modulation of post-synaptic receptors, and (potentially) short-term increases in the activity of neurotransmitter transporters for excitatory glutamate (EAATs) or inhibitory GABA (GATs), which are critical for shaping the spatiotemporal transient of neurotransmitter in the synaptic cleft or extracellular space (Deken et al., 2003; Beenhakker and Huguenard, 2010; Jin et al., 2011).

STP has been shown to play key roles in signal processing in multiple brain areas, including (but not limited to) the synapse between auditory hair cells and spiral ganglion afferent fibers (Cho et al., 2011; Goutman and Glowatski, 2011), the Calyx of Held (von Gersdorff and Borst, 2002), thalamocortical projections (Chung et al., 2002), specific types of synapses between pyramidal neurons and various classes of cortical interneurons in auditory cortex (Reyes, 2011), and many other cortical and subcortical regions. Although the functional role of STP varies from synapse to synapse, and from brain area to brain area, it is clear that dynamic STP will allow rapid changes in the ability of particular synaptic inputs to drive wide-scale activity or outputs in a way that is dependent on input frequency and recent synaptic history (Reyes, 2011). In addition, the

13

transient vs. sustained and synchronous vs. delayed components of sensory signals will be strongly filtered by STP at individual synapses (Szalisznyo et al., 2008).

So, STP of lateral IPSCs (L-IPSCs) at the Mb terminal would likely be dependent on presynaptic Ca^{2+} influx or "residual Ca^{2+}" at AC boutons that release GABA (or glycine), and may be mediated by changes in vesicle release probability or availability, or by post-synaptic processes such as $GABA_A R$ desensitization or allosteric modulation of $GABA_A R$ or $GABA_C Rs$. It is also possible that STP at this synapse could be influenced by the activation of pre- or post-synaptic $GABA_B Rs$ (Song and Slaughter, 2010) or GATs (Hull et al., 2006a). Furthermore, we hypothesized that this STP would be dependent on the frequency of light stimulation, and would decay over the range of hundreds of milliseconds to seconds. Such dynamic regulation would allow for frequency-dependent, rapid changes in the strength and timing of surround contrast adaptation (in the case of STF of L-IPSCs) or sensitization (in the case of STD of L-IPSCs). However, full interpretation of the impact of STP (of both size and timing) of lateral inhibition at the Mb terminal ultimately depends on our understanding of its ability to shape Mb glutamate release and GC encoding of relevant stimulus properties. We will return to this issue in **Chapter 2**, and in the Summary and Conclusions.

Summary

In **Chapter 1**, we examined light-evoked L-IPSCs at the axotomized Mb terminal in a slice preparation of the goldfish retina. We identified temporally separate components of L-IPSCs that were relatively phase locked to the onset ("ON") and offset ("OFF") of the light stimulus, and characterized the relative rod and cone PR contributions, pharmacology, and synaptic origin of these responses. In **Chapter 2**, we independently characterized the STP of ON and OFF L-IPSC size and timing, and explored its

14

underlying pharmacological sensitivity and mechanisms. Next, we further explored the dependence of ON and OFF L-IPSC amplitude, charge transfer (i.e. size), and onset latency (i.e. timing) on background light adaptation state, signaling at AMPARs in outer retinal feedback circuits, and signaling at $GABA_ARs$ in inner retinal "nested loop" networks of serial connections between ACs. Finally, we performed paired recordings of synaptically connected ACs and Mb terminals to determine the classes of ACs that mediate these responses, and to assess the contribution of AC integration and intrinsic processes to the timing of L-IPSCs. Additional experiments in which we further explored the circuits and synaptic mechanisms that shape STP of ON and OFF L-IPSCs are presented in **Appendix I**. In **Chapter 3**, we identified ascorbic acid (Asc) as an endogenous positive allosteric modulator of both $GABA_AR$ and $GABA_CRs$ in the retina, and showed, in a heterologous expression system, that two extracellular cys-loop cysteines and histidine residue 141 (141) are the targets of Asc that mediate the observed increases in maximum current response and affinity, respectively. We also showed that intracellular Asc delays run-down of $GABA_CR$ mediated current, likely via prevention of reactive oxygen species (ROS) oxidation of C364, a cysteine residue located near the intracellular pore-region M3-M4 linker domain. Furthermore, we proposed a novel scheme in which glutamate-evoked release of Asc, potentially mediated by reversal of the SVCT2 Na^+/Asc cotransporter or some as-yet unknown mechanism, may allow for fast, activity-dependent regulation of inhibitory $GABA_AR$ and $GABA_CR$ mediated currents, especially during conditions of pathological excitotoxic neural activity.

CHAPTER 1

Light-evoked lateral GABAergic inhibition at single bipolar cell synaptic terminals is driven by distinct retinal microcircuits.

Jozsef Vigh[1], Evan Vickers[2], Henrique von Gersdorff [2]

[1]Dept. of Biomedical Sciences, Colorado State University, Ft. Collins, CO 80523

[2]The Vollum Institute, Oregon Health & Science University, 3181 SW Sam Jackson Park Road, Portland, OR 97239

J.V., E.V, and H.v.G designed research; J.V. and E.V. performed research; J.V., E.V., and H.v.G. analyzed data; J.V., E.V., and H.v.G. wrote the paper.

16

Abstract

Inhibitory amacrine cells (ACs) filter visual signals crossing the retina by modulating the excitatory, glutamatergic output of bipolar cells (BCs) on multiple temporal and spatial scales. Reciprocal feedback from ACs provides focal inhibition that is temporally locked to the activity of presynaptic BC activity, whereas lateral feedback originates from ACs excited by distant BCs. These distinct feedback mechanisms permit temporal and spatial computation at BC terminals. Here, we used a unique preparation to study light-evoked inhibitory postsynaptic currents (IPSCs) recorded from axotomized terminals of ON-type Mb BCs in goldfish retinal slices. In this preparation, light-evoked IPSCs could only reach axotomized BC terminals via the lateral feedback pathway, allowing us to study lateral feedback in the absence of overlapping reciprocal feedback components. We found that light evokes ON and OFF lateral IPSCs (L-IPSCs) in Mb terminals having different temporal patterns and conveyed via distinct retinal pathways. The relative contribution of rods vs. cones to ON and OFF L-IPSCs was light intensity-dependent. ACs presynaptic to Mb BC terminals received inputs via AMPA/KA and NMDA type receptors in both the ON and OFF pathways, and employed TTX-sensitive sodium channels to boost signal transfer along their processes. ON and OFF L-IPSCs, like reciprocal feedback IPSCs, were mediated by both $GABA_A$ and $GABA_C$ receptors. However, our results suggest that lateral and reciprocal feedback do not cross-depress each other, and are therefore mediated by distinct populations of ACs. These findings demonstrate that retinal inhibitory circuits are highly specialized to modulate BC output at different light intensities.

Introduction

Visual signals in the retina must pass through bipolar cells (BCs) on their way to the brain, because BCs form the sole direct excitatory connection between photoreceptors and ganglion cells (GCs), whose axons form the optic nerve. In the inner plexiform layer (IPL), BCs also excite amacrine cells (ACs) and receive inhibitory input from ACs. This input may be either reciprocal inhibition, originating from ACs directly excited by a given BC, or lateral feedback inhibition, originating from ACs excited by other BCs. Elegant immunocytochemical studies in the rabbit retina elucidated the complexity of this synapse; each rod bipolar terminal is contacted by varicosities from approximately 25 different S1-type ACs and 50 different S2-type ACs (Zhang et al, 2002). In the goldfish retina, a single Mb (mixed rod/cone bipolar cell) axon terminal receives approximately 350 inhibitory AC synapses in the IPL (Witkovsky and Dowling, 1969), of which 50% are reciprocal and 50% are lateral synapses (Marc and Liu, 2000). This suggests that a tremendous amount of synaptic computation takes place at bipolar cell terminals to determine the amount of glutamate that is released onto GCs.

Reciprocal feedback is thought to make the output of BCs more transient (Euler and Masland, 2000), tuning it to the dynamic range of GCs (Vigh and von Gersdorff, 2005), and preventing the rapid depletion of presynaptic vesicle pools (Singer and Diamond, 2006). Reciprocal feedback has also been shown to undergo use-dependent plasticity (Vigh et al, 2005; Li et al, 2007). Lateral feedback allows for spatial integration of signals (Cook and McReynolds, 1998), mediates center-surround organization of the receptive fields (Jacobs and Werblin, 1998; Ichinose and Lukasiewicz, 2005; Zhang and Wu, 2009) and contributes to GC orientation selectivity (Venkataramani and Taylor, 2010).

It is difficult to distinguish these forms of feedback when the retina is stimulated with its natural stimulus, light, because some ACs might provide both lateral and reciprocal feedback to a single BC. Here, we used a novel approach to achieve this goal in order to assess and isolate the retinal pathway that mediates lateral inhibition to an identified BC terminal. We recorded responses to full-field illumination in axotomized BC terminals embedded in goldfish retinal slices, in which visual information could only reach the BC terminal via the lateral inhibitory pathway (Figure 1.1A). We found that both rods and cones contributed to the lateral inhibitory postsynaptic currents (L-IPSCs) targeting Mb terminals during the illumination ("ON" inhibition), while L-IPSCs after the termination of light ("OFF" inhibition) were mediated primarily by a cone-driven retinal circuit. The L-IPSCs were GABAergic, involving both $GABA_A$ and $GABA_C$ receptors, much like reciprocal feedback at Mb terminals (Vigh and von Gersdorff, 2005). However, we show here that the ACs that mediate lateral IPSCs are distinct from those involved in reciprocal feedback.

Our study suggests that, in addition to reciprocal feedback, at least two distinct lateral circuits control the glutamate output of Mb BCs. Furthermore, we show that these circuits operate across a broad range of physiological light conditions.

Materials and Methods

Retinal slice preparation. Living retinal slices were prepared from the retina of goldfish (*Carassius auratus*) of either sex, as described previously (Palmer et al., 2003), except that all procedures were performed under infrared illumination with the aid of PVS-7 Night Vision Goggles and OWL Night Vision Scopes (both from BE Meyers, Redmond, WA) mounted on Olympus SZ51 stereo scopes to maintain the retina in a fully dark-adapted state. In some cases, parts of the dissection were performed under dim red light. Slices (200-250 µm thick) were superfused at 2–5 ml/min with a Ringer's solution containing (in mM): 100 NaCl, 2.5 KCl, 1.0 $MgCl_2$, 2.5 $CaCl_2$, 25 $NaHCO_3$, 0-0.2 ascorbic acid, and 12 glucose (osmolarity: 260±2 mOsm and pH: 7.45, set with NaOH). The Ringer's solution was gassed continuously with 95% O_2 and 5% CO_2. Drugs were bath applied in the perfusing medium. NBQX, CNQX, (*S*)-(+)-α-Amino-4-carboxy-2-methylbenzeneacetic acid (LY 367385), 6-imino-3-(4-methoxyphenyl)-1(6*H*)-pyridazinebutanoic acid (SR95531), 3-((R)-2-Carboxypiperazin-4-yl)-propyl-1-phosphonic acid ((R)-CPP) and D-AP5 were obtained from Tocris (Bristol, UK). Tetrodotoxin (TTX) was obtained from Alomone Laboratories (Jerusalem, Israel). All other chemicals and salts were obtained from Sigma (St. Louis, MO).

Electrophysiology and light stimulation. Giant terminals of Mb BCs with severed axons were identified in the inner plexiform layer (IPL) based on (1) Mb-shaped (bulbous) terminal morphology, (2) single-exponential membrane time constant, and (3) the presence of an L-type Ca^{2+} current and ΔC_m jump in response to depolarization. Axotomized bipolar cell terminals in retinal slices were voltage clamped in whole-cell mode using a HEKA Elektronik (Lambrecht/Pfalz, Germany) EPC-10 USB patch-clamp amplifier in conjunction with Patchmaster software (version 2.30), or an EPC-9 double

patch-clamp amplifier controlled by Pulse software. With either amplifier, the Sine+DC technique was used for real-time measurements of membrane capacitance, in which a 1 kHz sinusoidal voltage command (20-30 mV peak to peak) was added to the holding potential of -60 mV, and the resulting current was analyzed at two orthogonal phase angles by the lock-in amplifier (Gillis, 2000). Recordings were obtained using 6-12 MΩ patch pipettes pulled from 1.5 mm diameter thick-walled borosilicate glass (World Precision Instruments, Sarasota, FL) on a horizontal puller (Sutter, Novato, CA; model P-97), coated with dental wax (Cavex, West Chester, PA) to reduce pipette capacitance, and filled with solution containing (in mM): 95 Cs-gluconate, 25 HEPES, 10 TEA-Cl, 3 Mg-ATP, 0.5 Na-GTP, and 2 EGTA, adjusted to pH 7.2 with CsOH. In addition, methylamine HCl (10 mM) was included to buffer vesicular pH (Cousin and Nicholls, 1997; Vigh et al., 2005). In some cases, 10 methylamine HCl was left out and 95 Cs-gluconate was replaced with a combination of 60 Cs-gluconate and 40 CsCl to increase the amplitude of IPSCs at the holding potential of -60 mV. Some internal solutions contained 3 mM ascorbic acid and/or 3 mM reduced glutathione.

Voltage-clamp series resistance (R_s) errors were not electronically compensated and liquid junction potential was not corrected. Cells with uncompensated R_s > 30 MΩ (or leak > 50 (-pA) at a holding potential of -60 mV) were excluded from further evaluation. Recordings were performed at room temperature and in the daytime (morning/afternoon) to avoid circadian changes in transmitter release from bipolar cells (Hull et al., 2006b).

Full-field light stimulation of retinal slices was performed either with white (Allied Electronics, Beaverton, OR), 505 nm (green) or 660 nm (red) LEDs (American Bright Optoelectronics Corp, Chino, CA), positioned 3 cm above the preparation at a 30° angle. The intensities of 505 and 660 nm light pulses were reliably controlled with mV precision by the command voltage of EPC-10 DA output. In our stimulus range the number of

emitted photons was between 6.6×10^9 and 1.9×10^{12} *cm^{-2}* s^{-1} (λ=505 nm) and between

8.7×10^8 and 2.0×10^{12} *cm^{-2} *s^{-1} (λ=660 nm) as calibrated by an Optical Meter (model

1918-C) equipped with a low intensity sensor (model 918D-SL-OD3) (both form

Newport, Irvine CA).

For white light stimulation, slices were stimulated with a white LED connected via

soldered wire and BNC cable to an A/D input of the HEKA EPC-9 patch clamp amplifier.

Full-field light flashes were delivered by application of 400-500 ms voltage steps from 0

to 5 V. The full dynamic range of LED light intensity was evoked by voltage steps

between 2.5 V to 5 V, which evoked photon flux between 1.06×10^{11} and 7.32×10^{13}

photons*cm^{-2}*s^{-1}. The timing and amplitude of voltage steps was controlled from within

the Pulse Software (HEKA Elektronik) controlling the EPC-9 amplifier. Calibration of light

flash timing (onset and offset) was performed with a photodiode connected to the EPC-9

amplifier through an ITHACO 4302 dual 24 dB Octave Filter. Light flash onset and offset

had rise and decay time constants of 0.12 and 6.3 ms, respectively. Onset and offset

times did not vary as a function of flash duration between 100 and 1000 ms. Calibration

of white light intensity was performed with an ILT-1700 photometer and SE033 detector

from International Light Technologies (Peabody, Massachusetts). Factory calibration

determined the photic illuminance response sensitivity of the detector to be (2.60×10^{-8}

A)(ft^2)(lm^{-1}), or (2.415×10^{-9} A)(lux^{-1}), assuming 3215 K color temperature.

Data analysis. Off-line data analysis was performed using IgorPro software (version

5.03; Wavemetrics, Lake Oswego, OR). Because light-evoked lateral feedback

responses showed a degree of variability from stimulus to stimulus, we presented

averaged traces of a minimum of 5 individual light responses throughout the paper

unless otherwise noted. Consecutive light stimulations were applied with a stimulus

interval of at least 30 s. Quantification of light responses was performed by integrating

the charge transfer (Q) of light-evoked, lateral inhibitory postsynaptic currents (L-IPSCs)

for 500 (or 400) ms during the illumination (ON), and for 500 (or 300) ms after the

termination of the stimulus (OFF). Reciprocal feedback was quantified by integrating the

total current during a 100 ms depolarization from -60 to -20 or 0 mV. This method

provides a quick measure of the net charge transfer associated with I_{Ca} plus the

reciprocal GABAergic feedback that can be compared across subsequent

depolarizations, and has been used previously to quantify relative changes in reciprocal

feedback in the absence of I_{Ca} rundown (Vigh et al., 2005). When appropriate,

experiments were performed in the presence of LY 367385 to avoid reciprocal feedback

potentiation due to AC mGluR1 metabotropic glutamate receptor activation (Vigh et al.,

2005). Statistics were calculated using SigmaPlot (version 11; Systat Software Inc.).

Paired or unpaired two-tailed Student's t-tests were used to compare data sets. Multiple

sets of data were compared using ANOVA (Holm-Sidiak method), or the Mann-Whitney

U test, when appropriate. Data were reported as mean +/- SEM. Statistics were

performed on averaged traces, unless otherwise noted.

Results

Light evokes both ON and OFF lateral IPSCs in single bipolar cell terminals

Whole-cell voltage clamp recordings were made from Mb bipolar cell (BC) terminals in a goldfish retinal slice preparation. These large, bulbous structures are located in the ON sublamina of the inner plexiform layer (IPL), close to the ganglion cell (GC) layer. It is possible to make whole-cell voltage clamp recordings from a single axotomized Mb BC terminal (Palmer et al., 2003). This technique offers several advantages from a biophysical standpoint. For example, axotomized terminals allow accurate recording of membrane capacitance increases (ΔC_m jumps) associated with exocytosis (von Gersdorff and Matthews, 1999). It also allows isolation of reciprocal inhibitory feedback, which is observed at different types of bipolar cells (Dong and Werblin, 1998; Protti and Llano, 1998; Hartveit, 1999; Vigh and von Gersdorff, 2005). In the present study, another advantage of this preparation was exploited; severing the connection between the axon terminal and somatodendritic compartment of the BC results in light-evoked membrane currents of the terminal being exclusively mediated by the AC synapses that provide lateral feedback inputs from ACs to the axotomized terminal (Figure 1.1A).

Full field light stimulation (λ=505 nm, 500 ms) at increasing intensities triggered lateral inhibitory postsynaptic currents (L-IPSCs) in axotomized terminals voltage clamped at -60 mV (Figure 1.1Bi). The intensity range of the light stimuli spanned the mesopic light levels (Krizaj, 2000); the dimmest green flash was just below the cone activation threshold, and the intensity of the brightest light step was 1 log unit above rod saturation. Light triggered L-IPSCs during the illumination (ON), as well as after the termination of light stimulus (OFF) (Figure 1.1Bi). Note that in this representative terminal the second 505 nm flash which had an intensity (I=1.8×10^{10}, Figure 1.1Bi) around the cone threshold (~10^{10} photons*cm^{-2}*s^{-1}; Busskamp et al, 2010) evoked large

24

ON, but only tiny OFF L-IPSCs. In the mouse retina, the rod pigment's sensitivity to 500 nm light is nearly 2 log units higher than that of the M-cone pigment, and about 4 log units higher than that of the S-cone pigment (Lyubarsky et al., 1999). Although the spectral sensitivity of goldfish rods and cones (Palacios et al, 1998) are somewhat different from those of the mouse, this finding suggested that in Mb terminals ON L-IPSCs received larger rod input than OFF L-IPSCs.

The L-IPSCs were quantified as inhibitory charge transfer (Q, see Methods and Materials) to generate intensity-response curves for both the ON and OFF components (Figure 1.1Bii). Importantly, the quantification revealed that amplitudes of ON L-IPSCs appeared to plateau at the light intensities known to saturate rods ($\sim 10^{11}$ photons cm^{-2}s^{-1}). On the other hand, the intensity-response curve of OFF L-IPSCs did not saturate but rather increased linearly across the range of our (green) light intensities.

We found a large variation in the amplitude of light-evoked L-IPSCs from terminal to terminal. This variation might be physiologically relevant: it is possible that the number of lateral inputs is different across Mb terminals. Nonetheless, we cannot exclude the possibility that this variation was also caused by the slicing procedure, which may have destroyed a variable portion of long, wide-field AC processes targeting the recorded Mb terminal. Despite this variation, it was possible to generate cumulative intensity-response curves by first normalizing L-IPSCs evoked by a range of light intensities from a given terminal by reference to the largest L-IPSC amplitude. Then, the normalized values corresponding to each of the tested light intensities were averaged across multiple cells (Figure 1.1Biii). Statistical analysis confirmed that the differences between the normalized ON and OFF intensity/response data were significant (ANOVA, Holm-Sidiak method, p<0.001).

To further examine the possible differences between rod and cone contributions to L-IPSCs, we stimulated the retinal slices with full field red light flashes (λ=660 nm, 500

25

ms) of increasing intensity (between 8.7×10^8 and 2.0×10^{12} $^*cm^{-2}$ $^*s^{-1}$), superimposed on a

steady, rod-saturating 505 nm background ($I=10^{10}$ $^*cm^{-2}$ $^*s^{-1}$, Sterling, 2004), that barely

stimulated cones. With this steady green background, both ON and OFF L-IPSCs were

turned on at around the cone-sensitivity threshold ($\sim10^{11}$ $^*cm^{-2}$ $^*s^{-1}$, Figure 1.1Ci, 1.1Cii).

The intensity/response curves of ON and OFF L-IPSCs triggered by red flashes on the

green background ran parallel and no responses appeared to saturate within our

intensity range (Figure 1.1Cii). There was no statistical difference (ANOVA, P = 0.209)

between the normalized ON and OFF L-IPSC intensity/response data (Figure 1.1Ciii).

These results indicated that under these conditions both the ON and the OFF L-IPSCs

were mediated by cone-driven components.

More importantly, statistical analysis revealed a significant difference (Mann-

Whitney U Statistic, P<0.001) between the distribution of normalized data representing

the ON L-IPSCs triggered by a green flash intensity series on a dark background (Figure

1.1Biii, ON trace) and that of ON L-IPSCs triggered by a red flash intensity series

superimposed on rod-saturating green background light (Figure 1.1Ciii, ON trace),

indicating that rods substantially contributed to ON L-IPSCs in the mesopic intensity

range. Similar comparison of the corresponding OFF L-IPSC data sets revealed no

statistical difference (Mann-Whitney U Statistic, P=0.200). Thus the intensity/response

distribution of OFF LIPSCs was independent of the presence of background light. In

other words, the rod-saturating background illumination did not alter the sensitivity of

OFF L-IPSCs (despite the change in wavelength of the stimulating light flashes), but

reduced the sensitivity of ON L-IPSCs by approximately 1 log unit (compare cumulative

ON traces presented on Figure 1.1Biii vs. 1.1Ciii).

In summary, our data suggest that both ON and OFF L-IPSCs at Mb axon

terminals receive mixed rod and cone input. However, the relative contribution of rods

and cones to ON and OFF L-IPSCs is uneven. In the mesopic light intensity range, ON

L-IPSCs receive large rod- and cone-driven input, while OFF L-IPSCs are primarily driven by cones.

Differential contribution of ON and OFF retinal pathways to lateral feedback

The separation of light information into ON and OFF pathways, initially encoded as photoreceptor hyperpolarization, is accomplished by the existence of heterogeneous glutamate receptor populations in ON and OFF BCs, which depolarize and hyperpolarize in response to light, respectively. The retinal ON signaling pathway begins with a group III metabotropic glutamate receptor (mGluR), sensitive to L-AP4, a group III mGluR agonist (Slaughter and Miller, 1981). Indeed, L-AP4 (10-20 µM) significantly reduced the ON L-IPSCs in Mb terminals (Figure 1.2Ai, 1.2Aii) (to 23±3 % of control, p<0.02, n=5, paired Student's t-test, two-tailed) confirming that ON BCs provide excitatory input to the ACs that mediate light-evoked ON L-IPSCs. L-AP4 also tended to reduce OFF L-IPSCs (to 29 ± 5 % of control; Fig 1.2), although this effect was not statistically significant (p<0.13, N.S, n=5; paired Student's t-test, two-tailed). The L-AP4 effect on OFF L-IPSCs might be related to the presynaptic inhibitory effect of group III mGluRs on OFF BCs (Awatramani and Slaughter, 2001), which would reduce excitation of the ACs that mediate OFF L-IPSCs in Mb terminals. In addition, L-AP4 might act directly at group III mGluRs located on AC dendrites (Brandstätter et al, 1996; Koulen et al, 1996; Quraishi et al., 2007).

OFF BCs utilize ionotropic, AMPA/kainate type receptors (AMPA/KAR) to detect glutamate efflux from photoreceptors. Application of the AMPA/KAR antagonist 2,3-dihydroxy-6-nitro-7-sulfamoyl-benzo(f)quinoxaline (NBQX) (10 µM) markedly reduced the OFF L-IPSCs (to 30±6 % of control, p<0.0001, n=10, paired Student's t-test, two-tailed). Light responses of ACs are mediated by AMPA and NMDA receptors (Dixon and Copenhagen, 1992), with AMPARs thought to be more critical for transient ACs (Matsui

27

et al, 2001; Vigh and Witkovsky, 2004). Therefore, the NBQX effect on OFF L-IPSCs might have been also caused by inhibition the OFF BC➔AC synapse. By the same token, it was our expectation that NBQX would eliminate or reduce light-evoked ON L-IPSCs by blocking the ON BC➔AC synapse. Surprisingly, the opposite was observed: NBQX increased the ON L-IPSCs (Figure 1.2Bi, 1.2Bii; 1.2D; to 168±30 % of control, $p < 0.03$, n=10; paired Student's t-test, two-tailed). The fact that NBQX did not block the ON BC➔AC synapse suggests that glutamatergic receptors other than AMPA/KARs, perhaps NMDARs, not only contributed to glutamatergic synaptic transmission, but were also able to independently carry the visual information after pharmacological block of AMPA/KARs. To test this notion, we first applied NBQX (10 μM) with the NMDAR antagonist D-AP5 (50 μM). This cocktail markedly reduced both ON and OFF L-IPSCs (to 12±3 % of control, $p < 0.03$ and 24±10 % of control, $p < 0.03$, respectively n=5) (Figure 1.2D). Application of D-AP5 (50 μM) alone also reduced both the ON and the OFF L-IPSCs (to 33±8 % of control, $p < 0.05$ and to 65±14 % of control, $p = 0.3$, N.S., n=4). Similar results were obtained when we used another selective NMDAR antagonist, (R)-CPP. When (R)-CPP (20 μM) was applied together with NBQX (10 μM), the cocktail reduced both the ON and OFF L-IPSCs (to 6±2 % of control, $p < 0.04$ and 15±8 % of control, $p < 0.04$, respectively, n=6) (Figure 1.2Ci, 1.2Cii, 1.2D). Like D-AP5, (R)-CPP (20 μM) alone reduced both the ON and the OFF L-IPSCs (to 55±18 % of control, $p = 0.1$, NS, and to 47±8 % of control, $p < 0.03$, n=4). These results indicated that NMDARs contribute significantly to synaptic transmission between BCs and ACs that mediate lateral inhibition to Mb terminals (Figure 1.2D). The partial inhibition of L-IPSCs by D-AP5 alone also suggests that AMPA/KARs are present at both the ON BC➔AC and OFF BC➔AC synapse.

It is tempting to speculate that NBQX-evoked enhancement of ON L-IPSCs in Mb terminals might be mediated by horizontal cells (HCs) in the outer retina. For example,

28

an AMPA/KAR antagonist will hyperpolarize HCs (Krizaj et al, 1994), removing the HC

feedback to photoreceptors (Hirasawa and Kaneko, 2003; Fahrenfort et al, 2005, 2009;

Tatsukawa et al, 2005; Davenport et al., 2008; Thoreson et al, 2008) and, if present in

the goldfish retina, the GABAergic feed-forward inhibition from HCs to ON BCs (Duebel

et al, 2006). The resulting disinhibition would increase the light-evoked excitation of ACs

by ON BCs via NMDARs, leading to larger ON L-IPSCs at the Mb terminals.

GABAergic amacrine cells mediate lateral inhibition to Mb terminals

$GABA_A$ and $GABA_C$ receptors are expressed to different degrees in different types of

bipolar cells (Wässle et al., 1998; McCall et al., 2002). In previous studies we found that

reciprocal feedback at Mb terminals is mediated by both ionotropic $GABA_A$ and $GABA_C$

receptors, with $GABA_C$ receptors responsible for sustained inhibition (Vigh and von

Gersdorff, 2005). In retinas of other species, $GABA_CRs$, also located primarily on ON

BCs, primarily influence the ON pathway (Zhang and Slaughter, 1995; Eggers and

Lukasiewicz, 2010). Lateral inhibition to rod BCs in the rat retina, triggered by focal

pharmacological activation of ON BCs, was also mediated by $GABA_CRs$ (Chavez et al,

2010). We found that light-evoked lateral feedback IPSCs were reduced by the $GABA_CR$

antagonist 1,2,5,6-tetrahydropyridin-4-yl-methylphosphonic acid (TPMPA) (100-150 μM,

ON: to 42 ± 10% of control response, p <0.04; OFF: to 68 ± 8% of control response, p

<0.02; n=5, Figure 1.3Ai, 1.3Aii, 1.3C).

The specific $GABA_AR$ antagonist, 6-imino-3-(4-methoxyphenyl)-1(6H)-

pyridazinebutanoic acid hydrobromide (SR95531, 25 μM), markedly increased both

components of lateral feedback (ON: to 174± 15% of control response, p<0.02; OFF: to

233 ± 41% of control response, p<0.05; n=7) (Figure 1.3Bi, 1.3Bii, 1.3C). Similar effects

have been described in the inner retina, in that $GABA_AR$ blockers, such as the SR95531

not only block the $GABA_ARs$ on the (Mb) BC axon terminals, but also eliminate $GABA_AR$-

mediated serial inhibition between ACs (Zhang et al, 1997; Eggers and Lukasiewicz, 2010). This effect on serial inhibition is especially pronounced following full-field illumination. As a result, the presynaptic ACs providing lateral IPSCs (in this case to the Mb terminals) are disinhibited. Subsequent light-evoked excitation of ACs by BCs causes larger GABA release, which in turn, acts on $GABA_C$Rs of BCs. In our hands, however, TPMPA (up to 300 μM) reduced but did not completely block SR95531-elevated L-IPSCs (Figure 1.3Biii, blue trace). Subsequent application of picrotoxin (PTX, 100 μM), a strong blocker of both $GABA_A$ and $GABA_C$Rs in the goldfish retina (Vigh et al, 2005), eliminated the remaining lateral feedback IPSCs (Figure 1.3Biii, green trace). This finding raised the possibility that light-evoked lateral feedback IPSCs might have a glycinergic component, as PTX also inhibits ionotropic glycine receptors in the retina at the concentration we applied (100 μM; Li and Slaughter, 2007). However, strychnine (1 μM), a specific antagonist of ionotropic glycine receptors in the retina at these low concentrations (Protti et al, 1997), had no significant effect on ON or OFF L-IPSCs (control ON: 2.69+/-0.40 pC, Strychnine ON: 3.34+/-0.52 pC, p=0.38, n=3; Control OFF: 1.36+/-0.09 pC, Strychnine OFF: 1.44+/-0.10 pC, p=0.71, n=3; data not shown), consistent with the finding that spontaneous IPSCs recorded from Mb terminals were eliminated by TPMPA and SR95531 (Vigh et al, 2005). Therefore, it is most likely that the incomplete block of L-IPSCs by TPMPA in the presence of SR95531 resulted from an abnormally high synaptic GABA concentration. In other words, it is likely that full-field stimulation of the entire disinhibited AC network released large amounts of GABA, and that the competitive antagonist TPMPA was unable to block all $GABA_C$Rs.

GABAergic lateral inhibition is TTX-sensitive

TTX-sensitive voltage-gated sodium (Na_V) channels are known to mediate long-range dendritic signaling of wide-field ACs (Cook and McReynolds, 1998; Shields and Lukasiewicz, 2003), which are GABAergic (MacNeil et al, 1999; Masland and Raviola, 2000). TTX-sensitive, wide-field GABAergic ACs were found to contribute to surround responses of some ganglion cells (Taylor, 1999; Flores-Herr et al, 2001), and to mediate lateral feedback to rod BCs (Chavez et al, 2010). TTX-sensitive Na_v channels are also present in the somatodendritic compartment of a subpopulation of cone BCs in the goldfish retina, where they produce a small, rapidly inactivating current (Zenisek et al, 2001). In our experiments, TTX (1-2 μM) consistently reduced the OFF lateral IPSCs in each cells (to 44± 10% of control response, p<0.03, n=6). These data suggest that Na_v channels in OFF cone BCs in the goldfish retina could be functionally significant and/or that TTX-sensitive Na_v channels are capable of boosting OFF lateral inhibition in OFF ACs presynaptic to Mb terminals.

However, TTX effects on the ON lateral IPSCs were mixed, with inhibition in 4/6 and enhancement in 2/6 cells (Figure 1.4Ai, Aii). The TTX-evoked enhancement of ON L-IPSCs is interesting, because it suggests that the ON GABAergic ACs presynaptic to the Mb terminals may receive serial GABAergic inhibition (Zhang et al, 1997; Eggers and Lukasiewicz, 2010) that is, at least partially, Na_V channel-dependent. This effect was not present all the time, which might be related to the observation that the Na_V channel-possessing ACs are typically large, wide-field cells that might have been severed during slice preparation. If these connections are absent, the net TTX effect is inhibitory, implying that TTX-sensitive Na_V channels are capable of boosting the lateral inhibition of ACs presynaptic to the Mb terminals.

Lateral and reciprocal feedback is mediated by separate sets of amacrine cells

Our data demonstrates that lateral feedback inhibition of Mb terminals is accomplished via $GABA_A$ and $GABA_C$Rs, in a manner similar to that of reciprocal feedback inhibition (Vigh et al, 2005; Vigh and von Gersdorff, 2005). Reconstructions of synaptic connections to, and around Mb axon terminals, based on electron micrographs of ultrathin sections, led to the conclusion that reciprocal BC➔AC synapses are physically distinct from AC➔BC lateral feedback synapses (Marc and Liu, 2000). However, this systematic morphological study was unable to determine whether or not the same ACs give rise to both types of GABAergic feedback synapses.

The "in situ" axotomized Mb terminal offers the ideal preparation for addressing this question with a physiological approach. First, depolarization of a single Mb terminal will trigger primarily local, reciprocal feedback. This will cause GABA to be released from depolarized AC processes back onto $GABA_A$ and $GABA_C$ receptors on the Mb terminal (Figure 1.5A). If light evoked L-IPSCs and reciprocal IPSCs are mediated by the same population of AC processes, activation of reciprocal feedback immediately following light-evoked L-IPSCs, or *vice versa*, should result in depressed reciprocal (or lateral) inhibition, due to synaptic vesicle pool depletion in ACs and/or desensitization of $GABA_A$Rs. Depolarization of Mb terminals from a holding potential of -60 to 0 mV, in the presence of a Cs^+-based internal solution (see Materials and Methods), evoked a sustained inward current, associated with Ca^{2+} influx (I_{Ca}), and triggered glutamate release, as evidenced by an increase in membrane capacitance (ΔC_m). Reciprocal GABAergic feedback to the presynaptic terminal was evident as outward IPSCs superimposed on I_{Ca} (Figure 1.5Bi, black trace, arrow). In the presence of the mGluR1 antagonist LY367385 (100 μM), which has been shown to block progressive potentiation of reciprocal feedback inhibition (Vigh et al, 2005), consecutive depolarizations of presynaptic Mb terminals need to be applied at least 1 min apart in order to avoid short-

32

term depression (Figure 1.5Bi, compare black and red traces). Such short-term depression has been previously shown to be due to depletion of synaptic vesicle pools in the GABAergic ACs that mediate reciprocal feedback (Li et al, 2007).

Application of bright light stimulation to evoke L-IPSCs immediately prior to the triggering of reciprocal feedback, in an alternating stimulation protocol with triggering of control reciprocal feedback with an inter-trace interval of 60 s, did not alter the charge transferred by reciprocal feedback IPSCs ($103\pm7\%$ of control, $p<0.5$, N.S., n=6) (Figure 1.5Bii). With reverse-order stimulation, L-IPSCs in Mb terminals were evoked by bright full-field light stimulations 1 min apart, with the second light stimulus in each pair preceded by depolarization to trigger reciprocal feedback (Figure 1.5C). The results of light stimulation following depolarization were consistent with the results of depolarization following light stimulation, in that activation of reciprocal inhibitory synapses did not decrease the charge transfer of light-evoked lateral IPSCs (ON: $111\pm12\%$ of control, $p=0.62$, n=3; OFF: $105\pm7\%$ of control, $p=0.83$, n=3; unpaired Student's t-test, two-tailed). The results of these experiments strongly support the idea that light-evoked lateral and reciprocal feedback IPSCs at Mb terminals are mediated by separate populations of ACs.

Discussion

The present investigation dissected the reciprocal and lateral IPSCs that target Mb axon terminals, and studied the light-evoked, lateral IPSCs. The use of various light stimulation intensities, combined with the use of pharmacological tools, allowed us to infer the retinal circuitry underlying L-IPSCs (Figure 1.6). The major findings of our investigation were: (1) Both rods and cones drive lateral feedback to the Mb terminals, albeit with different temporal properties: depending on light intensity, both rods and cones contribute substantially to ON L-IPSCs, whereas OFF L-IPSCs are mediated primarily by cone-driven circuits, (2) Different populations of GABAergic ACs mediate ON and OFF L-IPSCs, (3) GABAergic ACs that mediate TTX-sensitive lateral inhibition receive serial GABAergic inhibition from other ACs, (4) GABA$_A$Rs and GABA$_C$Rs contribute to both ON and OFF L-IPSCs, and (5) lateral and reciprocal feedback inhibition to Mb BCs are mediated by separate populations of GABAergic ACs.

Rod signals are modulated by inner retinal inhibitory feedback

In mammalian retina under low scotopic conditions, the majority of rod signals are processed by a dedicated circuitry: the rod➔rod BC➔AII AC➔cone BC➔GC pathway (Bloomfield and Dacheux, 2001) is intersected at rod BC terminals by GABAergic reciprocal feedback inhibition from GABAergic A17 ACs (Hartveit, 1999; Zhang et al, 2002; Singer and Diamond, 2003; Chavez et al, 2006). The long processes of A17 could potentially carry inhibitory signals over tens to hundreds of microns (Menger and Wässle, 2000) and mediate lateral feedback inhibition of distant rod BCs. Nonetheless, the A17 appears to be specialized to provide reciprocal inhibition in a parallel fashion to many rod BCs independently along its processes, instead of participating in spatial (lateral) signaling (Grimes et al, 2010). Rod BCs in the mammalian retina receive lateral

inhibition from an as yet unidentified population of GABAergic ACs, which use TTX-sensitive (Na$_V$) conductances to transfer the signal (Bloomfield and Völgyi, 2007; Chavez et al, 2010). It is not known if scotopic signals are subject to further modulation by lateral and/or reciprocal feedback inhibition at cone BC terminals, which are the last step on the way toward GCs (DeVries and Baylor, 1995; Field and Chichilnisky, 2009; Gauthier et al, 2009).

In the goldfish retina, Mb BCs carry mixed rod-cone signals (Wong et al, 2005; Joselevitch and Kamermans, 2007) and make direct synapses onto GCs (Arai et al, 2010; Palmer, 2010). Regardless of this fundamental difference between the circuits that mediate scotopic vision in goldfish and mammals, Mb axon terminals are very similar to mammalian rod BCs in that they also receive robust GABAergic reciprocal feedback (Vigh and von Gersdorff, 2005), and, as demonstrated in the present study, lateral feedback. Importantly, the origin of lateral feedback IPSCs that arrive at the Mb axon terminal is consistent with the known inputs to Mb BC dendrites, as both rod and cone-driven components were found to contribute to light-evoked L-IPSCs (Figure 1.1Biii, 1.1Ciii).

ON and OFF pathways interact to mediate lateral feedback, but do not overlap
In the rabbit retina, L-AP4 sensitive, lateral inhibitory ("cancelling") feedback currents in rod BCs, which turn on at the onset of light stimulation, originate from neighboring ON BCs (Molnar and Werblin, 2007). Likewise, lateral feedback IPSCs to rod BCs in the rat retina could be more effectively triggered by pharmacological stimulation of ON BCs than by stimulation of OFF BCs (Chavez et al, 2010). We also recorded L-AP4 sensitive, ON L-IPSCs in Mb BCs (Figure 1.2Ai). The axotomized Mb terminals we recorded from were physically separated from their dendritic trees, where BCs receive excitatory inputs from photoreceptors. Thus, the onset of ON L-IPSCs relative to that of excitatory inputs

35

could not be determined. "Cancelling" L-IPSCs could contribute to the surround of the Mb receptive field (Saito et al, 1981). If the timing of ON L-IPSCs were slightly delayed relative to light-evoked excitation ("delayed cancelling"), its function would be similar to that of reciprocal feedback, which shortens sustained responses and inhibits low-frequency signal transfer, thereby enhancing propagation of high-frequency or transient stimuli (Molnar and Werblin, 2007). Future experiments involving recordings of light-evoked responses in intact Mb BCs will be needed to clarify these functionally important issues for the vertebrate retina.

We found that L-IPSCs in Mb BCs also have a strong, independent OFF component. Thus, Mb BCs are subject to "ON/OFF crossover inhibition," (Molnar et al, 2009) a configuration in which ACs with OFF responses deliver inhibitory inputs to ON cells, and *vice versa*. ON/OFF crossover inhibition has been demonstrated at synapses from ACs to GCs (Pang et al, 2007), ACs to ACs (Hsueh et al, 2008) and ACs to BCs (Molnar and Werblin, 2007; Zhang and Wu, 2009).

Glutamatergic excitatory postsynaptic currents (EPSCs) in GCs following depolarization of presynaptic Mb BCs are much longer than might be expected based on the duration of presynaptic depolarization, due to the spread of depolarization in the network of presynaptic Mb BCs coupled by gap junctions (Arai et al, 2010). As this coupling is strongest in the light adapted retina (Arai et al, 2010), it is tempting to speculate that cone-dominant OFF L-IPSCs (Figure 1.1Bi) might serve to terminate presynaptic release from Mb BCs in order to temporally restrict it to the period of light stimulation under photopic conditions.

In this study, we did not fully identify the ACs that evoked L-IPSCs in Mb BCs. We did, however, identify their GABAergic nature (Figure 1.3) and show that they receive serial GABAergic inhibition from other ACs (Dowling and Werblin, 1969; Zhang et al 2004) via GABA$_A$Rs (Zhang et al, 1997; Watanabe et al, 2000; Eggers and

36

Lukasiewicz, 2010). Due to the fact that ON and OFF L-IPSCs were differentially modulated by TTX (i.e. ON L-IPSCs were either reduced or enhanced, while OFF L-IPSCs were reduced, as shown in Figure 1.4Ai), it is unlikely that a single population of ACs receiving inputs from both ON and OFF BCs mediates all L-IPSCs in Mb BCs. To the contrary, we propose that ON and OFF L-IPSCs may be mediated by two functionally distinct sets of wide-field GABAergic ACs (Figure 1.6).

Lateral and reciprocal feedback IPSCs at Mb terminals are mediated by distinct ACs

There are many similarities between the synaptic events that underlie lateral and reciprocal feedback to Mb BCs (Vigh and von Gersdorff, 2005). The first similarity is that GABAergic ACs receive excitatory glutamatergic input from BCs via AMPA/KA and NMDA receptors in both cases. Interestingly, as seen at the Mb BC reciprocal feedback synapse, NMDAR activation can trigger L-IPSCs onto Mb terminals without AMPA/KAR "priming" to remove the Mg^{2+} block (i.e. in the presence of an AMPA/KAR antagonist, Figure 1.2B). This property of GABAergic feedback to Mb BCs is remarkably different from what has been reported in mammalian retina, where NMDARs have not been found to contribute to either lateral or reciprocal GABAergic feedback (Chavez et al, 2006; Chavez et al, 2010). Nonetheless, NMDARs have been shown to play a critical, direct role in releasing glycine from ACs in the mammalian retina (Chavez and Diamond, 2008).

Here, we have shown that GABAergic lateral feedback is mediated both by $GABA_ARs$ and $GABA_cRs$. Nonetheless, we were unable to describe a temporal difference between the contributions of these two receptor classes to L-IPSCs that matched that of reciprocal feedback events (i.e. $GABA_ARs$ mediate fast and transient events, while $GABA_cRs$ activate more slowly and mediate sustained inhibition). Prior to

this study, it was not known whether the same population of ACs could provide both lateral and reciprocal feedback inhibition to Mb terminals, depending on the spatial parameters of stimulation. However, when tested, we could not cross-deplete the GABAergic synaptic vesicle pools, or cross-desensitize the GABAergic synapses, that mediate reciprocal feedback by selectively activating lateral feedback inhibition with light stimulation (Figure 1.5Bii), or *vice versa* (Figure 1.5C). This suggests that different sets of GABAergic ACs are involved in reciprocal and lateral feedback inhibition in the goldfish retina, as has been previously suggested in rod BCs of rat retina (Chavez et al, 2010).

The vertebrate retina can be viewed as a spatiotemporal pre-filter that channels different aspects of the visual scene to the brain for final processing (Meister and Berry, 1999; Field and Chilinsky, 2007; Joselevitch and Kamermans, 2009; Gollisch and Meister, 2010). Morphologically and physiologically diverse BCs play fundamental roles in this pre-filtering process at the first retinal synapse, providing distinct postsynaptic processing of the photoreceptor signal (DeVries 2000; DeVries et al. 2006). Here we have shown that three different populations of ACs filter the output of a given BC in the inner retina (i.e. ACs providing reciprocal, lateral ON, and lateral OFF feedback) under different light conditions. This exemplifies the idea that inhibitory interactions in the IPL are highly specialized for the task of shaping BC output to GCs (Roska and Werblin, 2001). Such complexity ensures that the temporal properties of BC output are highly regulated in a way that is likely critical for proper control of GC spike latencies, which are thought to be a key component of GC information coding in the retina (Gollisch and Meister, 2008).
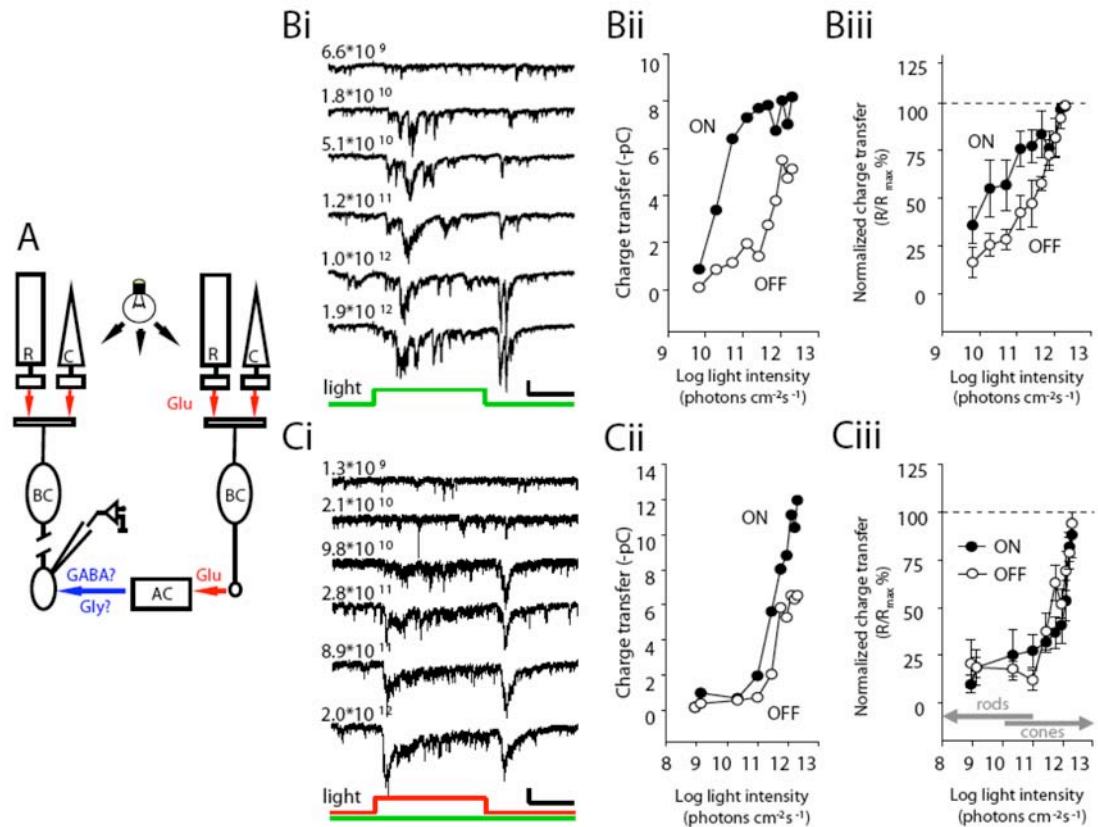
Figure 1.1. Both rod and cone signals are represented in the lateral inhibitory postsynaptic currents (L-IPSCs) of axotomized Mb terminals. **A:** Retinal pathway underlying L-IPSCs in axotomized Mb terminals. In the absence of direct visual input from the soma, a light signal can reach axotomized Mb terminals via the lateral inhibitory pathway. R: rod; C: cone; BC: bipolar cell; AC: amacrine cell; Glu: glutamate; Gly: glycine. **Bi**: Representative light evoked signals recorded from an axotomized Mb terminal. Averaged traces are shown (n=3). Light pulses (500 ms, λ=505 nm) were delivered once every 30 sec. Intensity of light pulses is given as number of photons (cm^{-2}s^{-1}), indicated at the top of each trace. Note that "ON" L-IPSCs first develop at much lower intensities than "OFF" L-IPSCs. Scale bar: 10 pA (vertical), 100 ms (horizontal). **Bii:** Quantification of L-IPSCs with Response/Intensity curve (Q/ I) for the same experiment shown on Bi. Note that our protocol consisted of flashes at 10 light intensities but only 6 are shown on Bi for clarity. Charge transfer was calculated by integrating the area under the current trace for 500 ms during the illumination ("ON"), as well as for 500

ms immediately following the offset of illumination ("OFF"). Charge values for each trace were plotted against the light intensity on a logarithmic scale. **Biii:** Summary Response/Intensity diagram (n=5) obtained with green light flashes (500 ms, λ=505 nm). R/R_{max} % calculation was performed for each cell before averaging values across cells at any given intensity. Error bars represent +/- SE. Note that sizeable ON responses were present at the lowest intensities applied in this study (in the high end of the rod sensitivity range), at intensities where OFF L-IPSCs were barely present. Also, ON L-IPSCs were nearly saturated at rod saturating intensities. Both of these observations support the notion that ON L-IPSCs are rod-dominant, whereas OFF L-IPSCs are cone-dominant. The difference between the ON and OFF data set was statistically significant (ANOVA, Holm-Sidak method, p<0.001). **Ci:** Representative light evoked signals recorded from an axotomized Mb terminal. Averaged traces are shown (n=2-4). Light pulses (500 ms, λ=660 nm) were delivered once every 30 sec, superimposed on a steady background (λ=505 nm). Intensity of light pulses is given as number of photons ($cm^{-2}s^{-1}$), indicated at the top of each trace. The intensity of the green background light was 10^{10} photons*cm^{-2}*s^{-1}. Note that both "ON" and "OFF" L-IPSCs were present, and that they developed at the same bright intensities. Scale bar: 10 pA (vertical), 100 ms (horizontal). **Cii:** Quantification of L-IPSCs with Response/Intensity curve (Q/ I) for the experiment shown in Ci. Charge transfer was calculated as in Bii. **Ciii:** Summary Response/Intensity diagram (n=5) obtained with red light flashes (500 ms, λ=660 nm) superimposed on a steady green background (λ=505 nm). Data is presented as in Biii. Note that in the presence of (rod-saturating) background light the "ON" and "OFF" Q/I curves overlap, and there was no statistical difference between the ON and OFF data sets (p=0.209, ANOVA, Holm-Sidak method).
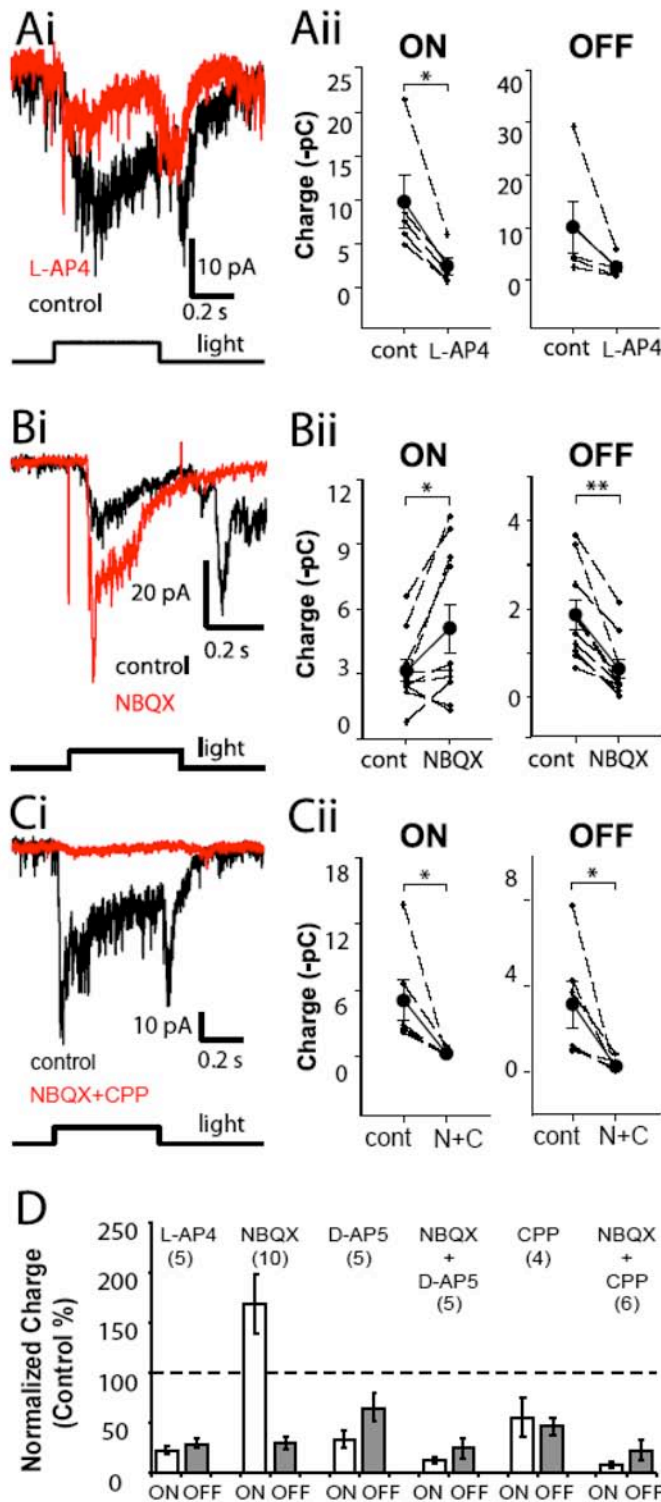
Figure 1.2. ON and OFF retinal pathways contribute to light-evoked lateral feedback at Mb bipolar terminals. Ai: Both the ON and the OFF portions of light-evoked (λ=505 nm, I=1.95x10^{12} photons cm^{-2}s^{-1}, 500 ms) L-IPSCs were reduced by the group III mGluR agonist L-AP4 (10-20 μM, red trace). Average traces are shown for each condition (n=5). **Aii:** Quantification of the effect of L-AP4 on the charge transfer ofON and OFF L-IPSCs. L-AP4 significantly reduced ON LIPSC charge (*p<0.02, paired Student's t-test, two-tailed), but the reduction of OFF L-IPSCs was not significant (p< 0.13, paired Student's t-test, two-tailed). Measurements, analysis and presentation of drug effects on L-IPSCs are performed this way throughout the paper. **Bi**: The AMPA/KAR receptor antagonist NBQX (10 μM, red trace) substantially reduced the OFF L-IPSCs evoked by bright white light (400 ms, I=7.32*10^{13} photons*cm^{-2}*s^{-1}), but markedly increased the ON

41

L-IPSCs. **Bii:** Quantification of the NBQX effect on ON and OFF L-IPSC charge transfers. NBQX significantly reduced the OFF L-IPSCs (**: $p<0.0001$, paired Student's t-test, two-tailed), and significantly enhanced the ON L-IPSCs (*: $p<0.03$, paired Student's t-test, two-tailed). **Ci**: L-IPSCs were essentially eliminated by the combination of ionotropic glutamate receptor antagonists NBQX (AMPAR/KAR, 10 μM) and (R)-CPP (NMDAR, 20 μM) (red trace). **Cii:** Quantification of the effect of combined ionotropic glutamate receptor antagonists (NBQX +(R)-CPP, "N+C") on the ON and OFF L-IPSCs. (R)-CPP +NBQX significantly reduced both the ON and OFF components of the red light (λ=660 nm, 500 ms, I=$2.02*10^{12}$ photons*cm^{-2}*s^{-1}) evoked the L-IPSCs charge (*$p<0.05$, paired Student's t-test). **D:** Summary diagram of normalized effects of pharmacological agents affecting retinal glutamatergic signaling on light-evoked L-IPSCs. Data are presented as mean± SE.
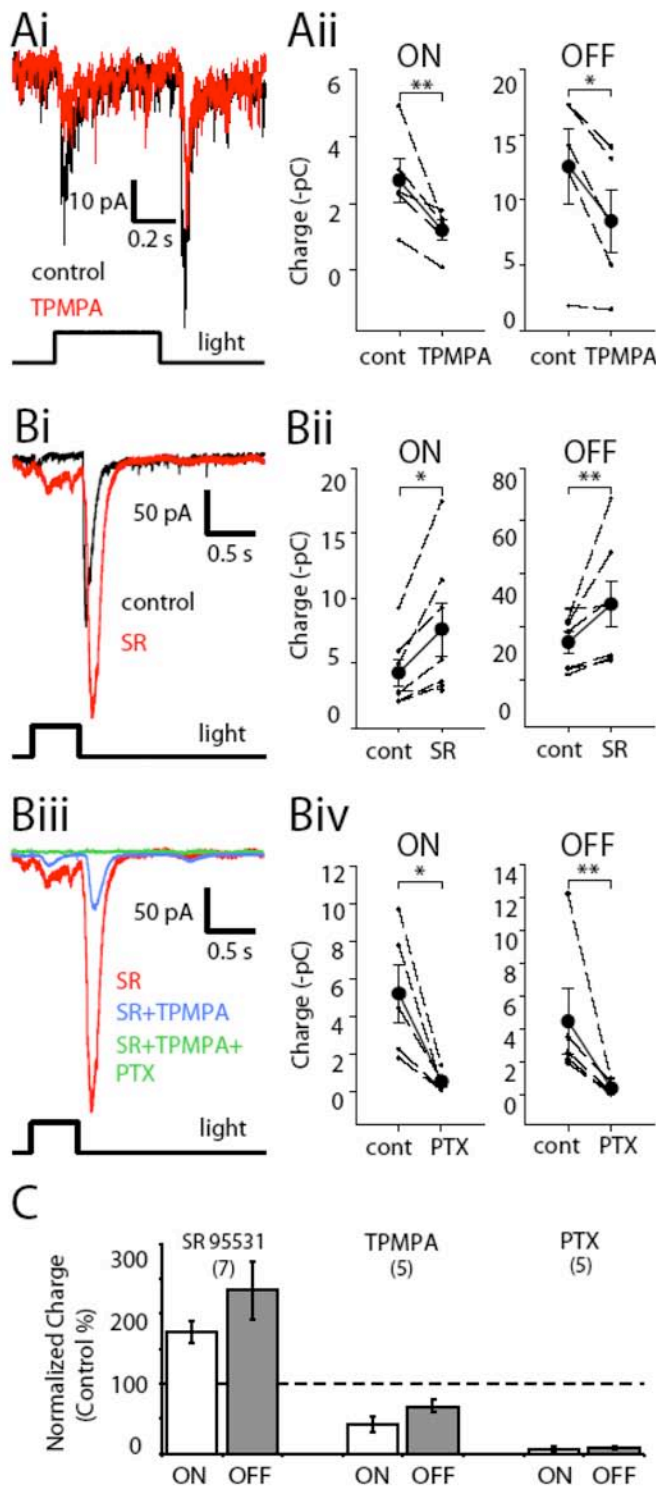
Figure 1.3. Light-evoked lateral feedback at Mb bipolar terminals is GABAergic. Ai: Both the ON and the OFF portions of the light-evoked (λ=505 nm, I=1.95x10^{12} photons cm^{-2}s^{-1}, 500 ms) L-IPSCs were inhibited by the GABA$_C$R antagonist TPMPA (150 μM, red trace). Average traces are shown for each condition (n=5). **Aii:** Quantification of the effect of TPMPA on ON and OFF charge transfer of L-IPSCs. Means are shown as filled circles connected with solid black lines. Error bars represent ± SE. TPMPA significantly reduced the charge of both ON and OFF L-IPSCs (*p<0.05, **p<0.02, paired Student's t-test, two-tailed). **Bi:** SR95531 (25 μM, SR, red trace) a GABA$_A$R antagonist markedly increased L-IPSCs, indicating that ACs providing GABAergic feedback to Mb terminals receive serial inhibition via GABA$_A$ receptors. **Bii:** Quantification of the effect of SR95531 on ON and OFF charge transfer of L-IPSCs. SR95531 significantly increased the charge of both ON and OFF L-IPSCs

43

(*p<0.05, **p<0.02, paired Student's t-test, two-tailed). **Biii:** Same cell as in **Bi**; traces obtained by consecutive treatments are divided into two panels for increased visibility. The SR95531‑elevated L‑IPSCs (SR, red trace) were reduced by TPMPA (here 300 μM shown, blue trace), but not eliminated completely. Complete LIPSC block of SR95531‑elevated L‑IPSCs could be achieved upon addition of PTX (100 μM, green trace). **Biv:** Quantification of PTX effect on the ON and OFF charge transfer of L‑IPSCs. PTX significantly decreased the charge of both ON and OFF L‑IPSCs (*p<0.05, **p<0.02, paired Student's t-test, two-tailed). **C:** Summary diagram of normalized GABAergic drug effects on light-evoked L‑IPSCs. Data are presented as mean ± SE.
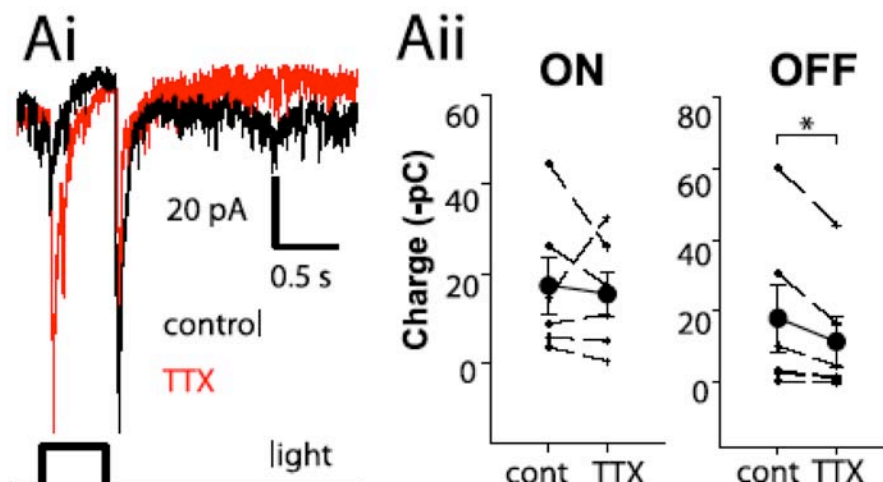
Figure 1.4. The propagation of GABAergic lateral feedback signals targeting Mb bipolar terminals involves TTX-sensitive mechanisms. Ai: Both the ON and OFF portions of the light-evoked (λ=505 nm, I=1.95x10^{12} photons cm^{-2}s^{-1}, 500 ms) L-IPSCs are affected by TTX, albeit differently. The example shown here depicts a cell in which the ON L-IPSCs were increased, whereas the OFF L-IPSCs were suppressed by TTX (2 μM, red trace). Average traces are shown for each conditions (n=5). **Aii:** Quantification of the TTX effect on the ON and OFF L-IPSC charge transfer (n=6). TTX significantly reduced OFF L-IPSCs charge (*$p < 0.03$, paired Student's t-test), but the effect of TTX on ON L-IPSCs was not significant ($p < 0.72$, paired Student's t-test). Note that TTX reduced ON L-IPSCs in 3/6 cells tested, and increased ON L-IPSCs in the other 3/6.
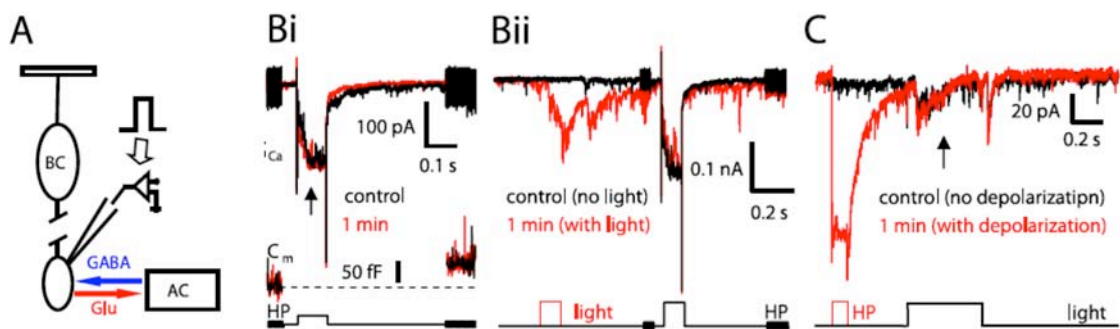
Figure 1.5. GABAergic lateral and reciprocal feedback at Mb axon terminals are mediated by separate populations of ACs. A: Diagram depicting exclusive triggering of reciprocal feedback by direct step depolarization of an axotomized Mb terminal. **Bi:** Depolarization of an axotomized Mb terminal from the holding potential (HP) of -60 to 0 mV for 100 ms activated calcium influx through voltage-gated calcium channels (I_{Ca}), which triggered glutamate release, as evidenced by a jump in ΔC_m. The protocol used is shown in the bottom trace. The fast voltage sinewave used to measure C_m was not delivered during the depolarization. The inhibitory feedback to the presynaptic terminal is expressed as a flurry of outward IPSCs superimposed on I_{Ca} (arrow). Experiments were performed in the presence of LY367385 (100 μM) to block mGluR1-dependent potentiation of reciprocal feedback. Under these conditions, consecutive depolarizations of the presynaptic terminal 1 min apart produced reciprocal feedback with similar magnitudes. There was no evidence of short-term depression (red trace). The resting C_m for this terminal was 5.5 pF. **Bii:** Same cell as in **Bi**. A light stimulus was applied (λ=505 nm, I=1.95x10^{12} photons cm^{-2}s^{-1}, 100 ms) to evoke pure lateral feedback between two reciprocal feedback steps (1 min apart), such that the light-evoked L-IPSCs preceded the second presynaptic depolarizations by 500 ms. However, the amplitude of reciprocal feedback did not decrease. **C,** The reverse of the experiment depicted in **Bii**.

46

Consecutive, bright white light-evoked (I=7.32*10^{13} photons*cm^{-2}*s^{-1}) L-IPSCs were

triggered 1 min apart, but a 100 ms depolarization from -60 to 0 mV was delivered to the

Mb terminal 300 ms before the second light pulse (red trace). No differences in the light-

evoked L-IPSCs were noted.
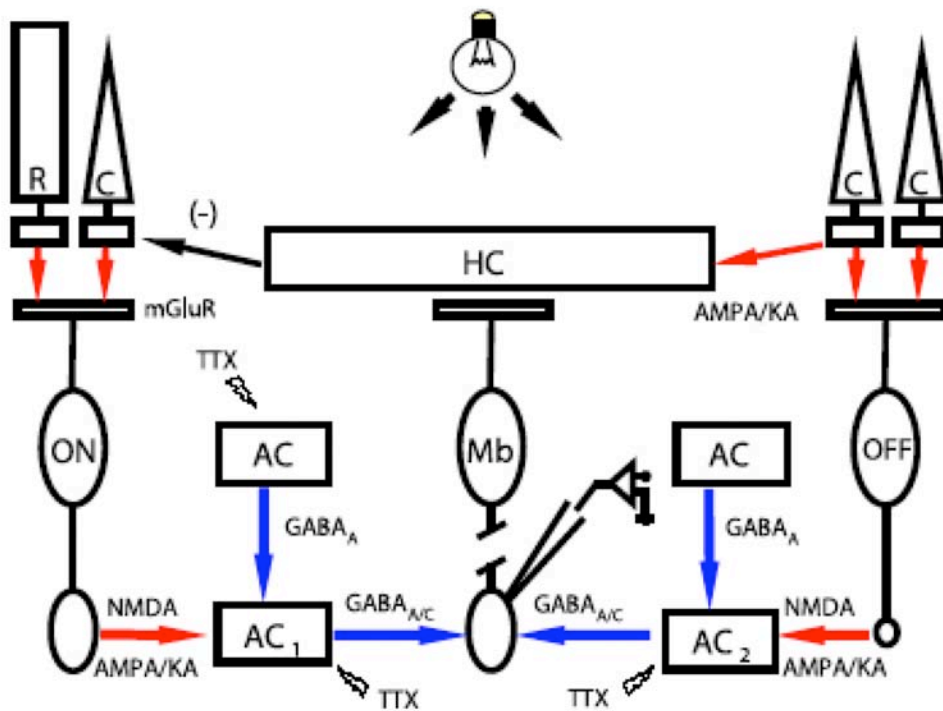
Figure 1.6. A proposed model for circuitry mediating lateral feedback to the Mb bipolar axon terminal. Light-evoked L-IPSCs in Mb terminals are triggered by at least two distinct retinal circuits, providing inhibition of Mb glutamate release with very different temporal characteristics under scotopic and photopic light conditons. R, Rod; C, cone; RED arrow, glutamatergic synapse; BLUE arrow, GABAergic synapse.

Paired pulse plasticity in the strength and latency of light-evoked lateral inhibition to retinal bipolar cell terminals.

Evan Vickers[1], Mean-Hwan Kim[1], Jozsef Vigh[2], Henrique von Gersdorff [1]

[1]The Vollum Institute, Oregon Health & Science University, 3181 SW Sam Jackson Park Road, Portland, OR 97239

[2]Department of Biomedical Sciences, Colorado State University, Ft. Collins, CO 80523

E.V, J.V. and H.v.G designed research; E.V. and M.H.K. performed research; E.V., M.H.K., and H.v.G. analyzed data; E.V., M.H.K., and H.v.G. wrote the paper.

Abstract

Synapses in the inner plexiform layer of the retina undergo short-term plasticity (STP) that may mediate different forms of adaptation to regularities in light stimuli. Using patch-clamp recordings from axotomized goldfish Mb bipolar cell (BC) terminals with paired-pulse light stimulation, we isolated and quantified STP of the size and timing of GABAergic lateral inhibitory postsynaptic currents (L-IPSCs). Bright light-evoked ON and OFF L-IPSCs in axotomized BCs had different onset latencies (~50-80 ms and ~70-150 ms, respectively) that depended on light adaptation state and were increased by block of $GABA_A Rs$ (ON and OFF responses) or voltage-gated Na^+ channels (OFF responses only). With paired light stimulation, latencies of ON L-IPSCs increased at paired-pulse intervals (PPIs) of 50 and 300 ms, while OFF L-IPSC latencies decreased at the 300 ms PPI. ON L-IPSCs showed paired-pulse depression at intervals < 1 s, while OFF L-IPSCs showed depression at intervals < 1 s and amplitude facilitation at longer intervals (1-2 s). This biphasic form of STP of L-IPSCs may underlie adaptation and sensitization to surround temporal contrast over multiple timescales. Block of retinal signaling at $GABA_A Rs$ and AMPARs differentially transformed STP of ON and OFF L-IPSCs, confirming that these two types of feedback inhibition are mediated by distinct and convergent retinal pathways with different mechanisms of plasticity. We propose that STP of strength and timing of L-IPSCs determines their ability to dynamically shape glutamate release from ON-type BC terminals to third-order retinal neurons, which may influence the strength of amacrine and ganglion cell inhibitory surrounds.

Introduction

Inhibitory networks in the inner plexiform layer (IPL) of the retina, consisting of amacrine cell (AC) inputs to BC presynaptic terminals, serial synapses between AC dendrites, and direct inputs to ganglion cell (GC) dendrites, perform computations that shape GC output to the brain. For example, these inputs mediate spatial integration and refine GC center-surround receptive fields (Cook and McReynolds, 1998; Jacobs and Werblin, 1998; Ichinose and Lukasiewicz, 2005) and GC orientation selectivity (Venkataramani and Taylor, 2010). The goldfish Mb BC, a counterpart of the mammalian rod BC (RBC) (Joselevitch and Kamermans, 2009), depolarizes in response to light stimulation (Wong et al., 2005) and has a large (~10 μm) synaptic terminal that stratifies in sublamina b (ON layer) of the IPL (Witkovsky and Dowling, 1969). It is thus possible to patch-clamp the Mb BC terminal in retinal slice preparations (Palmer et al., 2003), which makes it an excellent model for the study of inhibitory processing in the IPL.

Each Mb terminal makes ~50 synapses with GC dendrites, and ~300 synapses with AC boutons, of which ~50% are reciprocal and ~50% are lateral (Marc and Liu, 2000). Reciprocal synapses use AMPA and NMDA receptors on the AC, and $GABA_AR$ and $GABA_CR$ synapses on the Mb (Vigh and von Gersdorff, 2005), and lateral synapses exhibit unidirectional release in either direction (Marc and Liu, 2000). Several studies provide evidence that lateral and reciprocal synapses are spatially and functionally distinct (Fig 1.5; Marc and Liu, 2000; Vigh et al., 2011). Immunohistochemical (Koulen et al., 1998) and electrophysiological (Palmer, 2006) evidence suggests that $GABA_A$ and $GABA_C$ receptors are present at separate synapses. We have recently shown that light-evoked L-IPSCs at the Mb terminal consist of $GABA_A$ and $GABA_C$ currents, which arise from pathway-specific ON or crossover OFF inputs (Fig 1.1; Vigh et al., 2011).

Short-term depression (STD) of reciprocal inhibition at AC ➔ BC synapses is thought to modulate BC responses during high frequency light stimulation (Li et al., 2007), and has been shown to prevent STD at excitatory ON cone BC ➔ GC synapses in the mouse (Sagdullaev et al., 2011). However, light evoked STP of L-IPSCs at the Mb terminal has not been previously explored. STP of L-IPSCs likely acts to adjust the strength and spatial extent of post-synaptic AC and GC inhibitory surrounds by regulating Mb bipolar cell glutamate release during feedforward subthreshold depolarization (Joselevitch and Kamermans, 2007), and the ability of the Mb terminal to initiate regenerative Ca^{2+} action potentials (Zenisek and Matthews, 1998; Protti et al., 2000; Arai et al., 2010; Baden et al., 2011). Here, we recorded directly from axotomized Mb terminals, which allowed us to quantify L-IPSCs in the absence of reciprocal feedback, and stimulated with pairs of full-field light flashes to characterize STP of L-IPSCs. We found that STP differed for ON and OFF responses, and was altered differentially by blockage of $GABA_A$ and AMPA receptor signaling. Such dynamic regulation of lateral inhibition at the Mb bipolar cell terminal likely mediates rapid surround modulation and adaptation of GC and AC responses.

Materials and Methods

Retinal slice preparation and electrophysiology. Slices were prepared from pieces of

goldfish (*Carassius auratus*; 8-14 cm) retina, as described previously (Palmer et al.,

2003). For experiments in which paired recordings of ACs and Mb BC terminals were

performed, the goldfish retina was gently removed from the eyecup, embedded in low

gelling-temperature agar (3% w/v in slice solution; Agarose type VII-A, A-0701, Sigma-

Aldrich), as described in Kim et al., 2012. For all experiments, goldfish, of either sex,

were dark adapted for 1-2 hrs prior to dissection, and slicing solution contained the

following (in mM): 119.0 NaCl, 2.5 KCl, 3.2 $MgCl_2$, 0.3 $CaCl_2$, 12.0 glucose, 12.0

HEPES, and 0.2 ascorbic acid. The pH was set to 7.45 with NaOH, and osmolarity was

set to 260 – 265 mOsm. Dissection was performed under either dark or dim red light

conditions, and recording was performed under either mesopic ($1.01 \times 10^3 – 5.03 \times 10^3$

photons $\mu m^{-2} s^{-1}$) or scotopic (5.03×10^1 photons $\mu m^{-2} s^{-1}$) background conditions (Krizaj,

2000). Background light levels were measured with an ILT-1700 photometer and SE033

detector from International Light Technologies (Peabody, Massachusetts). Transverse

slices (250 μm thick) were cut with a Narishige ST-20 vertical slicer and transferred to a

Sylgard (Dow Corning, Midland, MI) recording chamber, where they were secured in

parallel lanes of petroleum jelly. For paired recordings, a diced agar block containing the

retina was cut into 200 μm thick slices using a Vibratome slicer (VT1000, Leica). The

chamber and slices were then moved to an upright microscope (Zeiss Axioskop;

Oberkochen, Germany), where the slices were constantly perfused with external

recording solution bubbled with 95% O_2 and 5% CO_2 mixed gas at 4-5 ml/min, and

viewed with infrared differential interference contrast (IR-DIC) optics through a 40x

water-immersion objective (Zeiss) coupled with 2.0 pre-magnification and an IR CCD

camera (XC-75, Sony). The output of the CCD camera was sent to a Hamamatsu

Camera Controller C2741-62, and then to a 13" Sony B/W monitor for viewing.

Axotomized bipolar cell terminals (i.e. with severed axons) were identified in the inner

plexiform layer (IPL) based on: (1) Mb-shaped (bulbous) terminal morphology (Fig 2.1A),

(2) single-exponential membrane time constant (not shown), and (3) the presence of an

L-type Ca^{2+} current, reciprocal feedback, and ΔC_m jump (Fig 2.1B) (Palmer et al., 2003)

associated with exocytosis (von Gersdorff and Matthews, 1999).

Axotomized bipolar cell terminals in retinal slices were voltage clamped at -60 or

-70 mV (uncorrected for liquid junction potential) in the whole-cell mode using a HEKA

Elektronik (Lambrecht/Pfalz, Germany) EPC-9 patch-clamp amplifier in conjunction with

Pulse software running the xChart extension (Pulse version 8.53). The Sine+DC

technique (Gillis, 2000) was used for real-time measurements of membrane

capacitance. Briefly, a 30 mV peak-to-peak, 1-2 kHz sine wave was superimposed on

the holding potential of the cells (-60 mV) and used by on-line analysis software to

calculate time-resolved membrane capacitance. Standard external recording solutions

contained (in mM) 100.0 NaCl, 2.5 KCl, 2.5 $CaCl_2$, 1.0 $MgCl_2$, 25.0 $NaHCO_3$, 0.2

ascorbic acid, and 12.0 glucose (pH 7.45; osmolarity, 260–265 mOsm). Patch pipettes

(6-12 MΩ) were pulled, with either a vertical (Narishige, PP-830) or horizontal (Sutter

Instruments, P-97) puller, from thick-walled, 1.5 mm outer diameter borosilicate capillary

glass from World Precision Instruments (1B150F-4; Sarasota, FL), and coated with

dental wax (Cavex, West Chester, PA) to reduce pipette capacitance. Internal pipette

solutions contained the following solutions (in mM): 60.0 Cs gluconate, 40.0 CsCl, 10.0

TEA-Cl, 25.0 HEPES, 3.0 Mg-ATP, 0.5 Na-GTP, and 2.0 EGTA. Internal solutions for

paired recordings contained 28.0 HEPES and 1.0 Na-GTP, but were otherwise the

same. Some internal solutions contained 3.0 mM ascorbic acid and/or 3.0 mM reduced

glutathione. All internals were set to pH 7.2 with CsOH, and osmolarity was adjusted to

250 mOsm with Cs gluconate and/or millipure H_2O. NBQX, TTX, TPMPA and gabazine

(SR95531) were obtained from Tocris (Bristol, UK). All other chemicals were obtained from Sigma (St. Louis, MO).

As in Vigh et al., 2011, recordings were performed at 20-22º C during the daytime (morning/afternoon) to avoid circadian variation in glutamate release from bipolar cells (Hull et al., 2006b). Voltage-clamp series resistance (R_s) was not compensated, and liquid junction potential was not corrected. Cells with R_s > 30 MΩ or |leak| > 50 pA at a holding potential of -60 mV were excluded from analysis. Average values for Rs and leak current at a holding potential of -60 mV were 22.0 ± 1.2 MΩ and -34.2 ± 2.6 pA, respectively (mean ± SE; n=75).

Light Stimulation. Slices were stimulated with a white LED connected via soldered wire and BNC cable to a digital-to-analog output of the HEKA EPC-9 amplifier, as described previously (Vigh et al., 2011). The LED was positioned at a ~30º angle above and behind the recording chamber, at a distance of 3 cm. Full field light flashes for all experiments were delivered by application of voltage steps from 0 to between 3 and 5 V, which evoked a photon flux at the slice of between 5.69 X 10^4 and 7.32 X 10^5 photons μm^{-2} s^{-1} (unless otherwise noted), which is above the threshold for cone photoreceptor activation (~10^2 photons μm^{-2} s^{-1}; Busskamp et al., 2010). The timing and amplitude of voltage steps was controlled from within the Pulse Software (HEKA Elektronik) running the EPC-9 amplifier. Calibration of light flash timing (onset and offset) was performed with a photodiode connected to the EPC-9 amplifier through an ITHACO 4302 dual 24 dB Octave Filter. Light flash onset and offset had rise and decay time constants of 0.12 and 6.3 ms, respectively. Onset and offset times did not vary as a function of flash duration between 100 and 1000 ms, or with the presentation of paired flashes with intervals ranging between 300 and 1900 ms. Calibration of light intensity was performed with an ILT-1700 photometer and SE033 detector from International Light Technologies

(Peabody, MA). Factory calibration determined the photopic illuminance response sensitivity of the detector to be 2.60 x 10^{-8} A ft^2 lm^{-1}, or 2.415 x 10^{-9} A lux^{-1}, assuming 3215 K color temperature.

Analysis of amplitude, charge and onset latency of L-IPSCs. Light responses at each paired pulse interval (PPI) were repeated at least five times per cell and averaged, unless otherwise stated. An interval of 20 or 30 s was presented between stimulations to allow for recovery from depression in neighboring Mb presynaptic terminals (von Gersdorff and Matthews, 1997), and stimulation with PPIs ranging from 50 – 2300 ms were interleaved to avoid systematic errors due to rundown of the light responses, which were generally stable during recordings of up to 30 minutes. For PPIs shorter than 300 ms, alternating single and double flashes were presented so that single responses could be subtracted from double responses. This allowed for isolation of the first OFF response and second ON response so that amplitude, charge transfer, and onset latencies could be reliably measured at short intervals (i.e. 50 ms). L-IPSC amplitude was calculated by subtracting a baseline ON and OFF current (first 20 ms following onset and offset of light flash, respectively) from the peak current amplitude during the 400 ms light flash and the 300 ms following the offset of the light flash for ON and OFF responses, respectively. Charge transfer was calculated by integrating current traces during these ON (400 ms) and OFF (300 ms) response windows following baseline subtraction.

L-IPSC onset latencies were determined using a custom IGOR procedure that detected the time at which the L-IPSC crossed a threshold current set at baseline minus 2 standard deviations (SD), where the baseline and SD were calculated from the 20 ms period at the beginning of either the ON or OFF response windows. The threshold crossing was determined by moving backwards in time from the peak of the L-IPSC,

which was detected as the global minima of the current recording during the response window. Due to the uncertainty introduced to these measurements by the possibility of small, asynchronous events, latency outliers that exceeded the population mean by more than 10 SD were excluded from further analysis. Latencies calculated with a similar technique where the threshold was set at 10% of the difference between baseline and peak current were not significantly different from those calculated with the 2 SD criteria. Manual, "by eye" detection of latencies also yielded comparable results, but showed significant ($p<0.01$) underestimation of paired Δ onset latency compared to the 2 SD criteria for ON L-IPSCs at the 300 ms PPI, and compared to the 10% baseline to peak criteria at the 50 ms PPI. None of the three techniques showed significant differences for OFF L-IPSC latencies at either the 50 or 300 ms PPIs ($p>0.05$). We report latencies using the 2 SD criteria throughout the paper, as this technique minimized discrepancies with the other two techniques.

Immunohistochemistry and Confocal Imaging. During paired patch-clamp recording, the Mb cell and AC were filled via the patch pipette with Alexa 555 and 488 hydrazide, respectively (100-200 µM, Molecular Probes). Immediately following the recording, retinal slices were transferred into 4% (wt/vol) paraformaldehyde in phosphate buffer solution for 30 min. Slices were mounted onto Superfrost slides (Fisher Scientific) in aqueous mounting medium with GEL/MOUNT anti-fade solution (Biomeda corp, Foster City, CA). Alexa containing Mb BCs and ACs were viewed with laser lines at 488 and 555 nm using a 40x water-immersion objective on a confocal laser-scanning microscope (LSM 710, Carl Zeiss). Stacked confocal images were reconstructed with Imaris software (Bitplane Scientific Software).

DIC/Epifluorescence Overlays. During some recordings of single axotomized Mb terminals, the internal solution contained 150-200 µM Alexa 555 hydrazide. DIC montage images were recorded in iMovie (Apple) by connecting the Hamamatsu Camera Controller to a MacBook Pro (Apple) via a Dazzle Hollywood DV-Bridge frame-grabber. Epifluorescence imaging was performed post-recording by illumination of the preparation with an AttoArc HBO 100 W mercury lamp (Zeiss). A filter cube matching the emission range of Alexa 555 was placed between the objective and the CCD camera. Fluorescence images were also acquired with iMovie, and were later aligned with DIC montages using ImageJ (NIH) and Photoshop (Adobe).

Statistical Analysis. Statistics were performed on averaged traces, unless otherwise noted, by using Prism (version 4; GraphPad Software, San Diego, CA). Two-tailed paired or unpaired Student's t-tests were used to compare data sets where appropriate, and one-sample t-tests with a hypothetical mean of 0 or 1 were used to test paired-pulse plasticity of onset latency or size, respectively, at each PPI. Data are reported as mean ± SEM, and values of $p < 0.05$ were considered statistically significant.

Results

Isolation of light-evoked GABAergic ON and OFF L-IPSCs at the Mb BC terminal

In order to examine the synaptic properties of light-evoked lateral inhibition, we performed direct whole-cell voltage-clamp recordings of axtomized goldfish Mb bipolar cell terminals (Fig 2.1A and 2.1B). By recording with intracellular solution containing 40 mM CsCl and 10 mM TEA-Cl (E_{Cl} = -20.1 mV) and voltage clamping the axotomized terminal at -60 or -70 mV, we were able to evoke large inward L-IPSCs by stimulating the retinal slice with full-field, 400 ms duration, white light flashes (between 5.69 X 10^4

58

and 7.32 X 10^5 photons μm^{-2} s^{-1}, unless otherwise noted; see Materials and Methods)

under scotopic background conditions (5.03 x 10^1 photons μm^{-2} s^{-1}; Fig 2.1C). We refer

to these events as L-IPSCs because they are expected to be inhibitory under

physiological conditions, with an estimated E_{Cl} of -60 mV and resting membrane

potential (E_m) between -40 and -45 mV (Protti et al., 2000; Baden et al., 2011). The

control light response (Fig 2.1C, black trace) consisted of distinct fast ON (~50 ms

latency) and slow OFF L-IPSCs (~100 ms latency), which could both be blocked

completely by bath application of 25 μM SR-95531 and 150 μM TPMPA (Fig 2.1C, red

trace). Similar results were obtained with 12.5 µM SR95531 (not shown), a concentration

less likely to produce significant non-specific block of glycine receptors (GlyRs; Wang

and Slaughter, 2005). This block was reversible upon washout (Fig 2.1C, blue trace).

This result confirms our previous findings that both ON and OFF L-IPSCs at the Mb

terminal consist entirely of $GABA_A$ and $GABA_C$ receptor mediated responses, and are

not mediated by GlyRs (i.e. not blocked by 1 µM strychnine; Vigh et al., 2011).

In Figure 2.1D, we show a schematic of the patterns of connectivity that are likely

responsible for propagation of ON and crossover OFF lateral inhibition from the

dendrites of neighboring or distant ON and OFF BCs to the Mb terminal. ON lateral

inhibition is driven by mixed rod and cone inputs (Fig 1.1; Vigh et al., 2011), and arrives

via a direct trisynaptic pathway via neighboring ON BCs and ON ACs. However, OFF

lateral inhibition is primarily driven by cone inputs (Fig 1.1; Vigh et al., 2011), and travels

via either a direct trisynaptic pathway or an indirect, disinhibitory multisynaptic pathway

(Fig 2.1D). The direct pathway likely consists of an input from an OFF BC to an OFF AC

that forms synaptic contacts onto the Mb axon terminal, or an input from an OFF BC to a

bistratified or diffuse AC that makes synaptic contacts directly onto the Mb terminal. The

indirect OFF pathway could arise from an OFF BC via contacts onto an OFF AC that

then contacts either an ON, diffuse, or bistratified AC that makes direct synaptic contacts

onto the Mb terminal. These indirect pathways, or nested loops of serial AC ➔ AC

GABA$_A$ synapses (Fig 2.1D, dashed lines), are likely bidirectional between ON and OFF

AC pathways (Marc and Liu, 2000; Hsueh et al., 2008), and have been shown to

regulate the strength of BC inhibitory surround (Eggers and Lukasiewicz, 2010).

ON and OFF L-IPSCs exhibit different temporal profiles of STP

In order to determine the likely effects of dynamic surround stimulation on the size and

timing of lateral feedback inhibition at the Mb terminal, we tested STP of L-IPSCs over

the paired-pulse interval (PPI) range of 50-2300 ms. Here, PPI refers to the interval

between the offset of the first light flash and the onset of the second light flash. Short

PPIs (example: 300 ms, Fig 2.2Ai) tended to produce STD of ON and OFF L-IPSC

amplitude (~20%) and charge (~15%), while long PPIs (example: 1900 ms, Fig 2.2Bi)

tended to produce STD of ON L-IPSC amplitude and charge (10-15%) and short-term

facilitation (STF) of OFF L-IPSC amplitude (~25%). Subtraction of the first light response

(both ON and OFF components; windowed from t = 0 ms at light onset to t=700 ms at

termination of OFF response; ON response ends at t = 400 ms, OFF response begins at

t = 400 ms) from the second light response of the pair yielded difference traces that

showed clear STD of ON and OFF L-IPSCs at a PPI of 300 ms (Fig 2.2Aii; same cell as

2.2Ai, onset latencies shown in purple), and a combination of ON STD and OFF STF at

a PPI of 1900 ms (Fig 2.2Bii; same cell as 2.2Bi, onset latencies indicated in purple).

Note that, for the 300 ms interval, ON STD in the difference trace is seen as a positive

deflection relative to a baseline with an initial negative offset due to incomplete decay of

the first OFF L-IPSC (Fig 2.2Aii). For this reason, STP at the 50 ms PPI was determined

with a protocol of alternating single and double light flashes. This allowed for the

isolation of first and second ON and OFF L-IPSCs by subtraction of the single response

from the double response (see Materials and Methods).

ON and OFF L-IPSCs showed different temporal profiles of amplitude (Fig 2.3A) and charge transfer STP (Fig 2.3B). STP of both amplitude and charge transfer were quantified as paired pulse ratios (PPRs), and STD or STF were defined as PPRs that were less than or more than 1, respectively (green asterisks, Fig 2.3). In addition, we performed direct statistical comparisons between ON and OFF PPRs at each PPI (purple asterisks, Fig 2.3). ON L-IPSC amplitude STD was highly statistically significant at PPIs of 50 ms (PPR = 0.57 ± 0.05; n = 14; p<0.001, one-sample t-test) and 300 ms (0.78 ± 0.06; n = 34; p<0.001) recovered at 1100 ms (p>0.05), and showed small but significant STD at 1900 ms (0.87 ± 0.04; n=39; p<0.01) that recovered by 2300 ms. In contrast, OFF amplitude STD was sometimes strong at a PPI of 50 ms, although high variability at this short PPI prevented the STD from reaching statistical significance (PPR = 0.94 ± 0.16; n = 6; p>0.05). OFF STD was present at 300 ms (0.82 ± 0.07; n=32; p<0.05), but was replaced by STF at 1100 ms (1.21 ± 0.10; n=32; p<0.05) that continued at 1900 ms (1.26 ± 0.09; n=37; p<0.01) before recovery at 2300 ms. ON L-IPSCs were significantly depressed relative to OFF L-IPSCs at PPIs of 50 ms (Δ PPR = -39.4%; p<0.01) and 1900 ms (Δ PPR = -30.6%; p<0.001, unpaired Student's t-test, two tailed). These differences in the STP profiles of ON and OFF L-IPSC amplitude likely allow them act as independent temporal filters on the early and late phases of light responses at Mb terminals. When taken together, they suggest a mechanism for regulation of the balance between surround temporal contrast adaptation (i.e. OFF STF) and sensitization (i.e. ON and OFF STD) at Mb ➜ GC and Mb ➜ AC inputs. This balance is likely adaptive during rapid transitions between visual environments containing high and low contrast (Kastner and Baccus, 2011).

Next, we analyzed the total integrated charge transfer of baseline subtracted ON and OFF L-IPSCs (Fig 2.3B). ON L-IPSC charge transfer exhibited strong STD at a PPI

of 50 ms (PPR = 0.39 ± 0.08; n=14; p>0.001, one-sample t-test). This STD recovered at

300 ms, and small but significant STD re-emerged at PPIs of 1100 ms (0.78 ± 0.08;

n=34; p<0.05) and 1900 ms (0.79 ± 0.06; n=39; p<0.01). ON STD was not significant at

2300 ms. OFF charge transfer STP (Fig 2.3B) followed a time course of recovery from

STD that was similar to that of the ON response, with strong STD at 50 ms (PPR = 0.47

± 0.20; n=6; p<0.05), recovery at 300 ms, moderate STD at 1100 ms (0.78 ± 0.06; n=32;

p<0.001), and recovery at 1900 and 2300 ms PPIs. Similarly to the result for amplitude

PPR, ON L-IPSCs were significantly depressed relative to OFF L-IPSCs at the 1900 ms

PPI (Δ PPR = -24.9%; p<0.05, unpaired Student's t-test, two tailed).

ON and OFF L-IPSCs exhibit differential onset latency STP

Interestingly, ON and OFF L-IPSCs also exhibited distinct STP of onset latency (Fig 2.4).

Such changes in the timing of presynaptic lateral inhibition may strongly determine the

degree to which L-IPSCs inhibit or shunt light-evoked EPSPs (Oltedal et al., 2009) or

Ca^{2+} action potentials (Protti et al., 2000; Hull et al., 2006a) at the Mb BC terminal,

whether ACs act to either inhibit or disinhibit GC spiking (Manu and Baccus, 2011), and

whether L-IPSCs primarily shape BC representations of either temporal contrast or

mean luminance (Oesch and Diamond, 2011). In order to quantify this effect, we

identified ON and OFF L-IPSC onset latencies as the crossing point of a threshold

defined as baseline current minus two standard deviations of the baseline, working

backward from the peak of the L-IPSC toward the beginning of the response window

(see Methods, vertical dotted lines in Fig 2.4Ai, 2.4Aii).

We found that ON and OFF L-IPSCs exhibited different forms of onset latency

plasticity. ON L-IPSCs showed a strong paired-pulse delay (i.e. increase) in onset

latency (Fig 2.4Ai, 2.4Bi; blue) at PPIs of 50 ms (Δ onset latency = +75.0 ± 28.3 ms; n=9;

p<0.05, one-sample t-test, green asterisks) and 300 ms (+34.0 ± 11.3 ms; n=34; p<0.01). These effects were large relative to mean onset latency of the first L-IPSCs of each pair (50 ms PPI: +96 ± 38.6%; 300 ms PPI: +60.2 ± 18.3%; Fig 2.4Bii). ON onset latency STP was not significant at PPIs of 1100 and 1900 ms (not shown). This delay of ON L-IPSCs at short PPIs may be caused by depletion of the readily releasable vesicle pool at ON BC ribbon synapses (von Gersdorff and Matthews, 1997), which would result in a strong reduction of the initial, fast component of glutamate release onto AC dendrites.

OFF L-IPSCs, in marked contrast to ON L-IPSCs, showed paired-pulse advances (i.e. decreases) in onset latency at short PPIs. OFF onset latency (300 ms PPI example, Fig 2.4Aii) showed a significant advance at the 300 ms PPI (Δ onset latency = -29.8 ± 10.1 ms; n=31; p<0.01, one-sample t-test; Fig 2.4Bi, red). There was no significant onset latency STP of OFF L-IPSCs at the 50 ms PPI (+5.4 ± 3.2 ms; n=5; p>0.05), or at the 1100 and 1900 ms PPIs (not shown). When normalized to first L-IPSC latencies, OFF Δ onset latency was relatively modest (50 ms PPI: +5.0 ± 3.8%; 300 ms PPI: -13.9 ± 5.8%; Fig 2.4Bii). Importantly, OFF Δ onset latency was significantly different from ON Δ onset latency at both the 50 ms (ON - OFF Δ onset latency = +63.8 ± 15.2 ms; p<0.0001, unpaired Student's t-test, two tailed; Fig 2.4Bi, purple asterisks) and 300 ms PPIs (ON - OFF Δ onset latency = +69.5 ± 28.5 ms; p<0.05). There was no significant difference in Δ onset latency between scotopic (Fig 2.4Bi, open circles) or mesopic (Fig 2.4Bi, filled circles) background conditions at the 300 ms PPI for ON L-IPSCs (scotopic: +44.6 ± 27.1 ms, n=11; mesopic: +28.9 ± 10.9 ms, n=23; p=0.52, unpaired Student's t-test, two tailed), although there was a non-significant trend toward larger Δ onset latencies for OFF L-IPSCs under mesopic background (scotopic: +4.6 ± 27.1 ms, n=5; mesopic: -36.5 ± 11.0 ms, n=26; p=0.14).

ON and OFF L-IPSC size and timing differentially adapt to background light

Feedforward light responses in the intact Mb terminal consist either of analog EPSPs with an onset latency of ~30 to 50 ms under mesopic background conditions (Wong et al., 2005), or a combination of EPSPs and Ca^{2+} action potentials with onset latencies ranging from ~50 to 100 ms (Joselevitch and Kamermans, 2007) or ~75 to 90 ms (Protti et al., 2000; Baden et al. 2011) under scotopic background conditions, respectively. Therefore, functional interpretation of ON and OFF L-IPSC size and latency STP requires examination of the degree to which the absolute size and latency of single responses adapts to background light. Furthermore, the degree to which ON and OFF L-IPSCs overlap or act independently at the Mb terminal during exposure to naturalistic visual stimuli will depend on the difference between their onset latencies under different background illumination. In order to test the sensitivity of L-IPSC amplitude and onset latency to light adaptation state, we varied background light intensity from scotopic (5.03 x 10^1 photons μm^{-2} s^{-1}) to mesopic (5.03 x 10^3 photons $\mu m^{-2}s^{-1}$) levels (Fig 2.5).

Mixed rod/cone mediated ON L-IPSCs (Fig 1.1; Vigh et al., 2011) were expected to show delayed (i.e. increased) onset latencies when background light was shifted from mesopic to scotopic levels (Fig 2.5A), due to an increased relative contribution of slow rod inputs via mGluR6 (Wong et al., 2005). In addition, ON L-IPSCs were expected to increase in amplitude under scotopic background conditions, due to increased recruitment of rod inputs (Vigh et al., 2011; Wong et al., 2005), and decreases in both L-type Ca^{2+} channel inactivation and steady-state depletion of the readily releasable vesicle pool (Jarsky et al., 2011; Oesch and Diamond, 2011) in neighboring Mb terminals. Cone dominant OFF L-IPSCs were also expected to increase in amplitude under scotopic background, due to dopamine-mediated enhancement of voltage-gated Na^+ channel conductances in cone BCs (Zenisek et al., 2001; Ichinose and Lukasiewicz, 2007).

64

Consistent with these expectations, the amplitudes of ON (scotopic background = 45.4 ± 6.5 pA, n=20; mesopic background = 29.6 ± 3.7 pA, n=20; p<0.05, unpaired Student's t-test, two tailed; Fig 2.2B, upper left) and OFF (scotopic background = 34.9 ± 5.5 pA, n=18; mesopic background = 20.52 ± 2.6 pA, n=18; p<0.05; Fig 2.5B, upper right) L-IPSCs under scotopic background were larger than under mesopic background. These changes in L-IPSC amplitude were not due to significant dependence of $GABA_CR$ mediated standing leak current (Hull et al., 2006a) on background light (scotopic: -28.3 ± 3.0 pA, n=20; mesopic: -27.8 ± 3.1 pA, n=20; p=0.90, unpaired Student's t-test, two tailed). ON L-IPSC latency showed the expected delay (i.e. increase) following the transition to scotopic background (scotopic = 75.6 ± 7.4 ms, n=20; mesopic = 52.4 ± 2.6 ms, n=20; p<0.01; Fig 2.5B, bottom left). However, OFF L-IPSC latency surprisingly showed a significant advance (i.e. decrease; scotopic background = 68.7 ± 7.5 ms, n=18; mesopic background = 146.7 ± 12.3 ms, n=15; p<0.0001; Fig 2.5B, bottom right). This decreased latency of OFF L-IPSCs, which are driven primarily by the light responses of cone photoreceptors (Fig 1.1; Vigh et al., 2011), may have been due to acceleration of glutamate release from cone BC terminals caused by enhanced Na^+ channel amplification of cone BC responses under scotopic background (Ichinose and Lukasiewicz, 2007).

Although these experiments do not exclude the possibility that background light dependent changes in voltage-gated Na^+ channel amplification of OFF AC EPSPs, or effects on OFF AC action potentials, may have caused these changes in OFF L-IPSC latencies (Fig 1.4; Vigh et al., 2011). Interestingly, the advance of OFF L-IPSCs under scotopic background resulted in the elimination of significant differences in ON vs. OFF onset latency observed under mesopic background (mesopic: OFF – ON latency = +94.4 ± 12.0 ms, p<0.0001, unpaired Student's t-test, two tailed; scotopic: OFF – ON latency = -6.8 ± 10.8 ms, p>0.05). Thus, ON and OFF L-IPSCs evoked in response to naturalistic

stimuli containing rapid fluctuations in surround luminance would be expected to overlap

significantly under scotopic background, and to remain largely independent under

mesopic (or photopic) background light levels.

Contribution of feedback inhibition and serial inhibitory circuits to STP of ON and

OFF L-IPSCs

In order to explore the mechanisms that underlie differential STP of ON and OFF L-

IPSCs, we used a pharmacological approach to dissect the roles of circuits that mediate

HC ➜ PR feedback inhibition in the outer retina (Fahrenfort et al., 2005; Fahrenfort et

al., 2009), and AC➜AC serial inhibition in the inner retina (i.e. "nested loops," Fig 2.1D;

Zhang et al., 1997; Watanabe et al., 2000; Hsueh et al., 2008; Eggers and Lukasiewicz,

2010). Block of these circuits would be expected to increase the dynamic range of ON

and OFF BC voltage responses to light stimulation, and to disinhibit ACs that mediate

the direct pathway for L-IPSCs (Fig 2.1D), respectively. Thus, we hypothesized that

functional removal of these outer and inner retinal subcircuits would result in the

enhancement of vesicle depletion at AC (Li et al., 2007) and BC presynaptic terminals

(von Gersdorff and Matthews, 1997) at different locations in the trisynaptic circuits that

mediate ON and OFF L-IPSCs, and thus differentially shape light-evoked STD and STF.

First, we examined the effect of AMPAR blockade on STP of ON L-IPSC charge

transfer by bath applying 10 µM NBQX (Fig 2.6A, blue). We have previously shown that

ON L-IPSCs propagation at ON BC ➜ AC synapses can be mediated entirely by

NMDARs in the absence of AMPAR signaling, and that block of AMPARs both

eliminates OFF L-IPSCs and enhances ON L-IPSC charge transfer at the Mb terminal,

likely via block of HC ➜ PR feedback inhibition (Fig 1.2, 1.6; Vigh et al., 2011). Earlier

studies have demonstrated that this feedback is activated by PR release of glutamate

onto AMPA receptors on HCs in the dark, followed by HC depolarization and either pH

mediated or ephaptic inhibition of Ca^{2+} channels on PR terminals (Fahrenfort et al., 2005; Fahrenfort et al., 2009). Our examination of STP in the presence of NBQX (Fig 2.6C, left, blue) revealed that ON L-IPSCs exhibited strong STD of charge transfer at the 300 ms PPI (PPR = 0.19 ± 0.04; n=6; p<0.0001, one-sample t-test, green asterisks) that recovered at PPIs of 1100 and 1900 ms. STD in the presence of NBQX at the 300 ms PPI was significantly enhanced relative to control (p<0.0001, unpaired Student's t-test with Welch's correction; same control data as Fig 2.3B; purple asterisks).

Next, we tested the effects of blocking $GABA_A$Rs on ON and OFF STP over a range of PPIs from 50-1900 ms. Bath application of 25 μM SR95531 (SR), which blocks $GABA_A$Rs at reciprocal AC ➔ Mb (Vigh and von Gersdorff, 2005) and serial AC ➔ AC synapses (Dowling and Werblin, 1969; Zhang et al., 1997; Watanabe et al., 2000; Eggers and Lukasiewicz, 2010), caused a clear disinhibition of both ON and OFF L-IPSCs (Fig 2.6B; see also Fig 1.3; Vigh et al., 2011). In the presence of SR, ON STD was not significantly altered relative to control PPRs (Fig 2.6C, middle; same control data as Fig 2.3B). However, STP of OFF L-IPSC charge transfer (Fig 2.6C, right) and peak amplitude (not shown) were transformed in the presence of SR. STD of OFF charge transfer was significantly reduced relative to control at the 300 ms PPI (Control PPR = 0.87 ± 0.07, n=32; SR PPR = 1.20 ± 0.12, n=20; p<0.01, unpaired Student's t-test, two tailed), and STF of OFF peak amplitude was significantly reduced at PPIs of 1100 ms (Control PPR = 1.21 ± 0.10, n=32; SR PPR = 0.80 ± 0.10, n=18; p<0.01) and 1900 ms (Control PPR = 1.26 ± 0.09, n=37; SR PPR = 0.84 ± 0.06, n=18; p<0.01).

The contribution of $GABA_A$R desensitization to total STD was eliminated by bath application of SR, because $GABA_C$Rs do not exhibit desensitization (Matthews et al., 1994; Lukasiewicz et al., 2004). Therefore, these results are consistent with the idea that $GABA_A$R desensitization at lateral AC ➔ Mb synapses may contribute to OFF STD,

but not ON STD, at short PPIs. In addition, SR block of OFF STF at long intervals suggested that GABA$_A$ mediated signaling at serial AC ➔ AC synapses may primarily act to regulate STP at AC terminals that mediate OFF, but not ON L-IPSCs. However, ON STD, which remained intact following GABA$_A$R blockade, may depend primarily on a mechanism other than post-synaptic GABA$_A$R desensitization. For further exploration of the role of GABAergic signaling in STP of ON and OFF L-IPSCs, see **Appendix I** (Figs A.1-4).

Lateral IPSCs triggered by direct depolarization of ACs presynaptic to the Mb terminal display large latencies and asynchronous release

Consistent with the TTX sensitivity of glutamate puff-evoked lateral inhibition onto rod BCs in the rat IPL (Chavez et al., 2010), our previous work showed that TTX attenuated OFF L-IPSCs and had mixed effects on ON L-IPSCs (Fig 1.4; Vigh et al., 2011). This suggested that two separate populations of ACs, only one of which expresses voltage-gated Na$^+$ channels (OFF), might mediate ON and OFF L-IPSCs at the Mb terminal. Furthermore, differential effects of TTX (0.1 – 5 μM in the presence of 25 μM SR) on the onset latencies of ON L-IPSCs (SR latency = 68.3 ± 3.4 ms, n=29; TTX + SR latency = 74.9 ± 4.1 ms, n=23; p>0.05, unpaired Student's t-test, two tailed) and OFF L-IPSCs (SR latency = 158.8 ± 11.1 ms, n=22; TTX + SR latency = 205.6 ± 17.9 ms, n=10; p<0.05) supported the idea that voltage-gated Na$^+$ channels selectively amplify and accelerate light responses in the ACs that mediate OFF L-IPSCs (see **Appendix I**; Figs A.4, A.5). Such a role for voltage-gated Na$^+$ channels in AC light responses has been demonstrated previously for inhibitory inputs to GCs mediated by AII ACs in mice retina (Tian et al., 2010).

In order to discover the identity of the distinct AC classes involved in ON and OFF L-IPSCs, we performed paired recordings of intact Mb terminals and nearby ACs (Fig 2.7A, 2.7B). In a small percentage of ACs, a somatic step depolarization from -70 mV to 0 mV evoked L-IPSCs in the Mb terminal (only 3 out of 39 pairs; connectivity ~ 7.7%; Fig 2.7A and 2.7B). Of these three laterally connected ACs, none of which showed AC EPSCs following Mb depolarization (not shown), two were diffuse or bistratified (not shown), and one (Fig 2.7A) appeared to stratify primarily in the ON sublamina of the IPL. In the remaining 36/39 paired recordings, EPSCs were evoked in ACs following step depolarization of the Mb terminal from -70 mV to 0 mV, but stimulation in the reverse direction (from AC ➔ Mb) failed to evoke L-IPSCs. Although it is possible that ACs that exhibited unidirectional lateral synaptic connectivity in either direction (Mb ➔ AC or AC ➔ Mb) belong to separate functional classes, we were not able to discern clear morphological differences between these two groups based on reconstructions from confocal images. Because all ACs selected were within 50 μm of the soma of the recorded Mb, it is possible that we failed to characterize certain classes of wide-field ACs that may make the majority of the lateral inhibitory synapses onto the Mb terminal.

The AC➔Mb paired recordings revealed an unexpectedly slow L-IPSC onset latency of 106.06 ± 75.93 ms (n=3; Fig 2.7A, 2.7B). Such long latencies, which are much larger than the time-course of a typical synaptic delay (~1 ms), may have been due to incomplete voltage clamp of distal sections of AC dendritic arbors (Koizumi et al., 2005). This would produce slow depolarization and eventually activate voltage-gated Na^+ channels, triggering an escaping dendritic action potential (Koizumi et al., 2005) that would result in the relatively sharp, consistent IPSC onsets that we observed in the Mb terminal (Fig 2.7B, "IPSC latency"). A similar delayed dendritic Na^+ action potential in OFF ACs, subsequent to spatiotemporal summation of small EPSCs arriving from

69

multiple BC presynaptic terminals, could explain the long onset latencies that we observed for light-evoked OFF IPSCs, especially under mesopic background conditions (see Figs 2.4, 2.5). However, the rare occurrence and extreme technical difficulty of obtaining synaptically connected pairs of AC ➜ Mb recordings prevented us from further testing this mechanism with bath or focal application of TTX.

Interestingly, Mb L-IPSCs in paired recordings also showed strong asynchronous release following a somatic repolarizing step to -70 mV in the recorded AC (Fig 2.7B). Response duration in Mb terminals stimulated with a 200 ms depolarizing step in ACs was 383.85 ± 95.81 ms (n=3). A possible mechanism for this asynchronous GABA release from ACs (183.85 ± 95.81 ms duration), which could act both to truncate Mb glutamate release and impose a relative refractory period for light-evoked depolarization, is the accumulation of cytoplasmic Ca^{2+} subsequent to activation of voltage-dependent Ca^{2+} channels (VDCCs; Gleason et al., 1994). Such Ca^{2+} accumulation in the AC boutons mediating OFF L-IPSCs would provide a possible mechanism for light-evoked OFF STF (Fig 2.3; see Zucker and Regehr, 2002; also, see **Appendix I**, Fig A.6).

Discussion

We have shown that light-evoked, tri-synaptic ON and OFF L-IPSCs at Mb BC terminals exhibit distinct temporal profiles of STP. ON L-IPSCs (Fig 2.8, left, blue) exhibited amplitude STD of ~45% at 50 ms that recovered to ~10% at 1900 ms, and onset latency delay of ~95% at 50 ms that fully recovered at 1900 ms. OFF L-IPSCs (Fig 2.8, right, red) displayed amplitude STD of ~20% at 300 ms, amplitude STF of ~25% at 1900 ms, and latency advance of ~15% at 300 ms that recovered at 1900 ms. The recovery of ON and OFF STD ($\tau \sim 500$ ms) was rapid in comparison to STD of Mb exocytosis ($\tau \sim 8$ s;

70

von Gersdorff and Matthews, 1997) and reciprocal inhibition ($\tau \sim 12$ s; Li et al., 2007), and therefore likely acts as a temporal high pass filter of Mb glutamate release onto AC and GC dendrites (Sagdullaev et al., 2011). To clarify the functional roles of L-IPSC STP, we showed that changing background light from mesopic to scotopic increased the size and latency of ON L-IPSCs, while increasing the size and decreasing the latency of OFF L-IPSCs. Next, we used pharmacological methods to identify HC ➔ PR feedback and AC ➔ AC serial inhibitory circuits that shape ON and OFF STP, respectively (Fig 2.8, center). Finally, we showed that L-IPSCs evoked by depolarizing voltage steps at AC somata had long (~100 ms) latencies, consistent with the large delays of light-evoked OFF L-IPSCs, and exhibited sustained and asynchronous release (~200 ms), consistent with the idea that Ca^{2+} accumulation in AC boutons may account for OFF STF and latency advance (Fig 2.7). Together, these findings describe a novel scheme for STP of convergent, temporally independent lateral surround inhibitory inputs at the Mb BC presynaptic terminal.

Effects of L-IPSC STP on Mb terminal light responses likely depend on background light conditions

Under scotopic background, where the Mb resting potential (E_m) has been measured at between -40 and 45 mV (Protti et al., 2000; Baden et al., 2011), light responses at intact Mb terminals consist of either "analog" EPSPs with onset latencies of ~50 to 100 ms (Joselevitch and Kamermans, 2007) or "digital" Ca^{2+} action potentials with latencies of 75 to 90 ms (Protti et al., 2000; Baden et al., 2011). We expect, under these conditions, that ON L-IPSCs with latencies of ~75 ms and a conductance of ~1 nS (Fig 2.5) at a membrane potential of -40 mV would transiently hyperpolarize the Mb terminal by up to 10 mV, assuming an E_{Cl} of -60 mV and an input resistance of ~500 MΩ (Protti et al., 2000), or provide a roughly 70% block of the EPSP peak (Oltedal and Hartveit, 2009).

71

ON L-IPSC STD of 10 to 45% (Fig 2.8, left), then, would be expected to decrease the size of subsequent IPSPs to between 5 and 9 mV, and to reduce peak EPSP attenuation to between 40 and 60%. In addition, ON latency delay of 95% during high frequency surround stimulation (Fig 2.8, left) would eliminate block of the EPSP peak (Oltedal et al., 2009), but allow significant inhibition of the sustained component, which can last from ~200 to 500 ms (Joselevitch and Kamermans, 2007). We expect that OFF L-IPSCs, with latencies of ~70 ms and amplitudes of ~35 pA (Fig 2.5), would have effects similar to ON L-IPSCs under these conditions during naturalistic transient changes in surround luminance, but would exert increased influence over the EPSP peak during repeated surround stimulation at intermediate and long PPIs, due to ~15% latency advance and ~25% amplitude STF (Fig 2.8, right).

Under scotopic background, the Mb terminal can generate Ca^{2+} spikes when E_m is >-48 mV (Baden et al., 2011). Thus, hyperpolarization of 5 mV provided by ON or OFF L-IPSCs would be sufficient to prevent spike initiation at the Mb terminal. In addition, shunting inhibition by L-IPSCs likely exerts significant control over Ca^{2+} spike initiation at the Mb terminal (Hull et al., 2006a). Therefore, STD of ON and OFF L-IPSCs may be permissive for "digital" signaling at the Mb terminal. Furthermore, latency delay of ON L-IPSCs at short PPIs may decrease their ability to prevent spikes by shifting the time of their arrival to after threshold crossing. However, under circumstances where surround stimulation is dominated by low frequency decreases in luminance (i.e. 1900 ms PPI), STF of OFF L-IPSCs may result in reduced probability of Mb terminal Ca^{2+} spikes.

The effects of L-IPSC STP on Mb EPSPs under mesopic background would be expected to differ from those described above for scotopic background for two reasons. First, the latency of light-evoked EPSP at the Mb terminal are likely to advance under mesopic conditions (~35-50 ms; Wong et al., 2005) and decrease the effect of ON L-IPSCs on the EPSP peak. This decreased inhibition will be exacerbated during high

frequency stimulation, when ON L-IPSCs are even further delayed (Fig 2.8, left).

Second, the arrival delay between ON and OFF L-IPSCs in response to rapid,

naturalistic fluctuations in surround luminance will increase following the shift from

scotopic to mesopic conditions, from near coincidence to ~100 ms (Fig 2.5B). Thus, we

would expect ON and OFF L-IPSCs under these conditions to exert independent

frequency dependent effects, acting to truncate the transient and sustained components

of the "analog" Mb light response, respectively. This would allow ON L-IPSCs to shape

the Mb representation of temporal contrast, and OFF L-IPSCs to shape its

representation of mean luminance (Oesch and Diamond, 2011). Thus, while ON and

OFF L-IPSCs might act in concert to exert gain control and gate spike initiation at the Mb

terminal under scotopic background, they may perform separate computational roles

under cone dominant conditions.

ON and OFF L-IPSC STP profiles are shaped by distinct mechanisms

Because block of GABA$_A$Rs had little effect on ON L-IPSC STD (Fig 2.6), it is unlikely

that ON STD was due to GABA$_A$R desensitization or the influences of plasticity at

upstream GABA$_A$ synapses. In addition, enhancement of ON STD at the 300 ms PPI

(Fig 2.6) following block of AMPARs with NBQX (see Fig 2.8, center) suggested that

surround feedback inhibition from HCs to PRs (Fahrenfort et al., 2005 & 2009) may

significantly compress the dynamic range of ON BC light responses, minimize vesicle

depletion at ON BC ribbon synapses, and enable rapid recovery of ON L-IPSC STD

under control conditions. Thus, elimination of HC membrane potential fluctuations via

block of AMPARs on HC dendrites would allow ON BCs to be more hyperpolarized in

the dark, and to experience greater depolarization upon light stimulation of PRs. This

might both accelerate recovery of the readily releasable pool of glutamatergic vesicles at

the Mb terminal in the dark, and enhance STD due to increased vesicle depletion during

73

the light stimulus (Jarsky et al., 2011). Therefore, it seems likely that ON STD and

latency delay under control conditions are driven by a combination of vesicle depletion at

neighboring BC terminals (von Gersdorff and Matthews, 1997) and presynaptic ACs (Li

et al., 2007), and that these mechanisms are enhanced by removal of feedback

inhibition in the outer retina.

STP of OFF L-IPSCs was regulated by mechanisms distinct from those involved

in ON STP. OFF STD at short PPIs was diminished or absent following blockade of

$GABA_A$Rs (Fig 2.6). This result suggested that $GABA_A$R desensitization at the Mb

terminal might contribute to OFF STD. This is consistent with the previous finding that

Mb $GABA_A$Rs can recover fully from desensitization within 1-2 s (Li et al., 2007). OFF

amplitude STF at long PPIs (Fig 2.8, right), which was attenuated by SR block of

$GABA_A$Rs at AC ➔ AC synapses, may be due to disinhibition via serial AC pathways

(i.e. STD within "nested loops"; see Fig 2.8, center). In addition, the sustained and

asynchronous L-IPSCs evoked in our paired recordings (Fig 2.7), along with the latency

advances displayed by paired OFF L-IPSCs (Fig 2.8, right), are both consistent with the

idea that OFF STF may be driven, in part, by intracellular residual Ca^{2+} accumulation

and increased release probability at OFF AC presynaptic boutons (Gleason et al., 1994;

Zucker and Regher, 2002).

Potential physiological roles of L-IPSC STP at the Mb BC terminal

Filtering of transient or sustained glutamate release by STP of ON and OFF L-IPSCs at

the Mb terminal may enable post-synaptic GCs (and ACs) to rapidly modify the strength

and extent of their inhibitory surrounds following changes in surround temporal contrast.

Such dynamic spatial coupling may play a role in the rapid coding of spatial information

as relative GC spike onset latencies (±30 ms) following saccadic gaze relocation,

wherein local spatial contrast determines the ratio between convergent fast OFF and

slow ON BC inputs onto individual GC dendrites (Gollisch and Meister, 2008). STP in the

size and timing of ON and OFF L-IPSCs driven distally by these same BC inputs would

introduce frequency dependent correlations between spike latencies across a population

of GCs, thus enabling the extraction of spatial information by downstream decoders

(Usrey et al., 2000; Chase and Young, 2007).
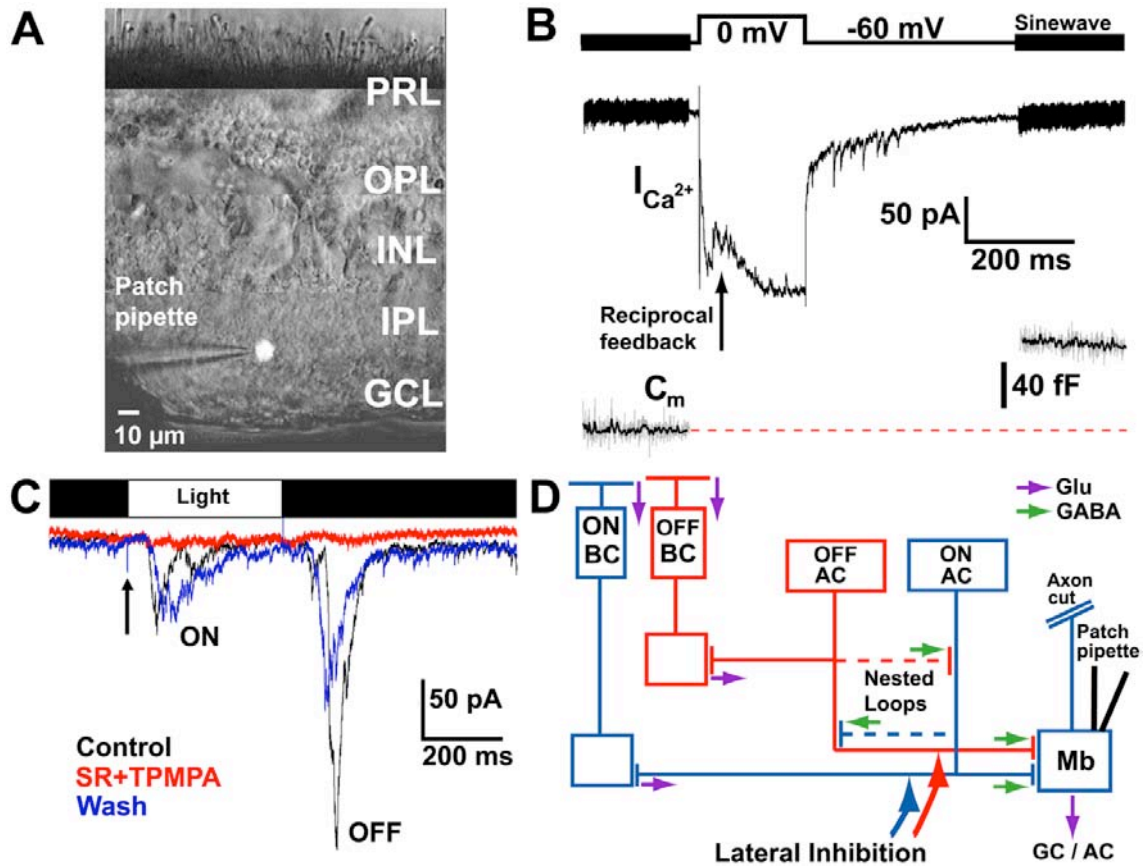
Figure 2.1: Light-evoked lateral inhibition in axotomized Mb bipolar cells (BCs) consists

of distinct ON and OFF lateral inhibitory post-synaptic currents (L-IPSCs) that are

mediated by $GABA_A$ and $GABA_C$ receptors. **(A)** Infrared differential interference contrast

(IR-DIC) montage and epifluorescence overlay of whole-cell patch clamp recording from

an axotomized Mb bipolar cell presynaptic terminal in the innermost layer of the inner

plexiform layer (IPL). PRL: photoreceptor layer; OPL: outer plexiform layer; INL: inner

nuclear layer; IPL: inner plexiform layer; GCL: ganglion cell layer. **(B)** Voltage clamp

recording of an axotomized Mb BC terminal revealed a large capacitance jump (ΔC_m),

Ca^{2+} current (I_{Ca2+}), and reciprocal feedback inhibition. Raw C_m measurements are

shown in gray, and smoothed data are shown in black (bottom). **(C)** Under dark-adapted,

scotopic background conditions (5.03 X 10^1 photons μm^{-2} s^{-1}), a 400 ms duration, full-

field light flash evoked distinct ON and OFF L-IPSCs (black trace; average of 20

stimulations). Both ON and OFF L-IPSCs were nearly completely blocked by bath application of 25 μM SR-95531 (SR) and 150 μM TPMPA (red trace; average of 4 stimulations), and this effect was reversible upon wash out (blue trace; average of 3 stimulations). Arrow indicates light flash stimulation artifact. **(D)** Schematic of circuitry likely to underlie ON and OFF L-IPSCs recorded from the axotomized Mb BC terminal shown in (C). The ON pathway (blue) travels across a trisynaptic pathway from rods and cones (not shown) to a monostratified ON BC, to an ON amacrine cell (AC), to the Mb BC terminal. ON ACs also provide "nested loop" feedback to OFF ACs via GABA$_A$ synapses. The OFF pathway (red) follows either an indirect, multisynaptic (disinhibitory: cones ➔ OFF BC ➔ OFF AC ➔ ON AC ➔ Mb BC) or direct, trisynaptic (inhibitory: cones ➔ OFF BC ➔ OFF AC ➔ Mb BC) route through a bistratified or diffuse AC. Glu, glutamatergic synapse; GABA, GABAergic synapse.

Figure 2.2: Light-evoked ON and OFF lateral inhibitory post-synaptic currents (L-IPSCs) exhibit short-term plasticity (STP) in response to paired 400 ms full-field light flashes with paired-pulse intervals (PPIs) between 50 ms and 1900 ms. ON L-IPSCs exhibited short-term depression (STD; 2nd ON < 1st ON) at both short (300 ms; **Ai**) and long (1900 ms; **Bi**) intervals. OFF L-IPSCs exhibited STD (2nd OFF < 1st OFF) at short intervals (300 ms; Ai), and short-term facilitation (STF; 2nd OFF > 1st OFF) at long intervals (1900 ms; Bi). Traces shown are averages of 5 stimulations from a single cell. **(Aii, Bii)** Windowed difference traces (2nd response – 1st response, ± SD) of light-evoked example ON and OFF L-IPSCs from (Ai, Bi) show both depression and facilitation. STD of both ON and OFF L-IPSCs was evident as positive deflections during and following the light flash, respectively (indicated below), for the 300 ms PPI (Aii). At the 1900 ms PPI (Bii), ON

STD was small while OFF STF (negative deflection) was pronounced. ON L-IPSCs are indicated in blue, OFF L-IPSCs are indicated in red, and L-IPSC onset latencies are indicated in purple. Examples shown were recorded under mesopic background conditions (5.03×10^3 photons μm^{-2} s^{-1}).
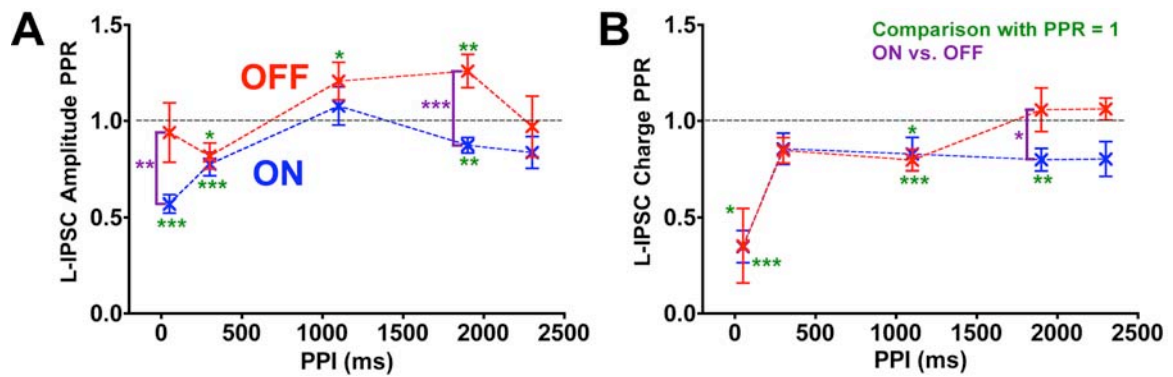
Figure 2.3: ON and OFF lateral inhibitory post-synaptic currents (L-IPSCs) exhibit

distinct profiles of short-term plasticity (STP) in terms of both amplitude and charge. **(A)**

The paired pulse ratio (PPR) of ON (blue) and OFF (red) L-IPSC amplitudes is shown as

a function of paired pulse interval (PPI). Data at each PPI (mean ± SE) were compared

to a null PPR of one (statistical significance indicated by green asterisks), indicated by

the dashed line (black). PPRs > 1 indicated short-term facilitation (STF), while values < 1

indicated short-term depression (STD). In addition, data for ON and OFF L-IPSCs at

each PPI were directly compared (purple brackets, asterisks). **(B)** Same cells and

presentation as in (A), except PPRs are shown for L-IPSC charge transfer. Number of

cells at each PPI and condition ranged from 6 to 39. *p<0.05, **p<0.01, ***p<0.001.
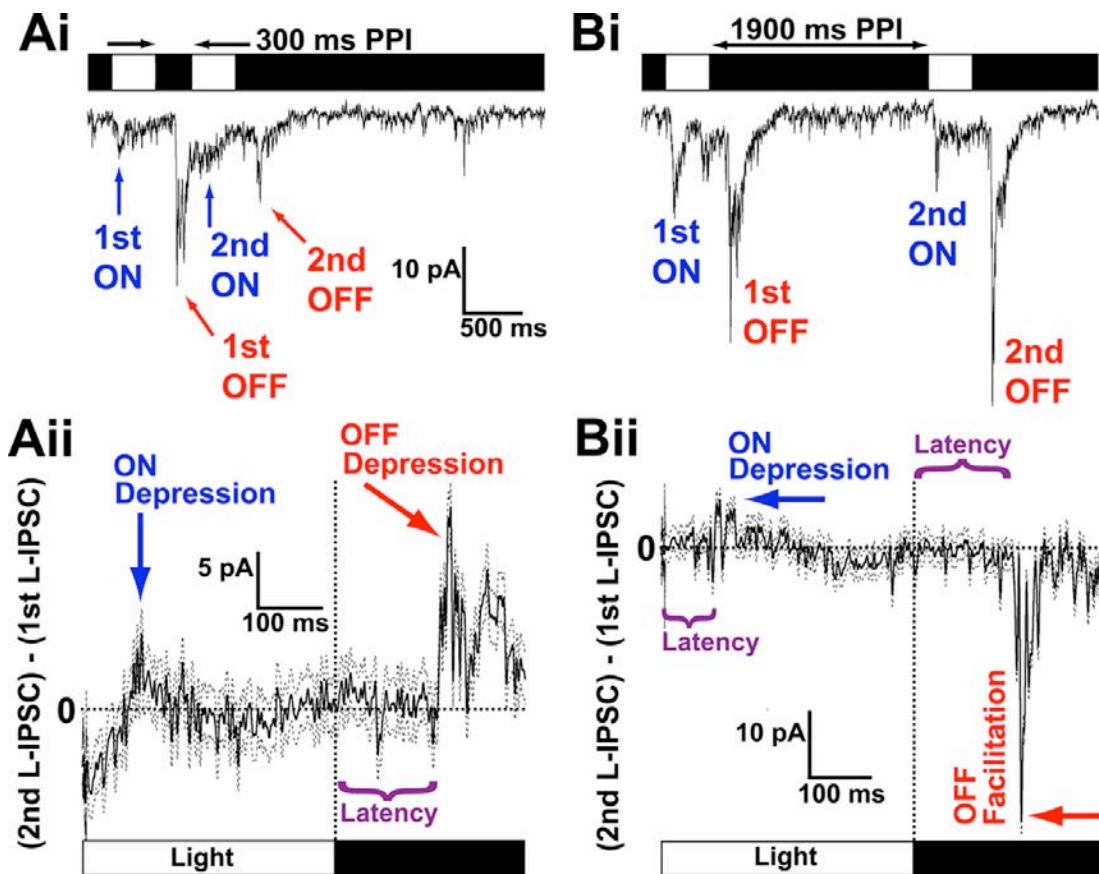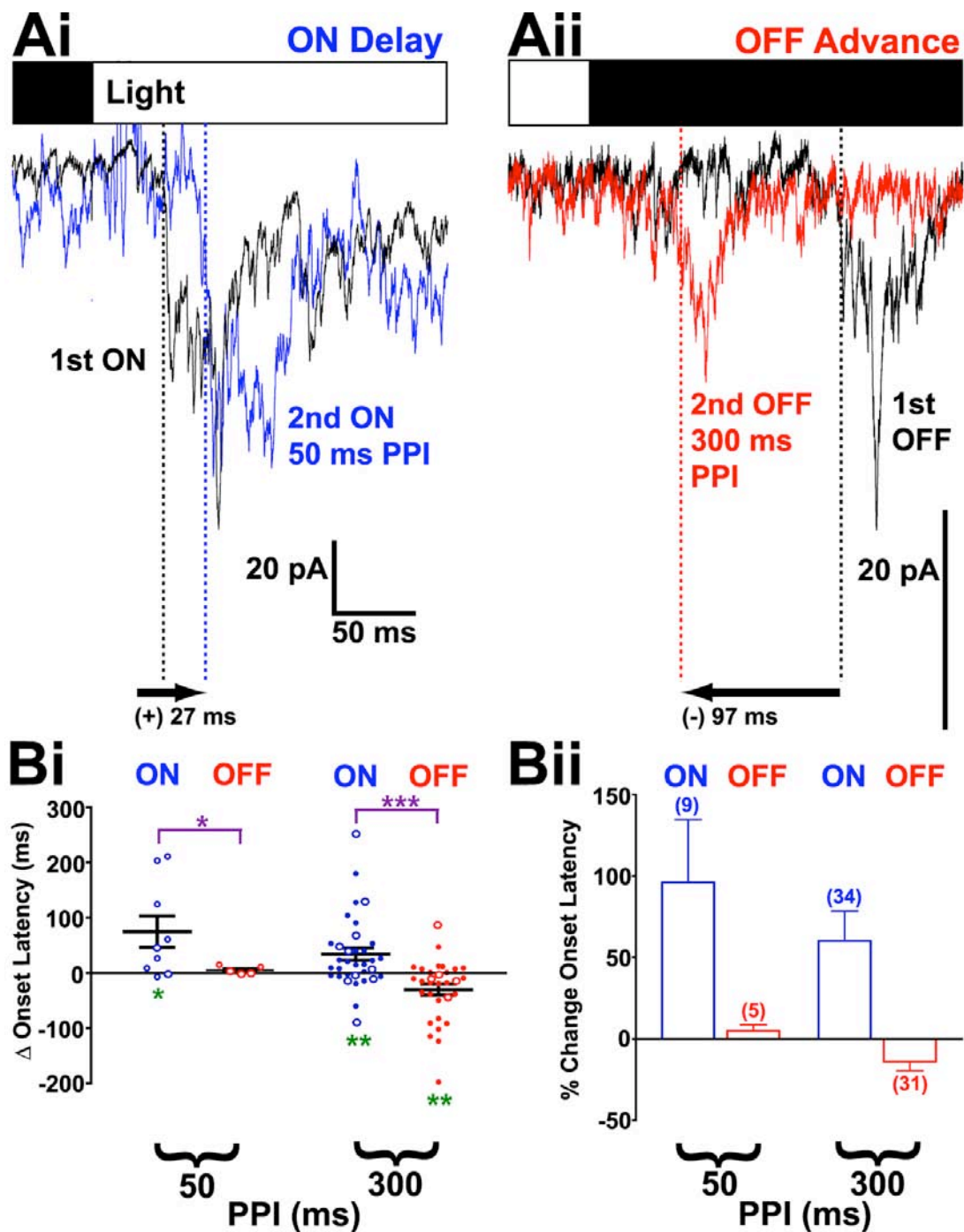
Figure 2.4: Light-evoked ON and OFF lateral inhibitory post-synaptic currents (L-IPSCs) exhibit differential short-term plasticity (STP) of onset latency. **(Ai)** Direct overlay of first (black) and second (blue) ON L-IPSCs at a paired-pulse interval (PPI) of 50 ms (left) showed a 27 ms delay (increase) of onset latency in an example cell recorded under

scotopic background (5.03 X 10^1 photons μm^{-2} s^{-1}). **(Aii)** Direct overlay of first (black)

and second (red) OFF L-IPSCs at a PPI of 300 ms (left) showed a 97 ms advance

(decrease) of onset latency in an example cell (different cell from (Ai)) recorded under

mesopic background (5.03 X 10^3 photons μm^{-2} s^{-1}). **(Bi)** Overall Δ onset latencies (=

onset latency of 2nd response - onset latency of 1st response) are shown for ON (blue)

and OFF (red) L-IPSCs at the 50 (left) and 300 ms (right) PPIs. Data at each PPI were

tested against a null Δ onset latency = 0 (delay > 0 ms, advance < 0 ms; green

asterisks), and ON and OFF Δ onset latencies were directly compared at each PPI

(purple brackets, asterisks). Filled circles indicate mesopic background; open circles

indicate scotopic background. All traces shown are averages of at least 5 stimulations.

*p<0.05; **p<0.01; ***p<0.0001. **(Bii)** Normalized data ((Δ onset latency / onset latency

of first L-IPSC) * 100; same cells as (Bi)) are shown for ON (blue) and OFF (red) L-

IPSCs at each PPI. Number of cells (n) in each condition is indicated in parentheses

(same as Bi). Error bars are mean ± SE.
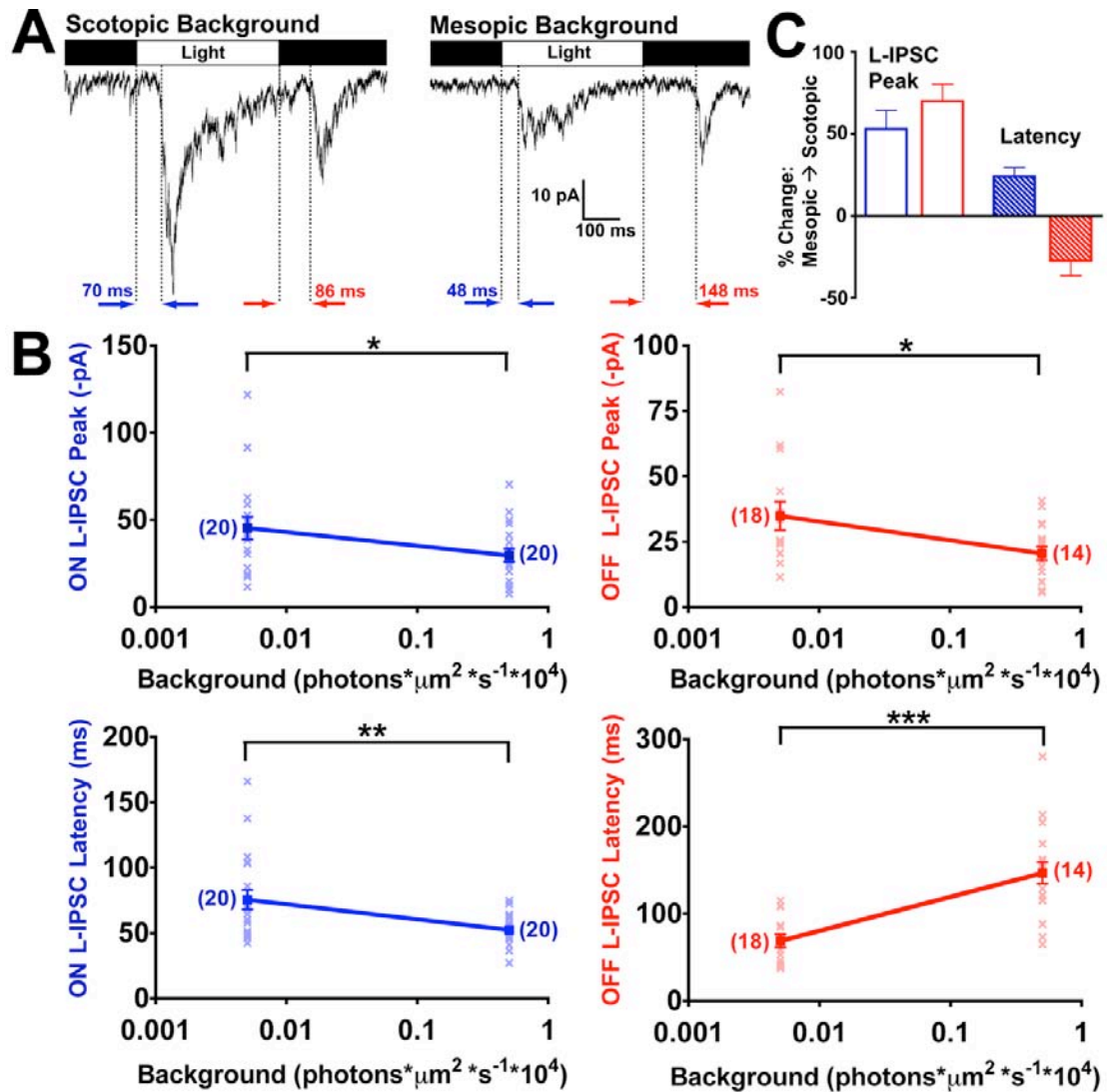
Figure 2.5: Switching from a mesopic background (5.03 x 10^3 photons μm^{-2} s^{-1}) to a scotopic background (5.03 X 10^1 photons μm^{-2} s^{-1}) alters both the amplitude and onset latency of ON and OFF lateral inhibitory post-synaptic currents (L-IPSCs). **(A)** Example L-IPSCs (black) recorded under either scotopic (left) or mesopic (right) background are shown with ON (blue) and OFF (red) onset latencies indicated by vertical dashed lines. Traces shown (average of 10 stimulations each) are from different cells. **(B)** Summary data for a group of cells are shown for ON (blue; left) and OFF (red; right) L-IPSC peak amplitude (top) and onset latency (bottom) as a function of background light intensity.

Data from scotopic and mesopic backgrounds were directly compared in each panel. All data shown are averages of 10-15 stimulations. Number of cells in each condition is indicated in parentheses. *p<0.05; **p<0.01, ***p<0.0001. **(C)** Normalized data showing the percent change from mesopic to scotopic conditions ((scotopic – mesopic) / mesopic)*100) are shown for ON (blue) and OFF (red) L-IPSC amplitude (left) and onset latency (right). Error bars are mean ± SE.
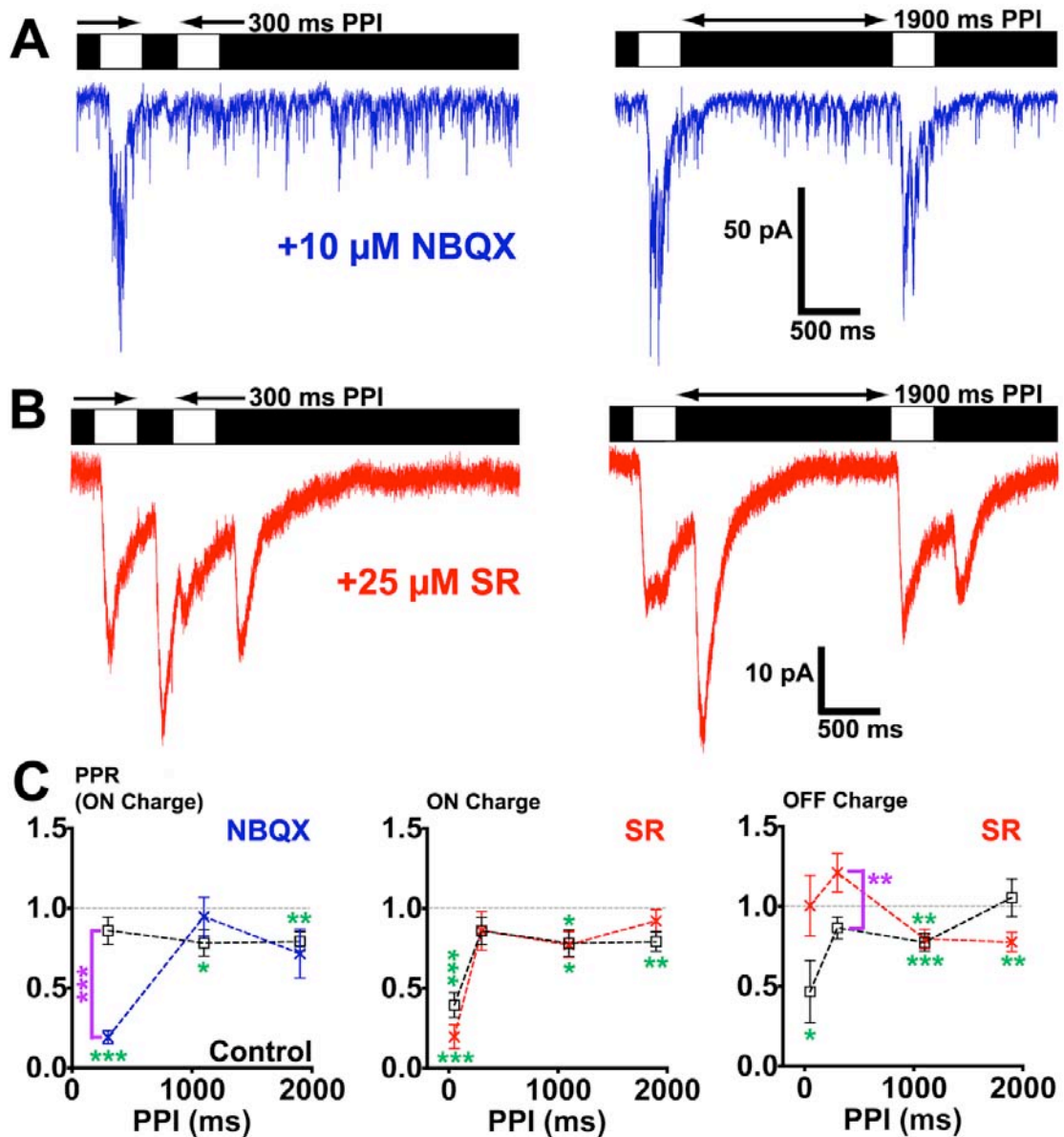
Figure 2.6: Block of signaling at AMPA receptors enhances short-term depression

(STD) of ON lateral inhibitory post-synaptic currents (L-IPSCs), while block of signaling

at $GABA_A$ receptors reduces STD of OFF L-IPSCs. **(A)** In an example cell recorded

under scotopic background (5.03 X 10^1 photons μm^{-2} s^{-1}), block of AMPARs with 10 µM

NBQX resulted in near complete STD of ON L-IPSCs at the 300 ms PPI (left). This ON

STD was nearly completely recovered at the PPI of 1900 ms (right). Traces shown (blue)

are averages of 5 stimulations. Light flashes are indicated by white rectangles above

traces. **(B)** Block of GABA$_A$Rs with 25 μM SR-95531 (SR) reveals purely GABA$_C$R

mediated L-IPSCs. In an example cell (different cell from (A)) recorded under mesopic

background (5.03 X 10^3 photons μm^{-2} s^{-1}), ON L-IPSCs exhibited STD at a paired-pulse

interval (PPI) of 300 ms (left) that recovered at a PPI of 1900 ms (right). OFF L-IPSCs

exhibited weak STD at a PPI of 300 ms (left) and strong STD at a PPI of 1900 ms (right).

Traces shown (red) are averages of 5 stimulations. **(C)** The paired pulse ratio for L-IPSC

charge transfer is shown for ON L-IPSCs in the presence of NBQX (left) and SR

(center), and for OFF L-IPSCs in the presence of SR (right). Data (mean ± SE) at PPIs

from 300 to 1900 ms were compared to a null PPR of one (statistical significance

indicated by green asterisks), indicated by the dashed lines (black). PPRs > 1 indicated

short-term facilitation (STF), while values < 1 indicated short-term depression (STD). In

addition, data for control (black) and NBQX (blue) or SR (red) at each PPI were directly

compared (purple brackets, asterisks). Number of cells in each condition ranged from 5

to 39. *p<0.05; **p<0.01, ***p<0.001.
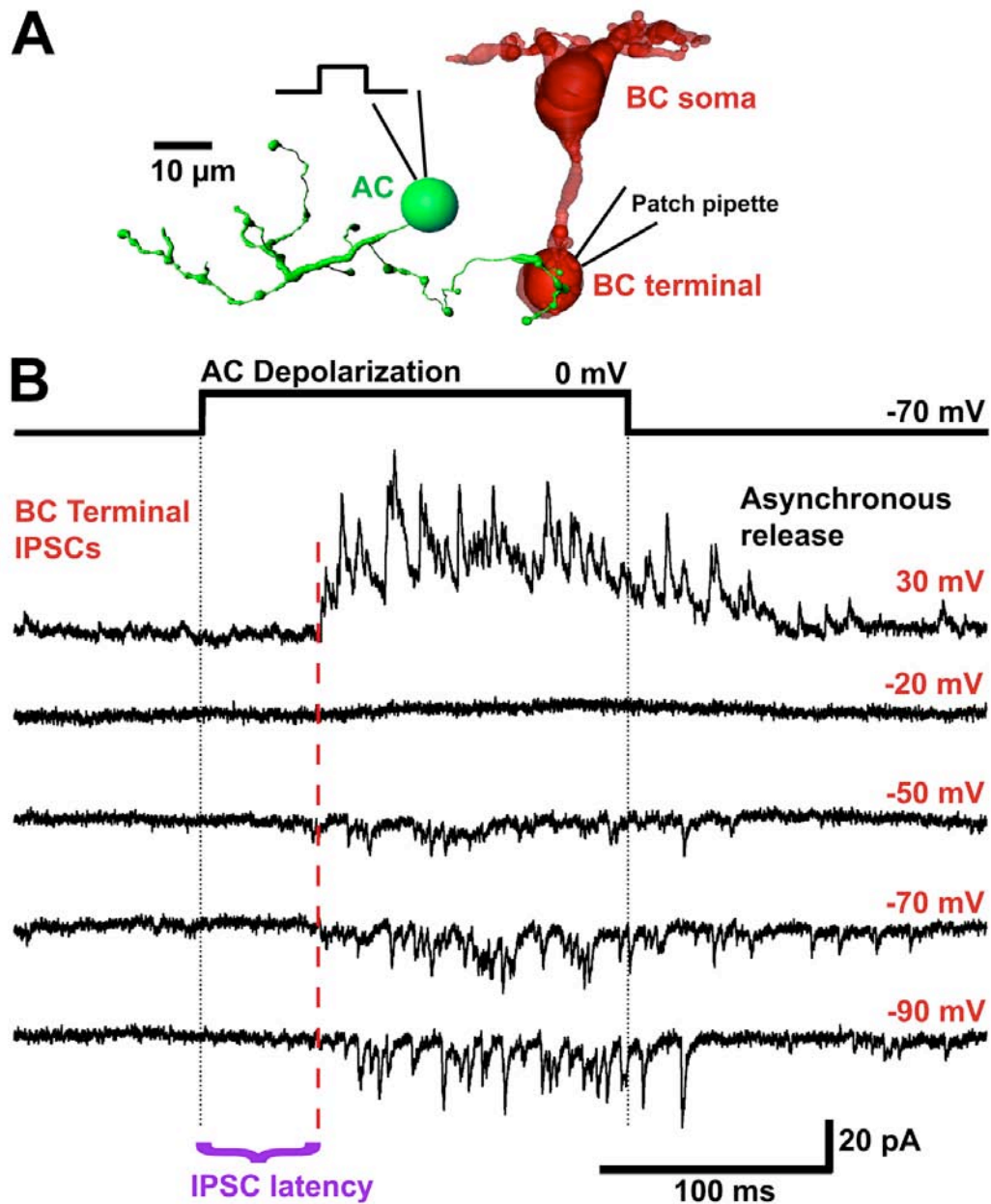
Figure 2.7: Lateral inhibitory post-synaptic currents (L-IPSCs) evoked by direct AC depolarization exhibit long onset latencies. **(A)** Reconstructed morphology of an Mb bipolar cell (BC; soma: top; axon terminal: bottom) and corresponding presynaptic amacrine cell (AC). The protocol used in (B) is indicated by the drawings of paired electrodes located at the AC soma and Mb BC terminal, the square wave voltage step applied to the AC, and the patch-clamp electrode used to voltage-clamp the Mb BC

terminal and record L-IPSCs. Note that the AC soma appears slightly displaced into the

inner plexiform layer (IPL), likely due to distortion of the slice during fixation. (**B**) A

depolarizing step from -70 mV to 0 mV in the AC soma (top) evoked L-IPSCs in the Mb

BC terminal (lower traces) with an onset latency between 50 and 100 ms (red dashed

line indicates IPSC latency at a holding potential of 30 mV). Note the persistence of

IPSCs following the voltage step, likely due to asynchronous release from AC boutons.

The holding potential in the Mb terminal (indicated in red) was varied between -90, -70, -

50, -20, and 30 mV. Note that no evoked L-IPSCs occurred in the Mb terminal at -20 mV

(the calculated Cl$^-$ reversal potential). Liquid junction potentials were not compensated.
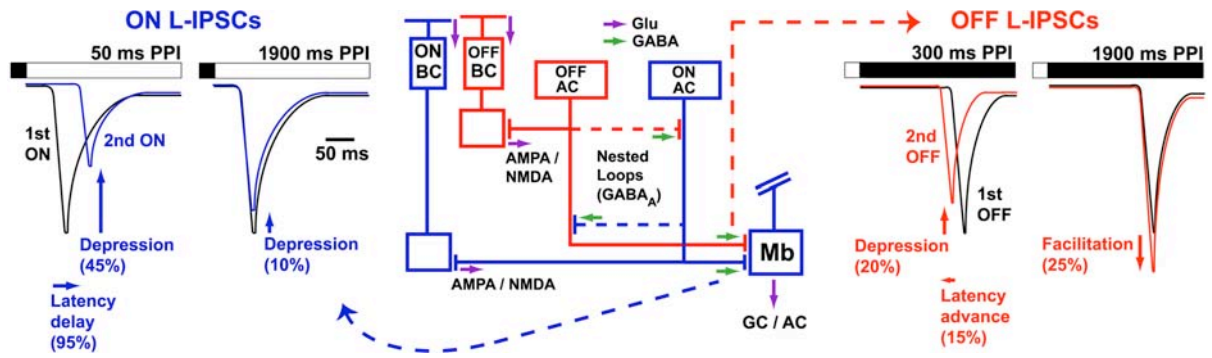
Figure 2.8: A schematic summary of the pharmacology and circuitry (center) of short-term plasticity (STP) in both size and latency of ON (left; blue) and OFF (right; red) GABAergic (GABA$_A$ and GABA$_C$) lateral inhibitory post-synaptic currents (L-IPSCs) recorded at the axotomized Mb bipolar cell (BC) presynaptic terminal. Note that while BC to amacrine cell (AC) synaptic transmission in both the ON and OFF pathways is mediated by a combination of signaling at AMPA and NMDA receptors (center diagram), ON L-IPSCs were potentiated (Fig 1.2; Vigh et al., 2011) and exhibited enhanced short-term depression (STD) in the presence of NBQX (Fig 2.6A). Similarly, while GABA$_A$ signaling occurs at nested loop synapses (center diagram; dashed lines) from ON ➔ OFF and OFF ➔ ON ACs, block of GABA$_A$Rs with SR-95531 reduced STD and short-term facilitation (STF) of OFF L-IPSCs but had little or no effect on short-term plasticity (STP) of ON L-IPSCs (Fig 2.6B). Temporal profiles of paired light flash STP of both size (depression and facilitation) and latency (delay and advance), taken from population means (Figs 2.3, 2.4), are illustrated by overlay of normalized and shifted L-IPSCs at paired pulse intervals (PPIs) of 50 and 1900 ms (ON, left) and 300 and 1900 ms (OFF, right). Idealized first L-IPSCs are shown in black, and second L-IPSCs are shown in blue (ON) or red (OFF). Arrows and percentages reflect normalized paired pulse ratios (PPRs; vertical arrows) and Δ onset latencies (horizontal arrows).

Allosteric modulation of retinal GABA receptors by ascorbic acid.

Cecilia I. Calero*[1], Evan Vickers*[2], Gustavo Moraga Cid[3], Luis G. Aguayo[3], Henrique von Gersdorff[2] and Daniel J. Calvo[1]

*These authors contributed equally to this work.

(1) Laboratorio de Neurobiología Celular y Molecular.

Instituto de Investigaciones en Ingeniería Genética y Biología Molecular (INGEBI).

Consejo Nacional de Investigaciones Científicas y Técnicas (CONICET).

Universidad de Buenos Aires (UBA).

Vuelta de Obligado 2490, CP 1428, Ciudad Autónoma de Buenos Aires, Argentina.

(2) The Vollum Institute

Oregon Health and Science University

Portland, Oregon 97239 USA

(3) Laboratorio de Neurofisiología

Departamento de Fisiología

Facultad de Ciencias Biológicas, Universidad de Concepción, Chile

Abstract

Ionotropic γ-aminobutyric acid receptors (GABA$_A$ and GABA$_C$) belong to the cys-loop receptor family of ligand-gated ion channels. GABA$_C$ receptors are highly expressed in the retina, mainly localized at the axon terminals of bipolar cells. Ascorbic acid, an endogenous redox agent, modulates the function of diverse proteins, and basal levels of ascorbic acid in the retina are very high. However, the effect of ascorbic acid on retinal GABA receptors has not been studied. Here we show that the function of GABA$_C$ and GABA$_A$ receptors is regulated by ascorbic acid. Patch-clamp recordings from bipolar cell terminals in goldfish retinal slices revealed that GABA$_C$ receptor-mediated currents activated by tonic background levels of extracellular GABA, and GABA$_C$ currents elicited by local GABA puffs, are both significantly enhanced by ascorbic acid. In addition, a significant rundown of GABA-puff evoked currents was observed in the absence of ascorbic acid. GABA-evoked Cl$^-$ currents mediated by homomeric ρ_1 GABA$_C$ receptors expressed in *Xenopus laevis* oocytes were also potentiated by ascorbic acid in a concentration-dependent, stereospecific, reversible, and voltage-independent manner. Studies involving the chemical modification of sulfhydryl groups showed that the two cys-loop cysteines and histidine 141, all located in the ρ_1 subunit extracellular domain, each play a key role in the modulation of GABA$_C$ receptors by ascorbic acid. Additionally, we show that retinal GABA$_A$ IPSCs and heterologously expressed GABA$_A$ receptor currents are similarly augmented by ascorbic acid. Our results suggest that ascorbic acid may act as an endogenous agent capable of potentiating GABAergic neurotransmission in the CNS.

Introduction

The ionotropic γ-aminobutyric acid (GABA) receptors, members of the cys-loop receptor family, are GABA-gated pentameric chloride (Cl⁻) channels (Moss and Smart, 2001; Zhang et al., 2001). They are usually divided into two classes, namely $GABA_A$ and $GABA_C$ receptors. $GABA_C$ receptors are composed by rho subunits, which are highly expressed in retinal bipolar cells (Wassle et al., 1998; McCall et al., 2002). They play an important role in the control of axon terminal excitability by mediating reciprocal synapses with amacrine cells (Matthews et al., 1994; Dong and Werblin, 1998; Protti and Llano, 1998; Hartveit, 1999). $GABA_C$ receptors also mediate tonic inhibitory currents, which arise in response to extracellular GABA concentrations controlled locally by GAT-1 transporters located on amacrine cells (Hull et al., 2006a; Jones and Palmer, 2009). Unlike $GABA_A$ receptors, $GABA_C$ receptors display both high affinity for GABA and a lack of desensitization (Johnston, 1996). These two properties allow them to mediate several modes of inhibitory signaling in the retina (Zhang and Slaughter, 1995; Lukasiewicz et al., 2004), including inhibition of vesicle recycling (Hull and von Gersdorff, 2004).

Ascorbic acid (vitamin C), an endogenous redox agent highly concentrated in the retina and other regions of the central nervous system, is accumulated in neurons and glial cells by specific transporters (Rebec, 1994; Rice, 2000; Harrison and May, 2009). In the retina, ascorbic acid levels rise above 100 times the concentration found in blood plasma (Rose and Bode, 1991; Hediger, 2002). Interestingly, the extracellular concentration of ascorbic acid can transiently undergo substantial increases during neuronal activity (Bigelow *et al.*, 1984; Grunewald, 1993). In retinal neurons, the ascorbate transporter SVCT2 mediates extensive sodium-dependent ascorbic acid extrusion through a mechanism regulated by neuronal depolarization and glutamate concentration (Portugal *et al.*, 2009). In addition, ascorbic acid has been shown to

modulate the activity of NMDA glutamate receptors and voltage-activated ion channels (Majewska et al., 1990; Fan and Yazulla, 1999; Alshuaib and Mathew, 2006; Nelson et al., 2007). Remarkably, its effects on cys-loop receptors have not been previously studied in the retina.

We analyzed here whether GABA$_C$ receptor function can be regulated by ascorbic acid. GABA$_C$ receptor-mediated currents were measured from Mb-type bipolar cell terminals in goldfish retinal slices and from *Xenopus laevis* oocytes expressing recombinant homomeric ρ_1 GABA$_C$ receptors. We show that the function of native retinal and recombinant GABA$_C$ receptors is significantly enhanced in the presence of ascorbic acid. Experiments involving the chemical modification of sulfhydryl groups and site-directed mutagenesis of the ρ_1 subunit indicate that cysteines 177 and 191 forming the cys-loop and histidine 141, all located in the N-terminal extracellular domain, are critical for the modulation of GABA$_C$ receptors by ascorbic acid. Additionally, we found that GABA$_A$ receptor-mediated mIPSCs at Mb retinal bipolar cell terminals, and ionic currents mediated by GABA$_A$ receptors heterologously expressed in HEK 293 cells, are potentiated by ascorbic acid. Together, our results suggest that ascorbic acid can be a powerful endogenous modulator of GABAergic neurotransmission.

Materials and methods

Retinal slice preparation and electrophysiology. Retinal slices were prepared from pieces of retina, taken from goldfish (*Carassius auratus*; 8-16 cm) of either sex, according to procedures described previously (Palmer et al., 2003). The slices (250 µm thick) were constantly perfused at 4-5 ml/min with 2.5 mM Ca^{2+} Ringer's solution for patch-clamp recording. Bipolar cell terminals with severed axons (axotomized) were identified in the inner plexiform layer (IPL) based on (1) single-exponential membrane

93

time constant, (2) the presence of an L-type Ca^{2+} current and DC_m jump, and (3) Mb-shaped (bulbous) terminal morphology (Palmer et al., 2003).

Axotomized bipolar cell terminals in retinal slices were voltage clamped in the whole-cell mode using a HEKA Elektronik (Lambrecht/Pfalz, Germany) EPC-9 patch-clamp amplifier in conjunction with Pulse software running the xChart extension (Pulse version 8.53). The Sine+DC technique was used for real-time measurements of membrane capacitance. Briefly, a 30 mV peak-to-peak 1 kHz sine wave was superimposed on the holding potential of the cells (-60 mV) and used by on-line analysis software to calculate time-resolved membrane capacitance. Standard external recording solutions contained (in mM) 100 NaCl, 2.5 KCl, 2.5 $CaCl_2$, 1.0 $MgCl_2$, 25 $NaHCO_3$ and 12 glucose (pH 7.45; osmolarity, 260–265 mOsm). In some cases, 3 mM ascorbic acid was added to recording solutions, which were then re-bubbled with 95% O_2 / 5% CO_2. In these cases, pH and osmolarity were readjusted following bubbling. Patch pipettes (6-8 MW) were pulled from borosilicate capillary glass and coated with dental wax to reduce pipette capacitance. Internal pipette solutions contained the following solutions (in mM): 60 Cs gluconate, 40 CsCl, 10 TEA-Cl, 25 HEPES, 3 Mg-ATP, 0.5 Na-GTP, and 2 EGTA. Some internal solutions contained 3 mM ascorbic acid and/or 25 μM SR95531. All internals were set to pH 7.2 with CsOH, and osmolarity was adjusted to 250 mOsm. APV, NBQX, TPMPA and gabazine (SR95531) were obtained from Tocris (Bristol, UK). All other chemicals were obtained from Sigma (St. Louis, MO).

For puff applications, GABA was dissolved in Ringer's solution along with, in some cases, 3 mM ascorbic acid and/or 25 μM SR95531. The pH was corrected to 7.45, and osmolarity was adjusted to 260 mOsm. This solution was then loaded in a patch pipette (see above) and puffed at 5 psi for 25 ms onto the axotomized Mb terminal at a distance of approximately 10-30 μM using a Picospritzer III (Parker Instrumentation, Cleveland, OH) driven by 100% N_2 gas. Miniature $GABA_A$ currents (mIPSCs) were

94

measured in recording solution containing 150 μM TPMPA, 1 μM TTX, 10 μM NBQX, and 50 μM D-APV. The holding potential was -60 mV, and data was acquired in a series of successive 60 s sweeps in continuous recording mode. mIPSCs were analyzed using a custom Igor procedure that utilized template matching and thresholding techniques. In some cases, noise distributions were determined by analysis of sweeps following addition of 25 μM SR95531. Standing $GABA_C$ leak current was measured using the Pulse xChart extension (16 Hz acquisition rate, up to 50 point averaging) in the presence of 25 μM SR95531. Holding potential was set at -60 mV, and the minimum period for determination of stable leak current, as determined by recording chamber volume replacement rate, was 18 s.

Statistical analyses were performed using Prism (version 4; GraphPad Software, San Diego, CA) with one-way repeated-measures ANOVA, Dunnett's or Tukey's post-hoc tests, and two-tailed unpaired or paired Student's t-tests for comparing data sets. One-sample t-tests were used to compare normalized data to a theoretical mean of zero. F-tests were used to compare fitted slopes from linear regression either with a theoretical value of zero, or between data sets. Data are reported as mean ± SEM. Statistics were performed on averaged traces where noted. mIPSC analysis was performed with Igor Pro v.5.04b (WaveMetrics).

RNA preparation, oocyte isolation, injection and electrophysiology. A human cDNA encoding the ρ_1 $GABA_C$ receptor subunit cloned in the vector suitable for *in vitro* transcription pGEM was used as a template to synthesize cRNAs *in vitro* (mMessage mMachine kit Ambion; Austin, TX, U.S.A.). Site-direct mutagenesis was achieved by the polymerase chain reaction overlap extension method using QuickChange Site-Directed Mutagenesis Kit (Stratagene, La Jolla, CA). cRNA solutions (0.1–0.3 ng/nl) were

prepared in RNase-free H_2O and stored at -70ºC. Oocytes, at stages V and VI were used for expression of exogenous cRNAs. Isolation and maintenance of cells were carried out as previously described (Miledi et al., 1989). Briefly, female *Xenopus laevis* frogs (Nasco, Modesto, CA, U.S.A.) were anaesthetized with 3-aminobenzoic-acid ethylester (~1 mg/ml) and ovaries surgically removed. Ovaries were incubated with 200 U/ml Type I or Type II collagenase (Worthington; Freehold, NJ, USA) for 30 min at room temperature (RT) and isolated oocytes maintained in an incubator at 17ºC in Barth's medium (in mM: 88 NaCl; 0.33 $Ca(NO_3)_2$; 0.41 $CaCl_2$; 1 KCl; 0.82 $MgSO_4$; 2.4 $NaHCO_3$; 10 HEPES and 0.1 mg/ml gentamycin; pH=7.4). After 1 day, each oocyte was manually microinjected (microinjector Drummond Sci. Co., Broomall, PA, U.S.A.) with 50 nl of a solution containing 50 ng of cRNA. Two-electrode voltage-clamp recordings were performed 3–7 days after oocyte injection with an Axoclamp 2B amplifier (Axon Instruments, Union City, CA, U.S.A.). Standard glass recording electrodes were made in a puller Narishige PB-7 (Narishige Scientific Instrument Lab., Tokyo, Japan) and filled with 3 M KCl. Pipette resistance values were approximately 1 MΩ. The holding potential was set to -70 mV and current traces acquired in a PC through Labmaster TL-1 DMA interface (Scientific solutions Inc, Solon, OH, U.S.A.) using pClamp software (Axon Instruments). Cells were placed in a chamber (volume 100 ml) continuously superfused (12 ml min^{-1}) with frog Ringer's solution (in mM: 115 NaCl; 2 KCl; 1.8 $CaCl_2$; 5 HEPES; pH 7.0). Drugs were applied through the perfusion system and all the experiments carried out at RT (23–24ºC). The agonist and all the drug and salts, HEPES, ascorbate analogs, 3-aminobenzoic-acid ethylester and RNase-free H_2O were purchased from Sigma-Aldrich (St Louis, MO, U.S.A.). Ascorbic acid, L-dehydroascorbic acid (DHA), calcium ascorbate ($Ca(Asc)_2$) and D-isoascorbic acid (D-iso Asc) solutions were prepared freshly each day in normal Ringer's solution and the pH always adjusted to 7.0 with NaOH (1 M). Data were analyzed with Prism v. 6.0 (MicroCal, Northampton, MA,

U.S.A.). Statistical analysis was performed using one-way ANOVA and Tukey´s or Dunnett´s tests. Dose–response curves (D–R) for GABA were fit with the expression of the mentioned logistic equation: $I_{max}= B\{1\text{-}1/[1+(A/EC_{50})^n]\}$, where A is the agonist concentration, B is the maximal response, EC_{50} is the concentration of agonist that elicits half-maximal responses, and n is the Hill coefficient.

Cell Culture, transfection and electrophysiology. HEK293 cells were cultured using standard methodologies (Yevenes et al., 2006). Transfections were done by using Lipofectamine 2000 (Invitrogen) with 2 µg of DNA for each plasmid studied per well. cDNA constructs encoding the α_1, β_2 and γ_2 rat $GABA_A$ was subcloned in the pRK5 vector (BD Pharmigen's). Whole cell recordings, at a holding potential of -60 mV, were performed as previously described 18-36 h after transfection. Patch electrodes were filled with (in mM) 140 CsCl, 10 1,2-bis-(2-aminophenoxy)-ethane-N,N,N,N-tetraacetic acid, 10 HEPES (pH 7.4), 4 $MgCl_2$, 2 ATP and 0.5 GTP. The external solution contained (in mM) 150 NaCl, 10 KCl, 2.0 $CaCl_2$, 1.0 $MgCl_2$, 10 HEPES (pH 7.4), and 10 glucose. The amplitude of the GABA current was assayed using a short (1-2 s) pulse of 30-40 µM GABA every 60 s. Bicuculline (1 µM) blocked all of the current mediated by $GABA_A$ receptors (not shown). GABA was unable to produce any response in more than 50 non-transfected cells. Statistical analyses were performed using ANOVA and results were expressed as the arithmetic means ± S.E.; values of p<0.05 were considered statistically significant. For all of the statistical analysis and plots, Origin 6.0 (MicroCal) software was used.

Results

GABA$_C$ currents in Mb retinal bipolar cell terminals are enhanced by ascorbic acid

Previous work has shown that both GABA$_A$ and GABA$_C$ receptors mediate chloride currents at Mb bipolar cell presynaptic terminals in goldfish retinal slices (Vigh and von Gersdorff, 2005). GABA$_C$ receptors at the bipolar cell terminals mediate a tonic current which is activated by background levels of extracellular GABA. This current corresponds to a standing leak current sensitive to the selective GABA$_C$ receptor antagonist (1,2,5,6-tetrahydropyridin-4-yl)methylphosphinic acid (TPMPA) and resistant to the GABA$_A$ receptor antagonist bicuculline-methiodide and SR-95531 (gabazine). Here we studied the effects of ascorbic acid on GABA$_C$ receptor-mediated responses using patch-clamp recording from axotomized Mb bipolar cell presynaptic terminals in the presence of 25 μM SR-95531 to block GABA$_A$ responses. Fig. 3.1A (left) illustrates a representative trace showing the effects of ascorbic acid on a GABA$_C$ tonic current recorded at -60 mV. Overall, the GABA$_C$ mediated standing leak current was significantly enhanced by bath application of 3 mM ascorbic acid (0 mM Asc = -49.17 ± 6.72 pA, 3 mM Asc = -61.44 ± 7.64 pA, Wash (0 mM Asc) = -48.66 ± 6.80 pA, n=11; repeated-measures ANOVA ($p<0.01$), Dunnett's Multiple Comparison Test ($p<0.01$), paired t-test p=0.0053). During wash-out, the leak current was significantly reduced to nearly baseline levels (summary data Fig. 3.1A, right; Dunnett's $p<0.01$, paired t-test $p<0.001$). Normalized measures of enhancement of leak current and wash-out were also significant (3 mM Asc = +30.43 ± 9.61%, 0 mM Asc = 0.24 ± 5.54%, one-sample t-test, hypothetical value = 0, 3 mM Asc: $p<0.05$, 0 mM Asc: p=0.01). Similar highly significant enhancement (0 mM Asc = -235.3 ± 57.65 pA, 3 mM Asc = -302.4 ± 55.79 pA, Wash (0 mM Asc) = -272.70 ± 45.40 pA, n=4; repeated measures ANOVA ($p<0.01$), Dunnett's ($p<0.01$), paired t-test p=0.0073) of leak current by ascorbic acid was obtained when the GABA$_C$ tonic current was recorded

in the presence of the GAT-1 selective blocker NO-711 (example trace: 3 μM NO-711,

Fig. 3.1B left; summary data: 1 or 3 μM NO-711, n=1,3, data collapsed, Fig. 3.1B right),

which increased the basal extracellular GABA concentration by inhibiting GABA uptake.

Wash-out of the effect of ascorbic was not significant in the presence of NO-711 (paired

t-test, p=0.058; Fig. 3.1B, right), which may be due to increased variability of

extracellular GABA concentration and difficulty establishing stable baseline leak current

in the absence of functioning GAT-1 transporters (Hull et al., 2006a). Normalized

changes in leak current in the presence of NO-711 also revealed significant ascorbic

acid mediated enhancement of leak current (3 mM Asc = +33.63 $\pm$ 8.78%, 0 mM Asc =

+21.97 $\pm$ 8.97%, one-sample t-test, hypothetical value = 0, 3 mM Asc: p<0.05, 0 mM

Asc: p>0.05). Bath application of 300 µM TPMPA in the presence of 25 µM SR-95531

(example trace, Fig. 3.1C, left) significantly reduced leak current (control: -31.5 $\pm$ 3.8 pA,

TPMPA: -14.2 $\pm$ 3.0 pA; n=4, paired t-test, p=0.015; Fig. 3.1C, right) in axotomized Mb

terminals, indicating the presence of a small, non-GABA$_C$ mediated leak current.

Subtraction of this non-GABA$_C$ leak current from recordings in the absence or presence

of NO-711 yielded estimated ascorbic acid potentiation of pure GABA$_C$ leak current of

+65.0 $\pm$ 30.2% and +36.5 $\pm$ 9.9%, respectively. This is consistent with enhanced

ascorbic acid-mediated potentiation of GABA$_C$ currents at low GABA concentrations.

We also evoked GABA$_C$ responses by GABA pressure ejecting (puffing) GABA

directly onto presynaptic terminals of bipolar cells (Fig. 3.2A; 25 ms puff, 30 s inter-

stimulus interval (ISI)). The amplitude of GABA$_C$ current responses to puff application of

GABA exhibited significant run-down (~30%) over 15 min in the absence of ascorbic acid

(example: Fig. 3.2A left; summary data: Fig. 3.2B, 0 mM Asc run-down linear regression:

-2.31 $\pm$ 0.08% per minute, slope significantly non-zero (p<0.0001)). Perfusion solution

contained 25 μM SR-95531 in all cases. Some experiments were performed with 25 μM

SR-95531 in the puff pipette, but showed no change in run-down kinetics (not shown).

Including 3 mM ascorbic acid in the bath solution, intracellular solution, and puff pipette significantly slowed and/or blocked this run-down over the same time period (example: Fig. 3.2A right; Fig. 3.2B, 3 mM Asc linear regression: -0.16 ± 0.11% per minute, slope not significantly non-zero (p>0.05)). This effect on run-down slope was highly significant (Fig. 3.2B; F=28.7, DFn=1, DFd=306, p<0.0001). The two conditions were compared at individual time-points, revealing significant block of $GABA_C$ current run-down by 3 mM ascorbic acid (in the puff pipette, patch pipette, and perfusion solution) at 5 min (unpaired t-test, n=7,7; p=0.0036) and 10 min (p=0.0031), but not at 14.5 min (p=0.0936). Addition of 3 mM ascorbic acid to the bath solution alone appeared to slow run-down during the first 5 min of puff application, but this effect did not reach significance over the entire 15 min period (data not shown). Summary data were collapsed across conditions where either 200 µM (n=4) or 1 mM GABA (n=3) was used for puff application, as analysis showed no difference in run-down slope between these conditions from 0-15 min (n=4,3; F=0.40, Dfn=1, DFd=112, p=0.53; data not shown).

We also quantified the amplitude of $GABA_C$ responses to puff application of GABA before (control), during, and after (wash) bath application 3 mM ascorbic acid (Fig. 3.3A, 3.3B). Puff applications of GABA, collapsed across 1 mM (n=7) and 200 µM (n=1), produced large TPMPA-sensitive (not shown) $GABA_C$ receptor-mediated inward currents at -60 mV (Fig. 3.3A). Ascorbic acid application significantly and reversibly (0 mM Asc = 661.2 ± 176.0 pA, 3 mM Asc = 729.8 ± 174.9 pA, Wash (0 mM Asc) = 579.7 ± 153.8 pA, Repeated Measures ANOVA (n=8, p=0.01), Tukey's Multiple Comparison Test (0 mM Asc vs. 3 mM Asc: p<0.05; 3 mM Asc vs. Wash (0 mM Asc): p<0.05) increased $GABA_C$ puff response amplitude by ~16% (Fig. 3.3A, bottom). Analysis of responses normalized to control amplitudes also showed a significant increase in 3 mM ascorbic acid (+16.29 ± 5.37%, one-sample t-test, p=0.019), while normalized amplitudes during wash-out were not significantly non-zero (-9.11 ± 6.98%, one-sample t-test, p=0.233).

Correction of averaged traces for $GABA_C$ run-down (based on linear regressions shown in Fig. 3.2), revealed a large effect of ascorbic acid that was nearly reversible during wash-out (Fig. 3.3B, bottom). Potentiation of $GABA_C$ mediated responses to puff application of GABA was highly significant following correction for run-down, although this potentiation was not significantly reversed during wash-out (Fig. 3.3B, bottom; 0 mM Asc = 675.5 ± 178.3 pA, 3 mM Asc = 826.6 ± 198.0 pA, Wash (0 mM Asc) = 746.8 ± 196.1 pA, Repeated Measures ANOVA (n=8, p=0.01), Tukey's Multiple Comparison Test (0 mM Asc vs. 3 mM Asc: p<0.01, 3 mM Asc vs. Wash: p>0.05). The lack of significant wash-out for corrected data is probably due to increased variability in run-down for data acquired more than 10 min after break-in (Fig. 3.2B). Analysis of corrected responses normalized to control amplitudes showed a highly significant increase in 3 mM ascorbic acid (+28.29 ± 6.73%, one-sample t-test, p=0.004), while normalized amplitudes during wash-out were not significantly non-zero (14.18 ± 9.17%, one-sample t-test, p=0.166). It is worth noting that, even though we know the exact concentration of GABA inside the pipette, it is difficult to quantitatively control the local concentration of GABA at bipolar terminal presynaptic receptors due to effects of transporters and extracellular diffusion. Thus, low concentrations of GABA applied to the bath or locally puff-applied often do not produce a robust, stable response. Despite these issues, a significant dose dependency of ascorbic acid mediated potentiation on the concentration of puffed GABA was observed between 1 mM and 10 mM, (1 mM GABA: +16.31 ± 6.20%, 10 mM GABA: -4.65 ± 6.70%; n=7,5; unpaired t-test, p=0.047; not shown). No difference in potentiation was seen between puff applications of 200 μM and 1 mM GABA (n=1,7; not shown). Taken together with the effect of ascorbic acid on standing leak current, these results demonstrate that endogenous $GABA_C$ receptor function is strongly modulated by ascorbic acid.

Responses mediated by homomeric ρ_1 GABA$_C$ receptors are enhanced by ascorbic acid

To further characterize the actions of ascorbic acid on GABA$_C$ receptors, we heterologously expressed recombinant GABA$_C$ receptors in frog oocytes. GABA applications to oocytes expressing homomeric ρ_1 GABA$_C$ receptors induced large inward Cl$^-$ currents displaying all of the features of retinal GABA$_C$ receptor-mediated responses. For example, they are bicuculline-insensitive, TPMPA and picrotoxin sensitive, non-desensitizing, and display the same pharmacological profile for agonists (Kusama et al., 1993; Woodward et al., 1993). In addition, this experimental model allowed us to control more precisely the extracellular concentration of ascorbic acid and the GABA concentration sensed by the GABA$_C$ receptors, thus, a more quantitative approach was possible. Fig. 3.4A shows GABAρ_1 responses measured in normal frog Ringer´s solution (control, 0.3 μM GABA) or immediately after the application of ascorbic acid to the recording solution. Current amplitude was significantly enhanced (~+160%) in the presence of 3 mM ascorbic acid. Similar effects were produced by brief exposures of the oocytes to a lower concentration of ascorbic acid (700 μM) during sustained GABA applications (0.3, 1.0 or 10 μM) (Fig. 3.4B). Ascorbic acid actions were strongly dependent on GABA concentration and were very rapid, stable and completely reversible after washout (Fig. 3.4B). No use-dependent effects were observed and no changes in activation, deactivation or desensitization of the GABAρ_1 responses were detected during ascorbic acid applications (not shown). Dose-response (D-R) curves for GABA were shifted to the left and slightly but significantly increased in their maximal values in the presence of ascorbic acid (Fig. 3.5A and Table 1b). Fig. 3.5B illustrates the effects of increasing concentrations of ascorbic acid on GABAρ_1 responses elicited by 0.3 and 1 μM GABA. Maximal values of potentiation obtained during applications of high

concentrations of ascorbic acid (30 mM) were substantial (~750%; Fig. 3.5C). No significant differences were observed, neither in the degree of potentiation at different membrane potentials (reflected by the change in I-V curves slopes), nor in the reversal potentials of Cl$^-$ currents, in the presence of ascorbic acid (Fig. 3.5D). The fast onset, fast offset, and reversible character of ascorbic acid effects on GABA$_C$ receptors, all suggest that these effects are not due to its entry into the cells. Based on this evidence, an extracellular superficial site of action is more likely. This is in agreement with the fact that short (0 to 10 sec) or persistent (up to 30 min) applications of ascorbic acid produced identical results in oocytes expressing GABAρ_1 receptors (not shown), and with data reporting that oocytes do not express ascorbic acid transporters (SCVT1 and SCVT2) (Dyer *et al.*, 1994). I-V curves showing that modulation is independent of the membrane potential also indicate regulatory sites located outside of the channel pore.

The specificity of ascorbic acid actions on GABAρ_1 responses was analyzed by testing structurally related analogs (Fig. 3.6A). L-dehydroascorbic acid (DHA) (3 mM) and calcium ascorbate (Ca(Asc)$_2$) (1.5 mM), two forms of ascorbate that lack antioxidizing activity, were unable to produce changes in currents elicited by 0.3 μM GABA (Fig. 3.6B and Table 1a). In contrast, the stereoisomer D-isoascorbic acid (D-iso-Asc) (3 mM) which shows the same antioxidizing power as ascorbic acid (Organisciak *et al.*, 1992), had a much lower efficacy (Fig. 3.6B and Table 1a) indicating that structural determinants are also essential for modulation. Kinetic analyses of the GABAρ_1 responses elicited by 0.3 μM GABA, recorded in normal frog Ringer´s solution or in the presence of ascorbic acid, Ca(Asc)$_2$, DHA or D-iso-Asc showed time courses of activation (t_a) and deactivation (t_{deact}) well fitted to single exponential functions. No kinetic changes were observed in the presence of 3 mM ascorbic acid, 1.5 mM Ca(Asc)$_2$, 3 mM

DHA or 3 mM D-iso-Asc (Table 1a). Desensitization values were negligible, thus t_{deact} was not included for analysis.

Involvement of cysteines forming the Cys-loop and histidine 141 in the modulation of GABAρ_1 receptors by ascorbic acid

We studied whether ascorbic acid effects on GABAρ_1 responses could be due entirely or in part to a direct interaction of this agent with specific aminoacidic residues at the receptor subunits. Previous studies have suggested that cysteine residues are commonly involved in the redox modulation of various ion channels (Ruiz-Gomez *et al.*, 1991; Ruppersberg *et al.*, 1991; Sullivan *et al.*, 1994; Lipton *et al.*, 2002; Chu *et al.*, 2006). GABA$_C$ receptor ρ_1 subunits carry only two cysteines (C177 and C191) at the extracellular domain forming the characteristic cys-loop. Mutations of these cysteines are precluded because they render non-functional receptors (Amin et al., 1994; Sedelnikova et al., 2005). Thus, to determine whether C177 and C191 are involved in the modulation of the homomeric ρ_1 GABA$_C$ receptors by ascorbic acid, we used the irreversible thiol alkylating agent N-ethylmaleimide (NEM), which forms covalent bonds with the free sulfhydryl groups preventing any further chemical reaction at these sites. NEM concentration was kept as low as possible and incubation periods very short to prevent unspecific effects. As shown in Fig 3.7A, NEM alone produced, on GABAρ_1 receptors expressed in oocytes, effects similar to those observed for ascorbic acid (Fig. 3.5A). D-R curves for GABA after NEM (30 μM) treatment were shifted to the left and their maximal values were significantly increased. As expected for a specific sulfhydryl reagent, NEM completely abolished dithiothreitol (DTT; 2 mM) potentiation of the GABAρ_1 responses (Fig. 3.7B). Next, we studied the actions of ascorbic acid on GABAρ_1 receptors previously treated with 30 μM NEM. D-R curves showed that the increase

produced by 3 mM ascorbic acid in GABAρ_1 maximal responses (evidenced in Fig. 3.5A) was entirely prevented after NEM treatment, whereas the leftward shift was partially resistant to NEM (Fig 3.7C). These results indicate that the extracellular cysteines that form the cys-loop of ρ_1 subunits are involved in the modulation of GABA$_C$ receptors by ascorbic acid. Effects of ascorbic acid may also be partially due to redox modulation of C177 and C191, so additional mechanisms may also be involved.

Previous studies have demonstrated that H141, located near the ρ_1 subunit extracellular Cys-loop, is essential for allosteric modulation of homomeric GABAρ_1 receptors (Wang *et al.*, 1995; Zhang *et al.*, 2001; Sedelnikova *et al.*, 2005). Thus, we used site-directed mutagenesis to study if this amino acid residue can also participate in the modulation of GABAρ_1 receptors by ascorbic acid. H141 was replaced with an aspartic acid to generate mutant homomeric GABAρ_{1H141D} receptors. When expressed in oocytes, these receptors had typical responses to GABA (bicuculline insensitive and TPMPA sensitive) and showed EC$_{50}$ values for GABA slightly higher than wild-type receptors (Fig 3.7D, also see (Wang et al., 1995)). The effects of ascorbic acid on mutant GABAρ_{1H141D} receptors were analyzed in D-R curves. Similarly to wild-type receptors, maximal responses to GABA were significantly increased in the presence of 3 mM ascorbic acid (Fig. 3.7E). However, the shift to the left produced by ascorbic acid on D-R curves performed on wild-type GABAρ_1 receptors (Fig. 3.5A) was completely abolished in receptors carrying the mutation H141D (Fig. 3.7E). In addition, ascorbic acid remained capable of potentiating responses evoked by low GABA concentrations (see inset Fig. 3.7E). We also analyzed the specific contribution of C177 and C191 to the effects induced by ascorbic acid on GABAρ_{1H141D} receptors in oocytes previously treated with NEM. Ascorbic acid-induced increases in maximal responses evoked by GABA on wild-type receptors was completely prevented by NEM treatment, but

potentiating effects of ascorbic acid on GABAρ_1 responses induced by low GABA concentrations on the mutant GABAρ_{1H141D} receptors remained unaltered (inset Fig. 3.7F). Ascorbic acid might exert pro-oxidant effects on membrane proteins through a selective metal catalyzed oxidation involving the modification of histidines (Stadtman, 1991, 1993; Nelson et al., 2007). However, this possibility was dismissed because ascorbic acid effects on GABAρ_1 responses were identical in the presence of the metal chelating agents EDTA and tricine (not shown). In addition, several oxidizing agents antagonize GABAρ_1 responses (Calero and Calvo, 2008), and Zn^{2+} interaction with histidine H141 also causes a reversible inhibition (Wang *et al.*, 1995). In contrast, we found that histidine H141 is critically involved in potentiation of GABAρ_1 receptor function by ascorbic acid. A proton transfer from ascorbic acid to the H141 was also disregarded because pH was constant during experiments (pH = 7.4). Moreover, critical residues for pH sensitivity are located within the first 60 N-terminal amino acids in ρ_1 subunits (Rivera *et al.*, 2000). Thus, H141 would be involved in an independent conformational change, allosterically induced by ascorbic acid at or near the Cys-loop of GABAρ_1 receptors, which might take place simultaneously with redox modification of C177 and C191 at ρ_1 subunits. All of these events would occur near the extracellular agonist-binding site.

Modulation of neuronal and recombinant GABA$_A$ receptors by ascorbic acid

Based on our findings, we decided to test if ascorbic acid could produce similar effects on GABA$_A$ receptors. Whole-cell patch-clamp recordings were performed on both presynaptic terminals of retinal bipolar cells and transfected cells expressing two types of recombinant GABA$_A$ receptors. Fig. 3.8A shows an example recording demonstrating a reversible increase in the amplitude of miniature GABA$_A$ receptor-mediated IPSCs (mIPSC) following extracellular application of 3 mM ascorbic acid. The mean mIPSC

waveforms for this example recording (Fig. 3.8B left) show a distinct, reversible increase in mIPSC amplitude. This effect can also be seen as a reversible rightward shift in the cumulative probability curve for mIPSC amplitude (same example cell) following addition of ascorbic acid (Fig. 3.8B, right). Although ascorbic acid appeared to increase mIPSC frequency (2.44 Hz Control vs. 5.34 Hz Asc) and preferentially affect larger mIPSCs (>12 pA) in this example cell (Fig. 3.8B, right), there was no overall significant effect of ascorbic acid on mIPSC frequency (Control (0 mM Asc) = 3.01 ± 1.26 Hz, 3 mM Asc = 3.80 ± 1.45 Hz, Wash (0 mM Asc) = 3.58 ± 1.39 Hz; Repeated measures ANOVA, n=5, p=0.28; Fig. 3.8C, right). It is possible that in some cells, ascorbic acid potentiation of mIPSCs raised their amplitude above our detection threshold, and thus caused an apparent increase in the frequency of small mIPSCs. However, examination of the mIPSC amplitude distribution (Fig. 3.8B, right) showed a clear shift in cumulative probability over the whole range of amplitudes, indicating that the effect of ascorbic acid was not specific for a small subset of mIPSCs. In fact, both the enhancement of mIPSC amplitude by bath application of 3 mM ascorbic acid, and the reversibility of this effect upon wash-out, were statistically significant (Control (0 mM Asc) = 15.42 ± 2.51 pA, 3 mM Asc = 18.45 ± 3.23 pA, Wash (0 mM Asc) = 15.62 ± 2.48 pA; Repeated Measures ANOVA, n=5, p=0.014; Tukey's Multiple Comparison Test, Control (0 mM) vs. 3 mM Asc, p<0.05; 3 mM Asc vs. Wash (0 mM Asc), p<0.05; Fig. 3.8C, left). These results show that ascorbic acid potentiation is effective at local GABA concentrations in the synaptic cleft seen under physiological conditions.

Native and recombinant $GABA_A$ receptors can be modulated by a number of redox agents whose effects depend on receptor subunit composition. In particular, the presence of the g_2 subunit was shown to reduce the sensitivity of $GABA_A$ receptors to exogenous and naturally occurring redox reagents (Amato et al., 1999; Pan et al., 2000). Thus, redox modulation at GABAergic synapses is predicted to vary throughout the

central nervous system depending on the $GABA_A$ receptor subtypes expressed. In order to examine the ascorbic acid sensitivity of $GABA_A$ receptors with known subunit compositions, two combinations of recombinant $GABA_A$ receptors were transfected in HEK cells, namely $a_1b_2g_2$ and a_1b_2 receptors. In fact, expression of α_1, α_2, α_3, β_1, β_2, β_3, γ_2 and δ subunits has been previously reported in retinal neurons (Wassle et al., 1998; Koulen, 1999; Zhang et al., 2003). $GABA_A$ receptor-mediated inward currents recorded in HEK cells at -60 mV were significantly enhanced by extracellular application of ascorbic acid over the entire range of concentrations tested (0.5 to 10 mM). Responses mediated by $GABA_A$ receptors lacking the γ_2 subunit were strongly potentiated by ascorbic acid (up to a ~600% by 10 mM), whereas responses mediated by $\alpha_1\beta_2\gamma_2$ receptors were also effectively increased by ascorbic acid, but to a lesser extent (up to a ~200% by 10 mM). Data were summarized in Fig. 3.9. These results indicate that ascorbic acid can produce on $GABA_A$ receptors similar effects to those exerted by other redox agents, and that $GABA_A$ receptor subtypes show a differential sensitivity to ascorbic acid modulation.

Discussion

We have shown a remarkably potent modulation of retinal and heterologous $GABA_C$ and $GABA_A$ receptors by physiologically relevant concentrations of ascorbic acid. Surprisingly, we believe that the present findings are the first to demonstrate that this ubiquitous and endogenous redox agent can regulate the function of cys-loop receptors.

Effects of ascorbic acid on $GABA_C$ receptors

The potentiating effects of ascorbic acid on native and recombinant $GABA_C$ receptors were similar to those shown by many reducing agents acting on different ionotropic

GABA receptors and other cys-loop receptors (Bouzat et al., 1991; Ruiz-Gomez et al., 1991; Pan et al., 1995; Amato et al., 1999; Pan et al., 2000; Calero and Calvo, 2008). Efficacy of ascorbic acid on retinal $GABA_C$ responses appears to be relatively lower than on responses mediated by $GABA\rho_1$ receptors, probably because experiments in the retina required higher concentrations of GABA to counteract the action of GABA transporters and extracellular diffusion. Additionally, differences may be due to variations in the sensitivity to ascorbic acid among receptors from different species (fish vs. human), the possible existence of heteromeric receptors in the retina (e.g: $GABA_C$ receptors containing ρ_2 or ρ_3 subunits), the interaction of native receptors with accessory subunits or regulatory proteins not present in oocytes, or endogenous redox buffers that could be absent or altered in heterologous systems.

Mechanisms underlying the modulation of $GABA_C$ receptors by ascorbic acid

We showed that the cys-loop residues C177 and C191, along with H141, all located near the extracellular agonist-binding site, take part in the modulation of $GABA_C$ receptors by ascorbic acid. The shift to the left produced by ascorbic acid on the $GABA\rho_1$ receptor D-R curve (Fig. 3.5A) can be explained by a decrease in the energy barrier for GABA activation induced by this agent. Ascorbic acid could bind to or modify one or more sites capable of allosterically modulating single-channel properties, for example by inducing an increase in GABA affinity that involves H141. In addition, to describe the simultaneous increase observed in the maximal response, which is more likely mediated by a redox modification of C177 and C191, a possibility is that ascorbic acid acts to favour the conversion from the last GABA-bound closed state to the open state (Goutman *et al.*, 2005). Alternatively, ascorbic acid could induce the channels to transition towards additional open states in which the receptor adopts lower energy

conformations with higher open probabilities. We found that GABAρ_1 channel deactivation from open states was not altered in the presence of ascorbic acid (Table 1a), which suggests that the first or the second alternatives are more likely. However, a combination of different mechanisms could also occur. Further analysis, including binding experiments, single channel recording, and kinetic studies, is necessary to address these questions.

We also showed that the intracellular application of ascorbic acid prevents run-down of GABA$_C$ receptor-mediated inward currents at the Mb presynaptic terminals. There are many intracellular targets of redox modulation, and mitigation of general oxidative stress is likely to also prolong the viability of a cell following dialyzation by the patch pipette. Run-down of GABA$_C$ currents during the course of a 15-20 min patch-clamp recording has been shown to depend on PKC phosphorylation, and to be inhibited by addition of phosphatases to the intracellular solution (Feigenspan and Bormann, 1994). Thus, a candidate could be the potential interaction of ascorbic acid at these signaling pathways. Interestingly, recent studies showed that the generation of reactive oxygen species (ROS) can induce run-down of currents mediated by neuronal acetylcholine receptors (nAChRs) (Campanucci et al., 2010). This run-down is triggered by ROS-induced oxidation of C239, an intracellular cysteine residue conserved in many nAChR subunits (e.g: α_3, α_4, β_2 and β_4) that forms a ring located at the M1-M2 linker near the inner mouth of the channel pore. Based on these data, and on the fact that ρ subunits in GABA$_C$ receptors also carry an intracellular cysteine (C364) at the M3-M4 linker, the prevention of GABA$_C$ current run-down exerted by ascorbic acid might act as a protective mechanism against ROS actions.

Effects of ascorbic acid on GABA$_A$ receptors

Redox modulation of GABA$_A$ receptors has been demonstrated in heterologous systems and in different areas of the CNS, including the retina (Pan *et al.*, 1995; Amato *et al.*, 1999). GABA$_A$ receptors from retinal ganglion cells are significantly inhibited by oxidants and potentiated by reducing agents (Pan *et al.*, 1995), but studies in retinal bipolar cells were lacking. We show that GABA$_A$ receptors located on the presynaptic terminals of Mb bipolar cells, which likely contain the γ_2 subunit (Wassle et al., 1998), can be modulated by ascorbic acid. This is a significant finding, because it directly shows that ascorbic acid can potentiate synaptic GABA$_A$ mediated currents in intact retinal tissue. Additionally, experiments performed on recombinant $\alpha_1\beta_2\gamma_2$ and $\alpha_1\beta_2$ GABA$_A$ receptors showed that ascorbic acid actions depend on subunit composition. GABA$_A$ receptors containing the γ_2-subunit had a decreased sensitivity to ascorbic acid (Fig. 3.9), in agreement with the reduced sensitivity to redox agents exhibited by hippocampal, cerebellar and ganglionic GABA$_A$ receptors (Amato *et al.*, 1999).

Potential physiological relevance of the modulation of GABA$_C$ receptors by ascorbic acid

Ascorbic acid is highly concentrated in the retina, both in extracellular (200–500 μM) and intracellular ($\leq$10 mM) compartments (Rose and Bode, 1991; Rice, 2000; Castro et al., 2001; Hediger, 2002; Hosoya et al., 2004). During and after neuronal activity, local levels of ascorbic acid surrounding retinal bipolar neurons can reach millimolar values due to SVCT2-mediated sodium-dependent extrusion (Portugal *et al.*, 2009). GABAρ_1 receptor potentiation by ascorbic acid can be significant at extracellular concentrations as low as 0.3 mM, with effects becoming substantial above 0.7 mM (Fig. 3.4B). Meanwhile, the activity of retinal GABA$_C$ receptors was considerably increased by extracellular ascorbic

acid in the low millimolar range (3 mM) (Fig. 3.1 and 3.2). Ascorbic acid effects on GABA$_C$ receptors strongly depended on GABA concentration. As GABA$_C$ receptors show relatively high affinity for GABA (compared to GABA$_A$ receptors), ascorbic acid modulation at low GABA concentrations could be ideally located within the dynamic range of ion channel activation. If so, the regulation of retinal GABA$_C$ receptors would be highly dependent on local ascorbic acid release and instantaneous extracellular GABA concentration. In particular, extrasynaptic receptors, which would presumably see lower concentrations of GABA, might be more powerfully modulated by ascorbic acid.

Tonic inhibition provides a constant shunt to the Mb terminal, which likely acts to prevent release in the absence of strong, high frequency inputs, and activation of the standing leak current is closely controlled by the GABA transporter GAT-1 (Hull *et al.*, 2006a). Reciprocal inhibition, which occurs when release of glutamate from the Mb terminal triggers direct GABA feedback from local amacrine cell presynaptic boutons, is comprised of a fast GABA$_A$ component and a slow, sustained GABA$_C$ component (Vigh and von Gersdorff, 2005). Reciprocal inhibition directly controls the duration and intensity of glutamate release from the Mb terminal. Finally, lateral inhibition, elicited when stimulation of a parallel bipolar cell pathway triggers unidirectional GABA release from a local amacrine cell bouton onto both GABA$_A$ and GABA$_C$ receptors on the Mb terminal, may act to shape the offset of bipolar cell light responses (Chavez et al., 2010). Strong modulation of tonic, reciprocal, and lateral inhibition at Mb terminals by ascorbic acid is likely to shape ganglion cell responses via control of glutamate release. However, given the previously described effects of ascorbic acid on T-type Ca^{2+} channels (Nelson et al., 2007) and K$^+$ channels (Fan and Yazulla, 1999), mechanisms of modulation of retinal physiological responses by this agent might be more complex.

We showed here that ascorbic acid enhanced standing leak currents and responses activated by local GABA puffs in the presence of gabazine, both of which are

112

mediated by $GABA_C$ receptors at the presynaptic terminals of retinal Mb bipolar cells. This suggests that ascorbic acid modulation can occur either during acute (similar to reciprocal or lateral synaptic inhibition), sustained (tonic standing leak current), or strong (under conditions of high rate of GABA release) activation of $GABA_C$ receptors. Additionally, ascorbic acid could be involved in a "negative feedback" phenomena following strong bipolar cell depolarization. This depolarization would cause strong glutamate release, which in turn would stimulate release of ascorbic acid into the extracellular space (Portugal et al., 2009). Increased concentrations of extracellular ascorbic acid can potentiate $GABA_C$ and $GABA_A$ mediated currents, enhancing local inhibition. In this context, ascorbic acid effects on both $GABA_A$ and $GABA_C$ responses would be consistent with the effects of glutamate on SVCT-2 mediated ascorbic acid extrusion. Unfortunately, the subcellular localization of SVCT-2 in neurons or glial cells still is unknown (Castro et al., 2001; Harrison and May, 2009). In conclusion, although the precise physiological role that ascorbate plays in the regulation of GABAergic neurotransmission needs to be further investigated, our results clearly indicate that ascorbic acid can act as an important endogenous modulator of ionotropic $GABA_C$ and $GABA_A$ receptors in the retina and probably also in other areas of the CNS.

Table 3.1

a. Effects of ascorbic acid and its analogs on GABAρ_1 responses

Compound	% Potentiation	n	τ_{ACT} (s)	τ_{DEACT} (s)	n
Control (GABA 0.3 μM)	-	6	24.8 ± 1.6	23.5 ± 3.8	6
3 mM Asc	139.5 ± 87.5**	7	22.6 ± 2.6	28.1 ± 3.3	6
3 mM D-isoAsc	33.5 ± 12.5*	4	28.5 ± 2.5	33.4 ± 1.9	6
3 mM DHA	-1.6 ± 4.2	3	26.1 ± 2.8	32.0 ± 2.8	6
1.5 mM Asc(Ca)$_2$	7.4 ± 4.8	6	22.5 ± 2.5	27.4 ± 4.3	4

b. Dose-response curves parameters

	EC$_{50}$ (μM)	n Hill	n
Control	0.74 ± 0.01	1.58 ± 0.04	5-10
3 mM Asc	0.49 ± 0.01*	1.88 ± 0.07	5-10
Control	1.52 ± 0.04	2.24 ± 0.05	4
30 μM NEM	1.29 ± 0.02	2.24 ± 0.10	4
30 μM NEM + 3 mM Asc	0.75 ± 0.01	2.44 ± 0.19	4
Control	0.86 ± 0.10	2.58 ± 0.30	3
30 μM NEM	0.78 ± 0.09	2.32 ± 0.10	3
30 μM NEM + 2 mM DTT	0.74 ± 0.06	2.04 ± 0.08	3
H141D	1.76 ± 0.21	3.41 ± 0.61	10
H141D + 3 mM Asc	2.07 ± 0.32	2.94 ± 0.38	5
H141D + 30 μM NEM	1.40 ± 0.16	3.24± 0.16	4
H141D + 30 μM NEM + 3 mM Asc	1.46 ± 0.24	3.48 ± 0.28	4

a. Potentiation (%) produced by ascorbic acid and its different analogs on GABAρ_1 responses and values obtained for kinetic parameters in the presence of the different compounds (**p<0.01 and *p<0.04)

b. Parameters of the D-R curves for GABA, performed for GABA ρ_1 wt and GABA ρ_1 H141D in the absence or presence of the different agents (*p<0.03).
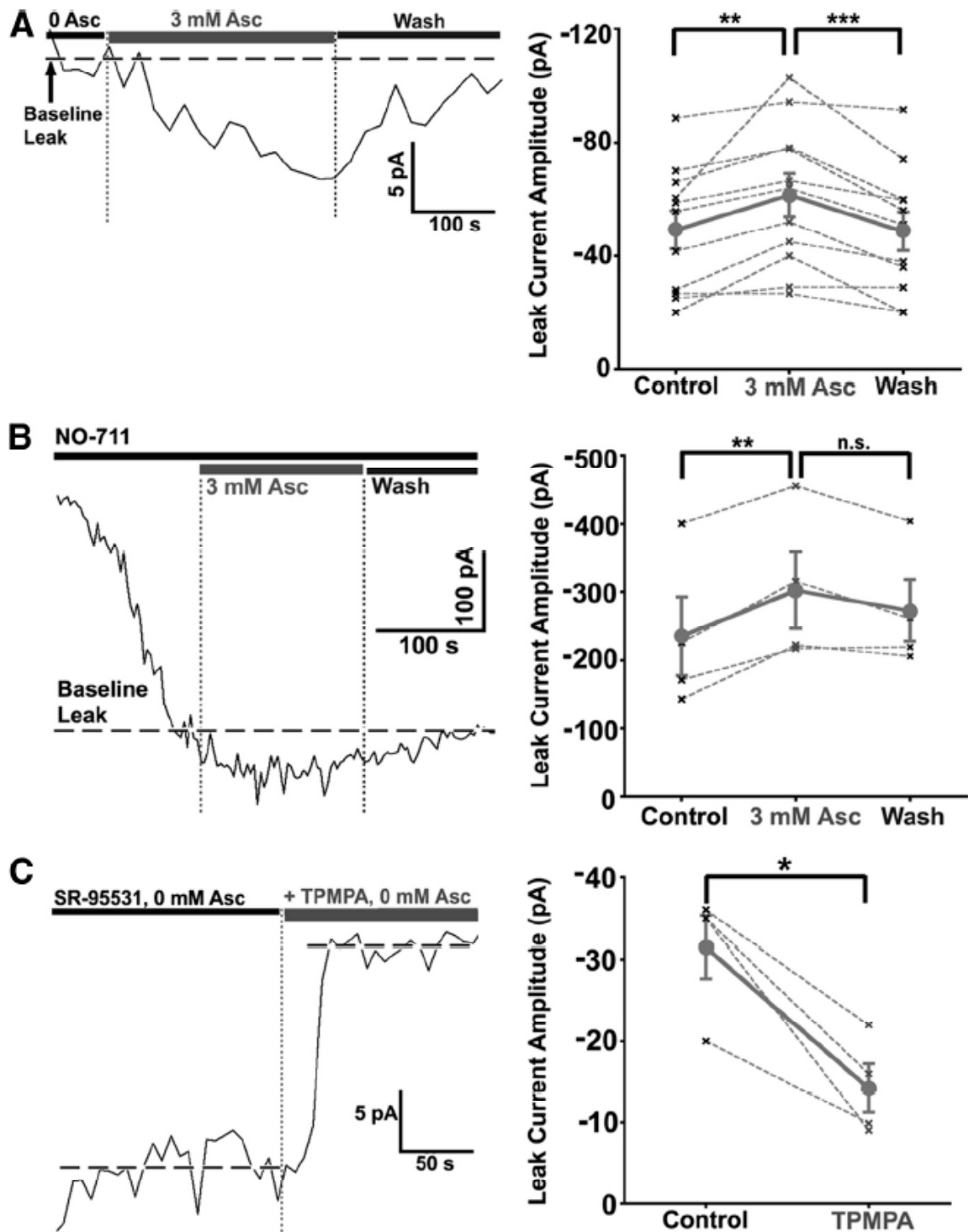
Figure 3.1: Ascorbic acid reversibly enhances $GABA_C$ mediated standing leak current in axotomized Mb bipolar cell presynaptic terminals. **(A)** $GABA_C$ leak current is enhanced by bath application of ascorbic acid (Asc). Whole-cell voltage clamp recording of an Mb terminal in the presence of 25 μM SR-95531 shows a $GABA_C$ mediated leak current of -

115

52.5 pA at -60 mV (left). The leak current was enhanced by 8 pA following bath application of 3 mM ascorbic acid. During wash (0 mM Asc), the leak current was reduced to nearly its original level. Ascorbic acid significantly and reversibly enhanced $GABA_C$ mediated leak current in the absence of NO-711 (n=11; right). The mean for all cells with SE shown in dark gray (circles) and is connected by a solid line; data from each single cell are shown in light gray ("x") and connected by dashed line. **(B)** Whole-cell voltage clamp recording of an Mb terminal in the presence of 25 μM SR-95531 and 3 μM NO-711 shows a $GABA_C$ mediated leak current of -400.6 pA at -60 mV (left). The leak current was enhanced by 55 pA following bath application of 3 mM Asc. During wash (0 mM Asc, 3 μM NO-711), the leak current was reduced to its original level. Ascorbic acid significantly enhanced $GABA_C$ mediated leak current in the presence of 1-3 μM NO-711 (n=4; right). Washout was nearly significant. **(C)** Standing leak current consists of both TPMPA-sensitive and TPMPA-insensitive components. Whole-cell recording (left) of an axotomized Mb1 terminal voltage-clamped at -60 mV shows a leak current of -34.7 pA that is stably reduced to -16.4 pA by bath application of 300 μM TPMPA in the presence of 0 mM ascorbic acid. Addition of 300 μM TPMPA in the presence of 25 μM SR95531 and 0 mM ascorbic acid produced a statistically significant reduction in leak current (n=4; right). $p<0.05$, $p<0.01$, $p<0.001$, n.s. $p>0.05$; all statistical tests reflect a repeated-measures design; all errors are expressed as ± SE, unless otherwise noted.

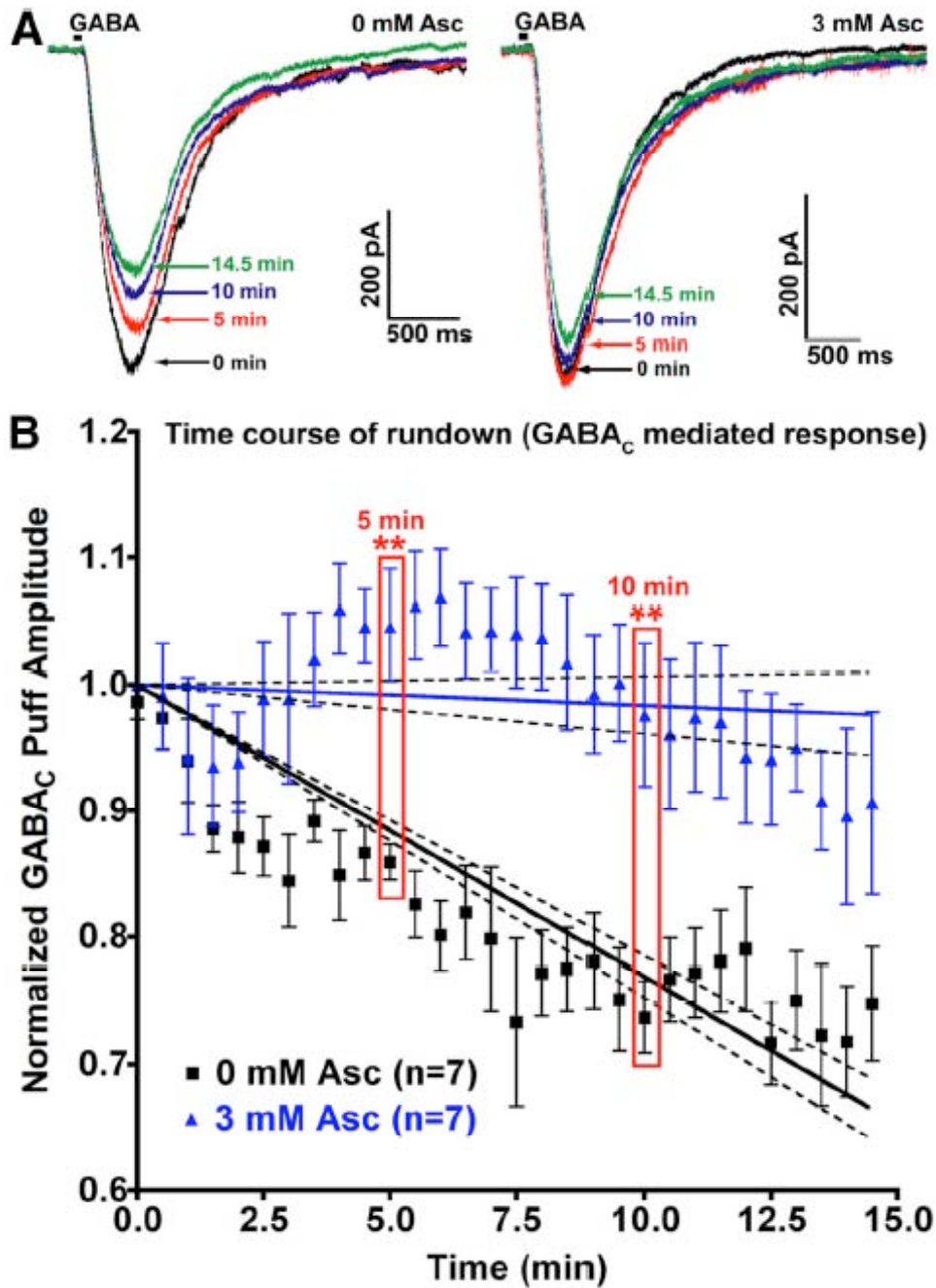**Figure 3.2:** Run-down of $GABA_C$ mediated responses to puff application of GABA in axotomized Mb bipolar cell presynaptic terminals is significantly slowed and/or prevented by the presence of intracellular and extracellular ascorbic acid. **(A)** Puff application of GABA (25 ms duration, indicated by black bar) was performed every 30 s for 15 min to assess the degree of run-down of the resulting $GABA_C$ mediated currents. Perfusion

solution contained 25 μM SR-95531 (a GABA$_A$ antagonist) in all cases. Some experiments were performed with 25 μM SR-95531 in the puff pipette, with no change in run-down kinetics (not shown). An individual example of GABA$_C$ current run-down shows that, in the absence of ascorbic acid either in the puff pipette, patch-clamp pipette, or perfusion solution, 25 ms puff application of 200 μM GABA with a 30 s (ISI) resulted in a 27.3% run-down in current amplitude over 14.5 min (left). Right panel: same as left, except that in this example 3 mM ascorbic acid was included in the puff pipette, patch-clamp pipette, and perfusion solution. Under these conditions, run-down of GABA$_C$ current amplitude over 14.5 min was 8.7%. Over the first 5 min, GABA$_C$ current amplitude increased by 3.7%. **(B)** The GABA puff experiments from (A) were repeated in the presence (n=7) or absence (n=7) of 3 mM ascorbic acid in the puff pipette, patch pipette, and perfusion solution, with 25 μM SR-95531 in the perfusion solution (and, in some cases, in the puff pipette). Shown are mean normalized GABA$_C$ current amplitudes for each 30 s interval at which GABA was puff applied for 25 ms. Error bars indicate mean ± SEM. The slope of run-down for each condition was fit with linear regression (solid lines). Dashed lines indicate 95% confidence interval boundaries for each condition. The effect of ascorbic acid on run-down was highly significant at 5 and 10 min. **$p<0.01$; all errors expressed as ± SE, unless otherwise noted.
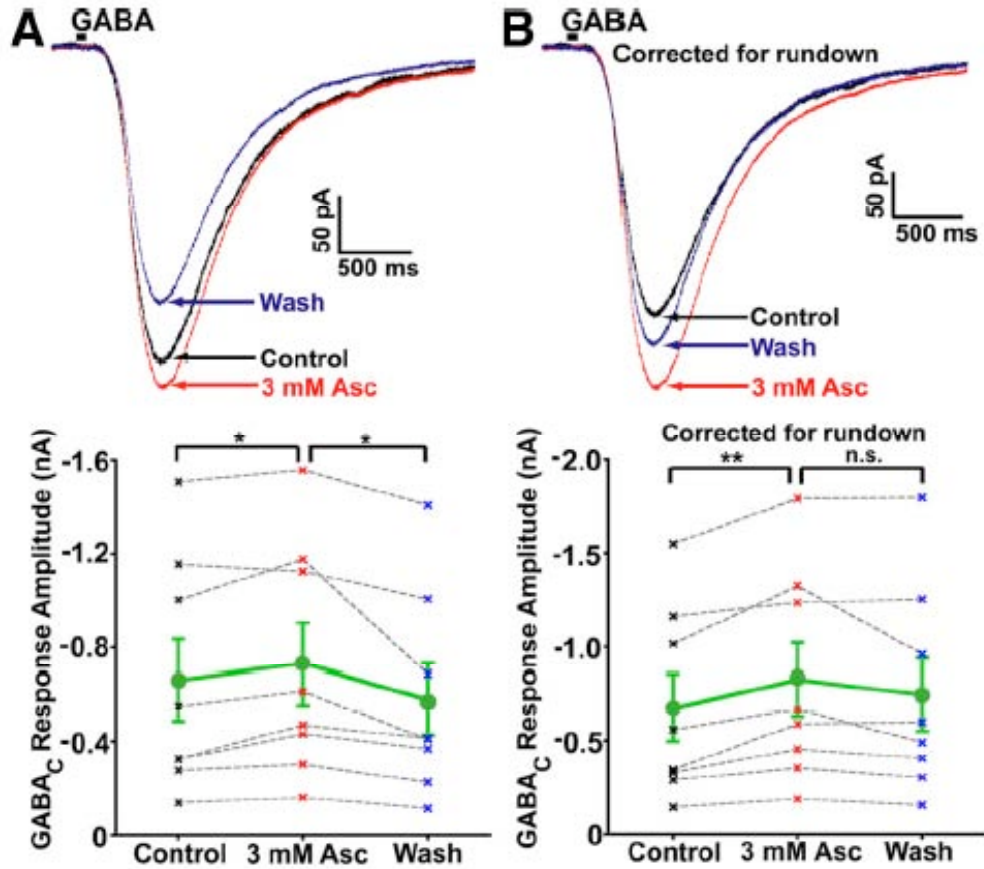
Figure 3.3: Response to puffing GABA directly onto axotomized Mb bipolar cell presynaptic terminals is enhanced by bath application of ascorbic acid. **(A)** Puff application of 1 mM GABA (25 ms duration, indicated by black bar) directly onto an axotomized Mb bipolar cell presynaptic terminal in the presence of 25 μM SR-95531 produced (upper) a large $GABA_C$ mediated inward current (black trace). Bath application of 3 mM ascorbic acid (red trace) increased the amplitude of this current in a reversible manner (washout; blue trace). Each trace is the average of three successive stimulations with an inter-trace interval of 20 s. Summary data (bottom; n=8) showed a significant and reversible increase in puff response amplitude caused by 3 mM ascorbic acid. Mean for all cells with SE shown in green (circles), data from each single cell ("x") connected by gray dashed line, control data points (0 mM Asc) shown in black, 3 mM

119

Asc shown in red, wash (0 mM Asc) shown in blue. **(B)** Run-down normalization of GABA$_C$ currents from cell in (A), calculated using mean time after initial GABA puff and the linear run-down regressions from Fig. 2B, show potentiation of nearly 25% in the presence of 3 mM ascorbic acid, with a nearly complete washout in 0 mM Asc (upper). Summary of corrected data (bottom; n=8) showed a significant increase in puff response amplitude caused by bath application of 3 mM ascorbic acid *$p<0.05$, **$p<0.01$, n.s. $p>0.05$; all statistical tests reflect a repeated-measures design; all errors are expressed as ± SE, unless otherwise noted.
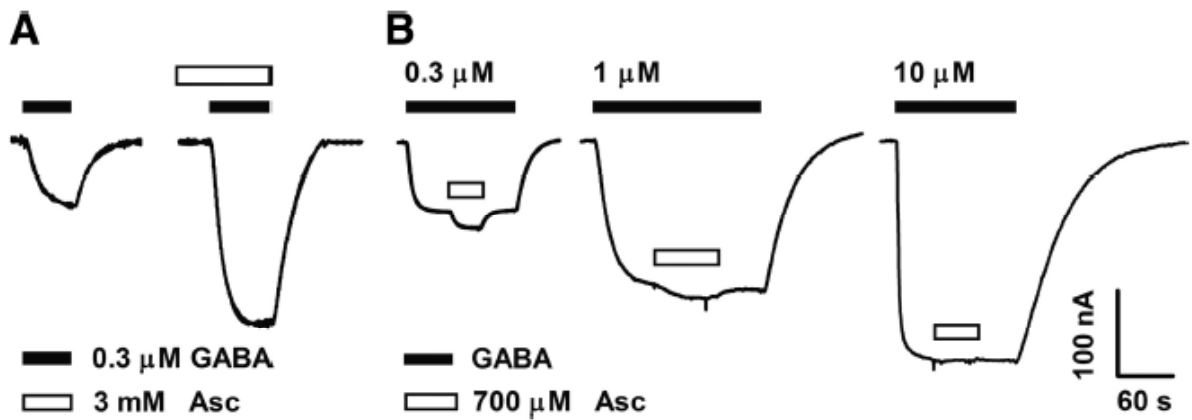
Figure 3.4: Homomeric ρ_1 $GABA_C$ receptor function is enhanced by ascorbic acid. Representative traces of ionic (Cl^-) currents elicited by different GABA concentrations in oocytes expressing homomeric GABAρ_1 receptors. Scale bars indicate current amplitude (y-axis) and time (x-axis). For this and the subsequent figures, oocytes were voltage-clamped at -70 mV. **(A)** GABAρ_1 responses recorded before (left, control) and after the application of 3 mM ascorbic acid (right). Potentiation of GABAρ_1 responses by ascorbic acid was 162 ± 22.6% (n=3). **(B)** Ionic currents elicited by increasing concentrations of GABA (0.3, 1 and 10 μM) were also enhanced during concurrent applications of 700 μM ascorbic acid.
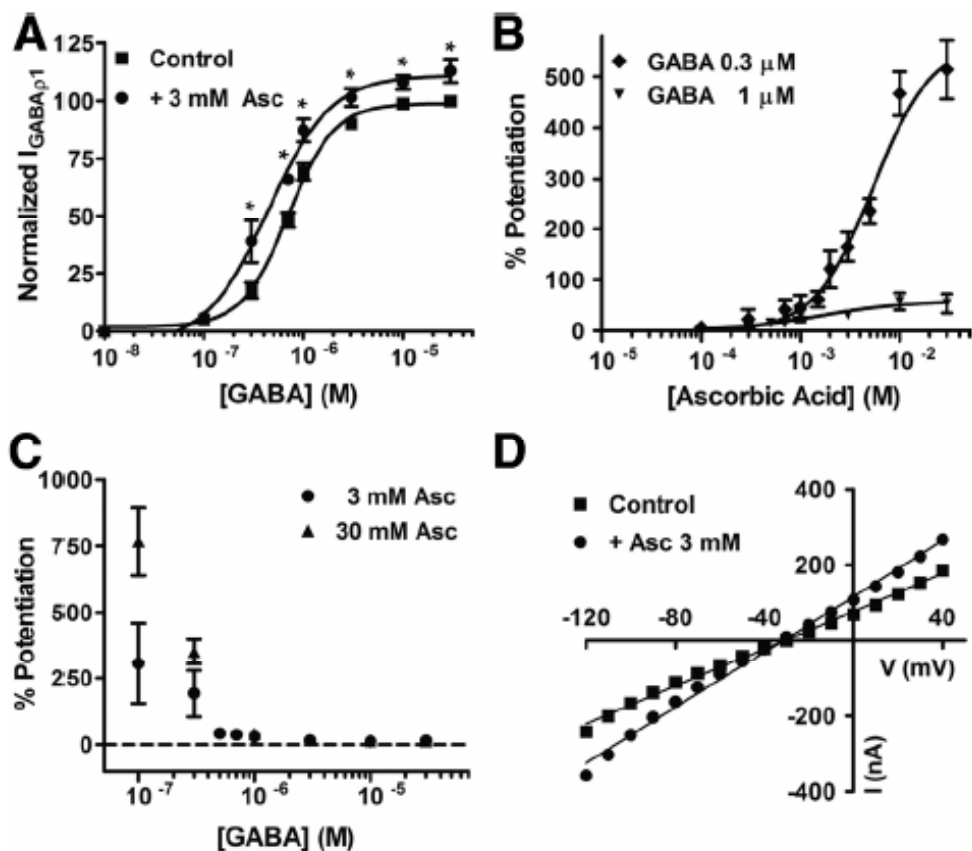
Figure 3.5: Analysis of ascorbic acid effects on GABAρ_1 receptor function. **(A)** Dose–response (D-R) curves for GABA performed in the presence or absence of ascorbic acid. Response amplitudes were expressed as fraction of maximal GABA-evoked currents (30 μM GABA). **(B)** Dose-effects curves for ascorbic acid acting on GABAρ_1 responses. Data were normalized to control values, obtained in the absence of ascorbic acid, for two different GABA concentrations. All the points tested >100 μM were significantly different from control. **(C)** Degree of potentiation of the GABAρ_1 responses by ascorbic acid for increasing concentrations of GABA. **(D)** I–V relationships of the GABAρ_1 responses measured in the presence or absence of ascorbic acid.
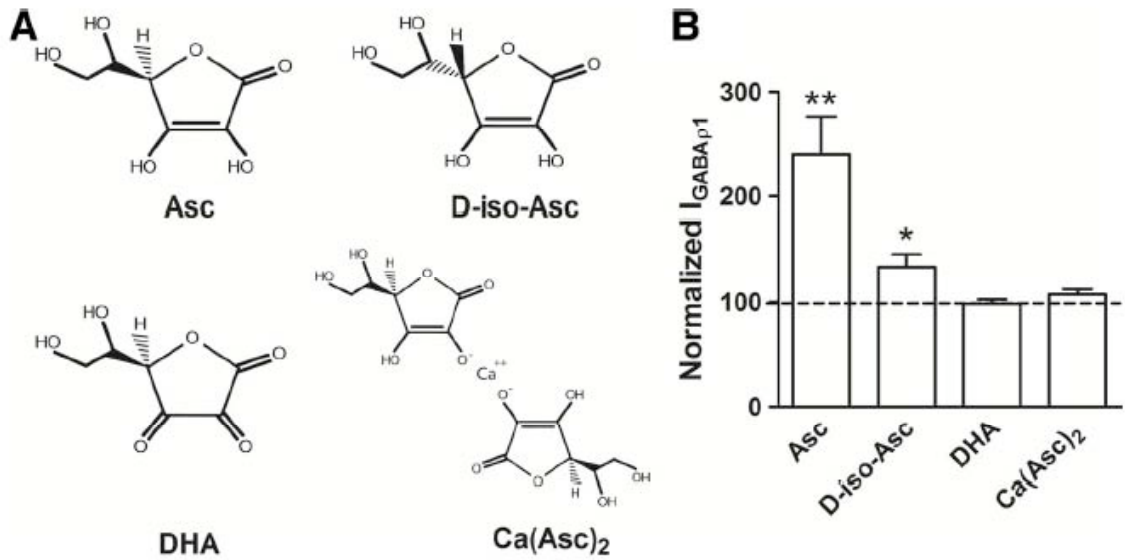
Figure 3.6: Effects of different ascorbic acid analogs on GABAρ_1 receptor function. **(A)** Chemical structures of the diverse compounds used. **(B)** Histogram summarizing the values obtained for GABAρ_1 responses evoked by 0.3 µM GABA recorded before (control, dotted line) and after exposure to the different ascorbic acid analogs (n=4).
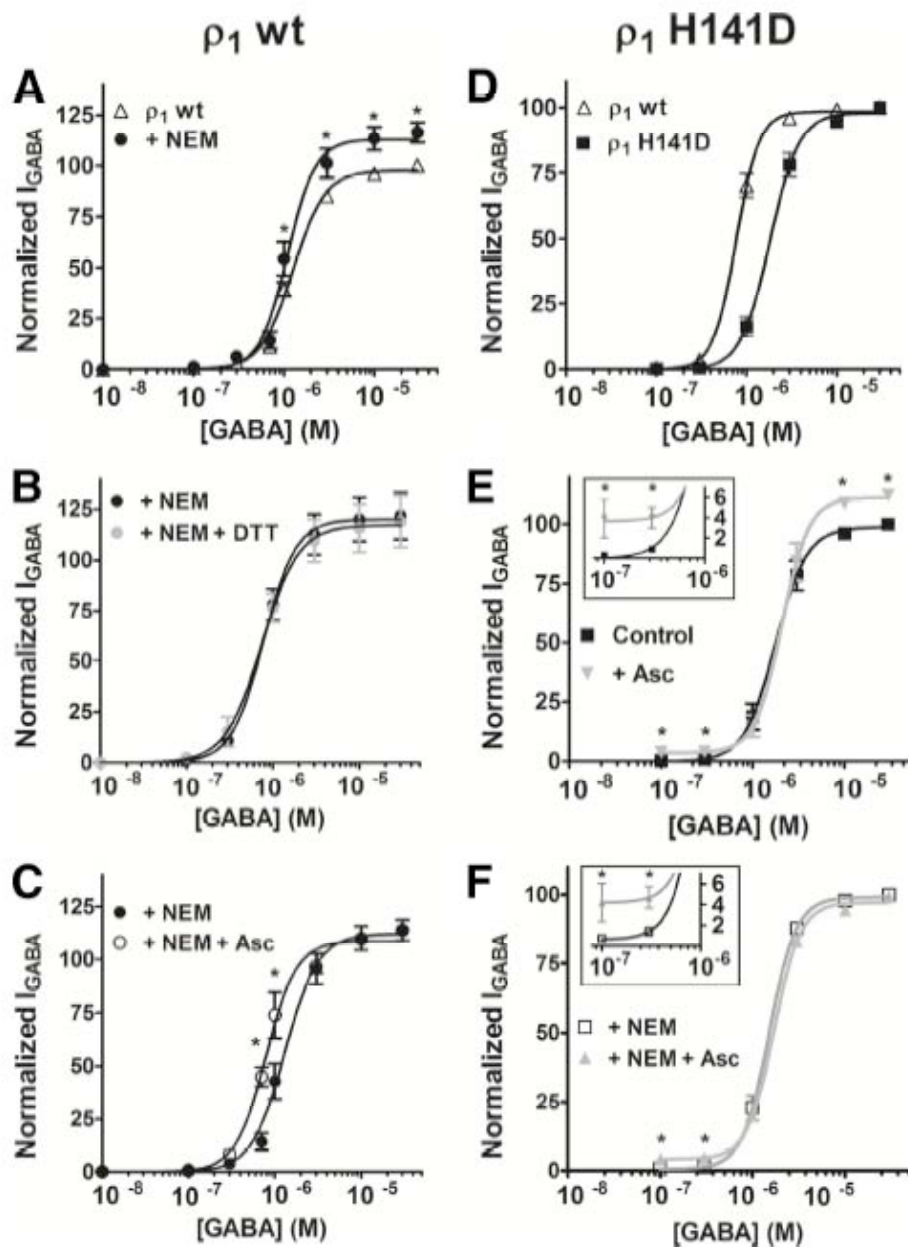
Figure 3.7: Identification of aminoacid residues involved in the modulation of homomeric ρ_1 GABA$_C$ receptors by ascorbic acid. **(A)** The irreversibly methylation of C177 and C191 at the Cys-loop, by pre-treatment of oocytes with 30 μM NEM, produced similar effects to those shown by ascorbic acid on D-R curves for GABA. **(B)** NEM pre-treatment completely abolished the potentiation of GABAρ_1 responses induced by 2 mM DTT. **(C)** NEM pre-treatment partially prevented the potentiation of GABAρ_1 responses by 3 mM

ascorbic acid. **(D)** D-R curves for GABA performed on wild-type GABAρ_1 and mutant GABAρ_{1H141D} receptors. **(E)** Mutation of H141 to D at the ρ_1 subunit partially prevented the potentiating actions of ascorbic acid. Effects of 3 mM ascorbic acid on D-R curves for GABA performed on GABAρ_{1H141D} receptors. Ascorbic acid significantly enhanced maximal responses and currents evoked by very low GABA concentrations (inset), but failed to induce a leftward shift in the D-R curve (as that observed in C), indicating that the H141 is critical for ascorbic acid modulatory actions. **(F)** NEM pre-treatment abolished the potentiation induced by ascorbic acid on maximal responses mediated by GABAρ_{1H141D} receptors, indicating that they are more likely mediated by C177 and C191, but effects at very low GABA concentrations were not prevented by NEM (inset). Response amplitudes were expressed as fraction of the 30 μM GABA-evoked currents (maximal response). Each point represents the mean and SEM of the responses obtained from 4-6 oocytes. Notice that many of the SE bars are hidden by the symbols.
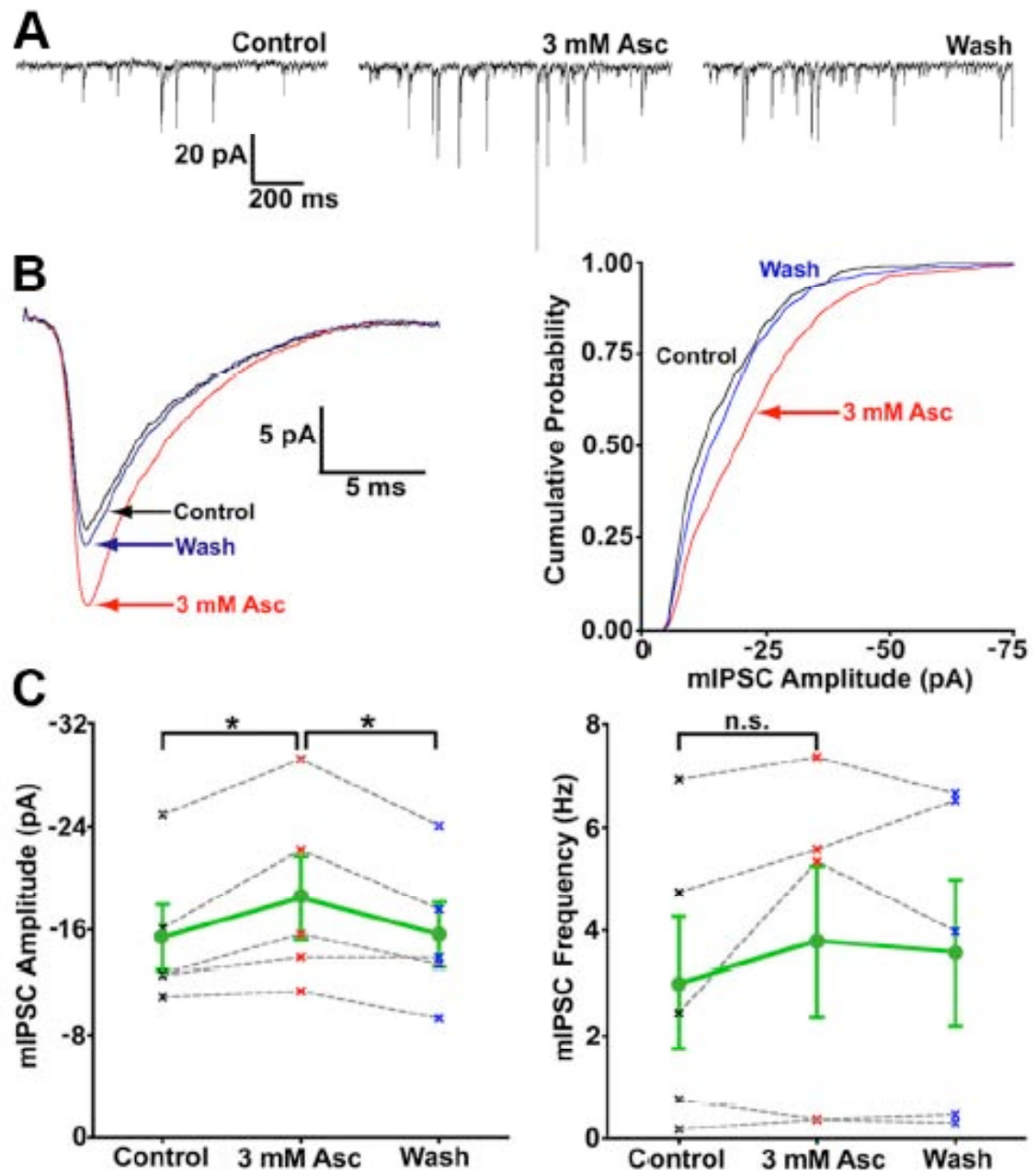
Figure 3.8: The amplitude of GABA$_A$ mIPSCs is enhanced by bath application of ascorbic acid. **(A)** Excerpts (1.3 s each) from continuous records of mIPSCs from a single axotomized Mb1 terminal (at least 120 s per condition) in the presence of 150 μM TPMPA (GABA$_C$ antagonist), 10 μM NBQX, 50 μM L-AP5, and 1 μM TTX show that 3 mM ascorbic acid reversibly increased the amplitude of GABA$_A$ mIPSCs without

126

significantly increasing mIPSC frequency. **(B)** The amplitude of the mean IPSC waveform of GABA$_A$ mIPSCs was reversibly enhanced by nearly 30% (left) following bath application of 3 mM ascorbic acid (same cell as in (A)). The mIPSC amplitude cumulative probability distribution (bin = 1 pA) for Control (0 mM Asc, count=353), 3 mM ascorbic acid (count=770), and Wash (0 mM Asc, count=574) conditions (right) showed a distinct, reversible rightward shift (larger amplitudes) in cumulative probability in the presence of 3 mM ascorbic acid. **(C)** Summary of data for all cells (n=5) shows a significant, reversible increase in GABA$_A$ mIPSC amplitude (left), with no significant effect on mIPSC frequency (right), following bath application of 3 mM ascorbic acid. Mean for all cells with SE shown in green (circles), data from each single cell ("x") connected by gray dashed line, control data points (0 mM Asc) shown in black, 3 mM Asc shown in red, wash (0 mM Asc) shown in blue. *p<0.05; n.s, p>0.05; all statistical tests reflect a repeated-measures design; all errors are expressed as ± SE, unless otherwise noted.
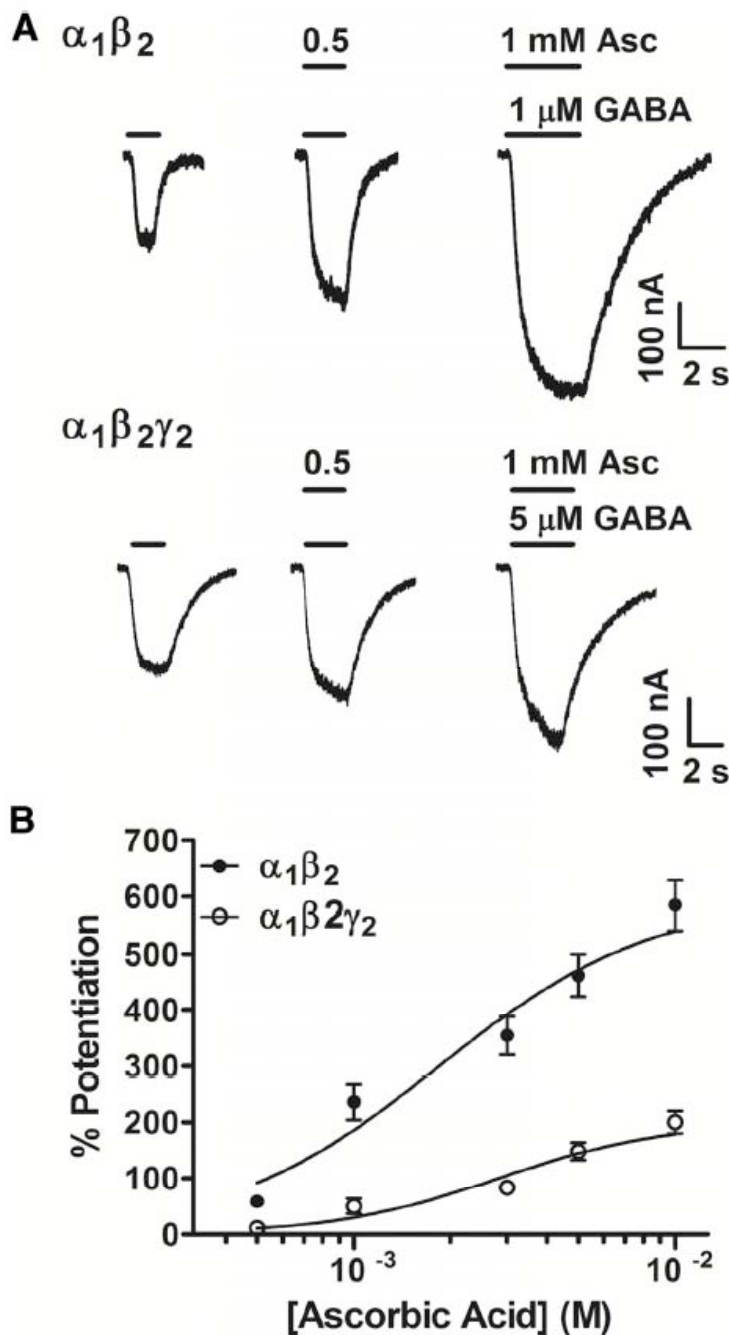
Figure 3.9: Potentiation of the $\alpha_1\beta_2$ and $\alpha_1\beta_2\gamma_2$ GABA$_A$ receptor function by ascorbic acid. **(A)** Representative traces of ionic (Cl$^-$) currents mediated by a_1b_2 and $\alpha_1\beta_2\gamma_2$ GABA$_A$ receptors expressed in HEK cells. Inward GABA$_A$ currents were elicited by bath applications of 1 or 5 μM GABA (the corresponding EC$_{50's}$ for GABA showed by $\alpha_1\beta_2$ and $\alpha_1\beta_2\gamma_2$ GABA$_A$ receptors respectively) and recorded by whole-cell voltage clamp at -60 mV. GABA$_A$ responses mediated by both $\alpha_1\beta_2$ and $\alpha_1\beta_2\gamma_2$ GABA$_A$ receptors were significantly enhanced in the presence of 0.5 or 1 mM ascorbic acid. **(B)** Dose-effect curves for ascorbic acid actions on $\alpha_1\beta_2$ and $\alpha_1\beta_2\gamma_2$ GABA$_A$ receptors (n=3; curves performed at the corresponding EC$_{50}$ values). Data were normalized to control values, obtained in the absence of ascorbic acid.

128

SUMMARY AND CONCLUSIONS

The main results of this thesis are best understood in the context of three important, general principles of retinal processing: (i) The responses of GCs, and to a large extent BCs, are based on differential light stimulation of the center (excitatory) and surround (inhibitory) areas of their receptive fields, which are shaped by lateral feedback and feedforward inhibition in both the outer and inner retina, (ii) The retina primarily encodes the temporal and spatial contrast, or variance about the mean, of light stimulation at the outer surface of the PR layer, and adapts to (or effectively subtracts) the mean light level (or, for some computations, the contrast as well) across different timescales, and (iii) GC responses exhibit predictive coding, wherein low-information content stimulus regularities are subtracted from the output, likely via dynamic adjustment of the synaptic strength of feedback (reciprocal or lateral) and feedforward (pathway-specific or crossover) inhibitory connections in the IPL. Here, we used a goldfish retinal slice preparation that allowed us to record directly from axotomized presynaptic terminals of ON-type, mixed rod/cone input (Mb) BCs and characterize light-evoked lateral inhibition, in the form of L-IPSCs, that was mediated by GABA receptor populations with different kinetics.

Our principle novel findings were the following: (i) L-IPSCs at this ON BC terminal originated from both ON and OFF pathways and were mediated entirely by $GABA_AR$ and $GABA_CRs$ at non-reciprocal synapses, and ON L-IPSCs were enhanced by AMPAR blockade while OFF L-IPSCs were highly dependent on the activation of voltage-gated Na^+ channels (**Chapter 1**); (ii) ON L-IPSCs have onset latencies of ~50 ms, exhibit paired-pulse STD that recovers over 2 s, and decelerate (or "delay") at short paired-pulse intervals (PPIs), while OFF L-IPSCs have onset latencies of ~120 ms, exhibit STD at PPIs < 1 s and STF at PPIs between 1 and 2 s, and accelerate (or

"advance" at short PPIs (**Chapter 2**); (iii) Ascorbic acid (Asc) in the retina is an endogenous positive allosteric modulator of $GABA_AR$ and $GABA_CRs$ that may exhibit activity dependent regulation under both physiological and pathological conditions (**Chapter 3**). Together, these results both describe a retinal microcircuit for lateral inhibition that exhibits dynamic, frequency-dependent synaptic plasticity, and provide a novel mechanistic scheme for allosteric modulation of the post-synaptic receptors that mediate the response. Furthermore, this microcircuit generates contrast information at a BC presynaptic terminal, is involved in the refinement of center-surround receptive field organization, and exhibits a combination of adaptation and sensitization that may contribute to effective predictive coding and spike onset latency coding in GC populations (Hosoya et al., 2005; Gollisch and Meister, 2008; Kastner and Baccus, 2011).

Expected effects of L-IPSC STP on Mb, GC, and AC light responses

Before examining specific novel results in detail and discussing future experiments that need to be done, it is necessary to carefully consider the effects that STP of ON and OFF L-IPSCs are expected to have on Mb glutamate release, GC responses, and, to draw parallels with the RBC to AII circuit in mammalian retina, the responses of ACs post-synaptic to Mb terminals that may distribute signals from rod PRs to diverse classes of cone BC.

Depending on the input resistance, membrane potential (-55 to -40 mV), and degree of L-type Ca^{2+} channel inactivation at an individual Mb terminal, light stimulation of the Mb center receptive field will likely evoke either an EPSP with a large transient component (up to ~20 mV) and a smaller sustained component (up to ~10 mV) at a latency of ~50 ms at the terminal (Joselevitch and Kamermans, 2007), or a large, regenerative Ca^{2+} spike at a latency of ~90 ms (Protti et al, 2000; Baden et al., 2011). As

130

soon as the rising phase of depolarization passes -50 mV, L-type Ca^{2+} channels will begin to open (Singer and Diamond, 2003) and exocytosis of glutamate-containing vesicles will occur in two discrete fast and slow phases, with an onset latency of ~0.8 ms and a duration of ~200 ms, respectively (von Gersdorff et al., 1998). For up to 30 s following a strong bout of exocytosis, release will be strongly suppressed due to depletion of the readily releasable pool of vesicles (von Gersdorff and Matthews, 1997). Because the resting membrane potential (E_m) at the Mb terminal likely sits very close to the activation voltage of L-type Ca^{2+} channels and the effective threshold for spike generation (roughly -45 mV; Baden et al., 2011), the amount of vesicular glutamate release elicited by a light stimulus will be highly sensitive to inhibitory feedback inhibition, which arrives in three forms: (i) rapid (~1-2 ms following initial release), transient pH mediated inhibition of L-type Ca^{2+} channels caused by release of protons from vesicles will inhibit the initial fast, synchronous phase of release (Palmer et al., 2003), (ii) reciprocal feedback inhibition, in the form of $GABA_AR$ and $GABA_CR$ mediated currents, arriving with a post-release latency of ~10 and ~50 ms, respectively (Vigh and von Gersdorff, 2005), will act either to hyperpolarize (if E_m > -60 mV, which is the expected reversal potential for Cl^- (E_{Cl^-})) or shunt (if E_m ~= -60 mV) the terminal, and (iii) lateral feedback inhibition, again in the form of $GABA_AR$ and $GABA_CR$ mediated currents, will, under mesopic (i.e. dim) background conditions (Fig 2.5), arrive with a latency of ~50 ms following the onset of the light stimulus, in the case of ON L-IPSCs, and ~120 ms following the offset of the light stimulus, in the case of OFF L-IPSCs (assuming the surround stimulus arrives simultaneously with the center stimulus).

Under this scenario, reciprocal feedback inhibition will act primarily to either hyperpolarize E_m and attenuate Ca^{2+} influx and glutamate release during the initial, fast phase of release (at $GABA_ARs$), and the second, sustained phase of release (at $GABA_CRs$; see **Appendix I**, Fig A.4), or to decrease the input resistance of the terminal

(shunt) and either shorten the transient phase of the EPSP by decreasing the membrane time-constant (at $GABA_A Rs$), or prevent the initiation of a regenerative Ca^{2+} spike by reducing the membrane input resistance or decreasing the slope of the rising phase of the EPSP (at $GABA_C Rs$). The effects of lateral feedback inhibition on glutamate release from the Mb terminal will, similarly to those of reciprocal inhibition, be dependent on the relationship between E_m and E_{Cl} at the time of the light stimulus. However, the timing of the $GABA_A R$ and $GABA_C R$ mediated components of ON and OFF L-IPSCS (see **Appendix I**, Fig A.4) appears to be more diverse and plastic than that of reciprocal inhibition (Li et al., 2007). Although we have not made direct, simultaneous measurements of Mb light-evoked vesicular glutamate release kinetics and L-IPSCs, it seems likely that the $GABA_A$ or early component of ON L-IPSCs may act to either directly influence or truncate the fast phase of release, depending on the temporal frequency of recent surround modulation (Fig 2.6). The $GABA_C$ or late component of ON L-IPSCs likely acts primarily to either attenuate the rising phase of the second, sustained component of release during low frequency surround modulation, or to prevent Ca^{2+} spike initiation during high frequency surround modulation (Fig 2.6). In the case where a light decrement in the surround coincides with a light increment in the center of an Mb receptive field, the $GABA_A$ component of OFF L-IPSCs will likely act to hyperpolarize E_m during either the sustained phase of release or the period of Ca^{2+} spike initiation. The $GABA_C$ component of OFF L-IPSCs, on the other hand, likely arrives later and acts to either prevent Ca^{2+} spike initiation, truncate the sustained phase of release, or to hyperpolarize E_m following the light response and thus decrease steady-state RRP depletion and L-type Ca^{2+} inactivation in preparation for subsequent center light responses (Jarsky et al., 2011; Oesch and Diamond, 2011). Following repeated high-frequency stimulation of the surround, OFF L-IPSCs will accelerate (or "advance"; Figs 2.4, 2.8) and therefore shift their influence toward the early phase of the concurrent

132

center light response, while ON L-IPSCs will decelerate (or "delay"; Figs 2.4, 2.8) and shift their influence toward the late phase of the Mb light response.

So, the effects of L-IPSCs on Mb light responses and glutamate release onto AC and GC dendrites will depend primarily on the difference between E_{Cl} and E_m, the relative temporal phase relationship between surround and center stimulation, and the frequency of surround stimulation. Furthermore, L-IPSCs will act to either attenuate glutamate release during periods of analog signaling at the Mb terminal, or to effectively gate the initiation of regenerative Ca^{2+} spikes during periods of digital signaling. However, it is also worth considering that contrast modulation of the surround during periods of either light decrements or constant light levels in the center, when the ON Mb is quiescent, will likely result in hyperpolarization of the Mb terminal by both ON and OFF L-IPSCs. This would be expected to decrease steady-state depletion of the RRP and reduce L-type Ca^{2+} inactivation (Jarsky et al., 2011; Oesch and Diamond, 2011), and possibly to shift E_{Cl} to a more depolarized level (i.e. to between -40 and -20 mV) where GABAergic Cl^- currents would depolarize the Mb terminal (Hull et al., 2006a). Both of these effects would, interestingly, likely act to enhance both transient and sustained Mb glutamate release following subsequent center light stimulation. In addition, L-IPSCs arriving during these quiescent periods may regulate E_m in a way that would either prevent or promote subsequent Ca^{2+} spike initiation, depending on whether the "resting" E_m sits either within or depolarized with respect to the critical window for spike initiation (roughly -45 to -35 mV; Baden et al., 2011).

Paired recordings have shown that Mb glutamate release results in both AMPAR and NMDAR mediated EPSCs at post-synaptic GCs, and that Mb exocytosis and EPSC charge transfer are linearly related (Palmer, 2010). This suggests that modification of either "analog" or "digital" glutamate release from Mb terminals by L-IPSCs likely exerts a significant effect on GC voltage responses and Na^+ spike generation. This idea is

133

supported by a recent study that showed that STD of $GABA_CR$ mediated feedback

inhibition at ON BCs was able to prevent STD of light responses (in terms of spike

count) at post-synaptic GCs (Sagdullaev et al., 2011). Although STD of reciprocal

inhibition at the Mb terminal (Li et al., 2007) is consistent with this finding, the effects of

light-evoked ON and OFF L-IPSCs that exhibit biphasic STP of charge, amplitude, and

onset latency on GC light responses (in terms of latency to first spike, spike frequency,

and response duration) is likely much more complex and nuanced. Future studies that

employ paired recordings of axotomized Mb terminals and post-synaptic GCs under

conditions of carefully controlled surround temporal contrast modulation are necessary in

order to explore these effects. In addition, direct examination of the frequency dependent

effects of L-IPSCs on intact Mb glutamate release and GC responses under conditions

of center light stimulation will be necessary to determine the exact relevance of L-IPSC

timing on the output of the retina. This may be possible under conditions in which

GABAergic transmission is blocked and reciprocal and/or lateral feedback currents are

introduced at the terminal via dynamic clamp (Veruki et al., 2008).

  As previously mentioned, it is also necessary to consider the effects of Mb

glutamate release onto AC boutons in the sense that this pathway is perhaps most

relevant to interpretation of the processing of dim light stimulation under dark

background conditions by the RBC to AII AC pathway in the mammalian retina.

Anatomical studies (Marc and Liu, 2000) and recent work with paired recordings in our

lab (Figure 2.7) has shown that there is a high rate of lateral connectivity from Mb

terminals onto ACs of multiple classes (both ON and diffuse bistratified). This is

somewhat consistent with the known divergence of RBCs onto both A17 and AII ACs

(Kolb and Nelson, 1983), although it should be noted that AIIs are thought to be the sole

route by which scotopic information diverges onto cone pathways via BC terminals and

GC dendrites (Kolb, 1979). It is, therefore, likely that Mb lateral outputs onto ACs

134

perform a similar role in the inverse multiplexing (i.e. organized divergence) of Mb

inputs, under either scotopic or mesopic (Krizaj, 2000) background light conditions, onto

an array of both ON and OFF cone BC pathways that vary in their kinetics and temporal

filtering properties. Under this scheme, L-IPSCs would, by virtue of their diverse and

plastic timing relative to feedforward light responses (i.e. passing via direct excitatory

connections), be well positioned to independently shape separate temporal components

of Mb or Ma outputs to ACs that are later split into different cone BC pathways.

Novel cellular and circuit mechanisms of inhibitory plasticity in the inner retina

In addition to these major findings, the present work also identified several novel results

that have potentially high significance for our understanding of inhibitory processing in

the retina. After briefly addressing these results and the future experiments that are

needed to explore their implications in terms of retinal processing, I will conclude with a

brief consideration of the possible role of STP of L-IPSCs in GC spike onset latency

coding of spatial contrast (Gollisch and Meister, 2008).

First, the findings that ON L-IPSCs were enhanced by block of AMPARs with

NBQX (**Chapter 1**), and that STD of ON L-IPSCs at PPIs < 1 s was enhanced under the

same conditions **(Chapter 2)**, suggests both that transmission from ON BCs to ON ACs

mediated entirely by NMDARs may be possible under some conditions, and that HC to

PR feedback inhibition, which requires AMPAR activation on HCs, acts to attenuate STD

of ON BC glutamate release and expand the dynamic range of lateral inhibition in the

IPL under physiological conditions. Thus, subthreshold membrane potential fluctuations

in ACs may critically regulate ON L-IPSCs by controlling the degree of Mg^{2+} block of

NMDARs on AC post-synaptic boutons, and, furthermore, dynamic inhibition in the IPL

may be more directly dependent on plasticity of OPL inhibitory mechanisms than has

been previously appreciated. Future experiments should be undertaken that directly

135

examine the properties of light-evoked, NMDAR mediated inputs at ACs that provide lateral input to Mb terminals. In addition, paired recordings of axotmized Mb terminals and HCs during light stimulation would provide crucial insight into the relative timing of HC voltage potential fluctuations and the onset latencies of ON and OFF L-IPSCs at the Mb terminal.

Second, the finding that OFF L-IPSCs depend on the activation of voltage-gated Na$^+$ channels (Figs 1.4, A.4-6), likely expressed in ACs that mediate tri-synaptic inhibition from cone PRs, suggests that OFF, but not ON, L-IPSCs at the Mb terminal depend on regenerative Na$^+$ spikes in ACs that mediate wide-field surround inhibition. This significant, novel finding suggests that OFF L-IPSCs, because they may be a form of "all-or-none" signaling, may play a role in permissively "gating" feedforward light responses at the Mb terminal. Such a gating function, especially in mammals, could be involved in the suppression of responses to global image movement during eye movements (Olveczky et al., 2007; Baccus et al., 2008). Direct paired recordings of Mb terminals and OFF ACs that mediate this response would allow further examination of the role of AC voltage-gated Na$^+$ channels in either boosting EPSPs or generating action potentials in a way that directly contributes to light-evoked OFF L-IPSCs at the Mb terminal.

Third, the mechanisms that underlie STP of L-IPSC strength and timing **(Chapter 2)** need to be more clearly dissected (see **Appendix I**). Although we have hypothesized that STD and onset latency delay (increase) may be due to RRP depletion at AC terminals, while STF and onset latency advance (decrease) may be due to accumulation of residual intracellular Ca^{2+} and enhanced release probability at AC terminals, the contribution of STP at the two upstream (PR to BC and BC to AC) synapses in the tri-synaptic L-IPSC pathway to overall STP of lateral inhibition at the Mb terminal needs to be further characterized. This will require a two-pronged strategy of paired recordings

between Mb terminals and either ACs or neighboring BCs during surround light stimulation, and focal pharmacological or electrical stimulation in the ON vs. OFF regions of the IPL, and at neighboring ON vs. OFF BC dendrites in the IPL.

Lastly, the locus, mechanisms and timescale of Asc (i.e. ascorbic acid) release in the IPL needs to be directly examined in order to understand the role that this positive allosteric modulator of $GABA_A R$ and $GABA_C R$ mediated currents **(Chapter 3)** may play in STP of L-IPSCs or reciprocal feedback inhibition at Mb terminals, and in the regulation of feedforward inhibition onto GC dendrites. Approaches that may prove useful include pharmacological blockade of the SVCT2 Na^+/Asc cotransporter or GLUT2 glucose transporter (Song et al., 2002), manipulation of extracellular Asc during paired-pulse light stimulation, and paired recordings of synaptically connected ACs and Mb terminals under conditions in which either cell is loaded with intracellular solution containing different (e.g. 0 vs. 1 vs. 10 mM) concentrations of Asc. We expect that perfusion of high concentrations of glutamate onto the IPL may evoke Asc release from either of these cells that is dependent on E_{Na+}, E_m, and pharmacological blockade of SVCT2, and that this Asc release would transiently potentiate standing $GABA_C R$ mediated leak current (Figure 3.1) or $GABA_A$ (and $GABA_C$) mIPSC amplitudes (Figure 3.8) at the Mb terminal. Also, it will be necessary to perform more quantitative studies of retinal Asc levels in the OPL vs. IPL *in vivo* under different background light conditions or behavioral states.

Overall, the major findings of this work constitute substantial contribution to our understanding of lateral feedback inhibition in the retina. In particular, the novel combination of physiological light stimulation and direct recording from an axotomized BC presynaptic terminal allowed characterization of the STP of strength and timing of small inhibitory currents that, despite their diminutive stature, likely exert significant control over the passage of visual information to GCs, where it is repackaged in the form of action potentials and transmitted to visual cortex via the thalamus.

137

Potential role of ON and OFF L-IPSC STP in GC onset latency coding of spatial contrast

The encoding of stimulus properties in the precise timing of individual action potentials following the presentation of a discrete stimulus or during ongoing active sensory acquisition, also known as latency coding, is thought to play a key role in the early neural coding of sensory information across multiple modalities (Land, 1999; Stecker and Middlebrooks, 2003; Greschner et al., 2006; Sawtell et al., 2006; Gollisch and Meister, 2008). Such a latency code has the advantage of being both fast, in that a large amount of information is contained in the initial spike, and metabolically efficient, in that long, high-frequency spike trains are not required for stimulus encoding (Reich et al., 2001; Gollisch and Meister, 2008). In the visual system of the tiger salamander, it has been shown that local spatial contrast in the visual image falling on the retina is efficiently encoded as the onset latency of the first action potential that an ON-OFF GC produces following a saccade (Gollisch and Meister, 2008). These latencies, which ranged from 60 to 120 ms as a function of the spatial phase of a grating stimulus presented in the receptive field of each GC, roughly matched earlier measurements of first spike onset latency in ON-OFF GCs of tiger salamander retina (~100 to 170 ms, Burkhardt et al., 1998). Importantly, the relative spike latencies (± 30 ms) of the population of ON-OFF GCs that tile the retina were shown to contain more spatial information than either the absolute GC spike latencies or spike counts (Gollisch and Meister, 2008). Thus, the complement of spatial information that describes the entire image is well represented in the population distribution of GC spike onset latencies across the retina.

It is hypothesized that spatial contrast at the level of photoreceptors may be converted to GC spike latency by convergence of early (i.e. fast) OFF BC and late (i.e. slow) ON BC inputs, which are separated by roughly 30 ms due to differences in

138

signaling speed between ionotropic AMPA / kainate receptors at OFF BC dendrites and metabotropic mGluR6 receptors at ON BC dendrites (Burkhardt et al., 1998; Burkhardt, 2011), onto the dendritic arbor of a single ON-OFF GC (Greschner et al., 2006; Gollisch and Meister, 2008). In this scheme, local negative contrast steps would produce an early GC spike, local positive contrast steps would produce a late GC spike, and mixtures of negative and positive contrast within an individual GC receptive field would produce spikes with intermediate latencies. In the tiger salamander retina, roughly 70% of GCs exhibit ON-OFF response characteristics (Burkhardt et al., 1998). Furthermore, the first spike onset latency of these ON-OFF GCs to negative contrast steps is between ~100 and 110 ms, while the latency to positive contrast steps is between ~120 and 170 ms (Burkhardt et al., 1998). These latency ranges are consistent with those that we observed for ON and OFF L-IPSCs in the goldfish retina (~50 to 150 ms; Fig 2.5), which suggests that information about surround contrast carried by L-IPSCs operates over a timescale consistent with their possible involvement in shaping the GC onset latency code.

In order for such a GC latency code for spatial contrast to be decoded by downstream neurons in the thalamus (i.e. LGN) or cortex (i.e. V1 or V4; Usrey et al., 2000; Reich et al., 2001), the population profile of spike times must be compared either to a fixed (i.e. saccade or other motor command) or relative (i.e. correlations between GCs) temporal reference frame (Gollisch and Meister, 2008). Interestingly, recent evidence has shown an active role for saccades and other guided eye movements in the acquisition of visual information in both zebrafish (Schoonheim et al., 2010) and goldfish (Schaerer and Kirschfeld, 2000; Angeles Luque et al., 2005). In mice, visual saccades occur every 100 – 500 ms (Sakatani and Isa, 2007), a period that roughly matches the range of PPIs for which we observed STP of L-IPSC amplitude, charge, and onset latency at the Mb terminal (Figs 2.3, 2.4, 2.8). Similarly, goldfish saccades observed

during constant smooth head movements occur roughly every 500 ms (Easter et al., 1974; Land, 1999), a period that we would expect to produce modest STD of ON L-IPSCs and STF of OFF L-IPSCs. Thus, goldfish saccades or other active eye movements, which occur over a range of frequencies similar to that observed in mammals, may allow the STP that we have described to actively shape (i.e. to compress or expand) the GC relative onset latency code for spatial contrast as saccade frequency is modulated under different behavioral conditions.

Even in the absence of a fixed reference frame provided by saccades, the convergence at Mb terminals of ON and OFF L-IPSCs carried by medium- or wide-field ACs will likely, due to their disparate timing (especially under mesopic background; Fig 2.5), act to differentially shape the transient and sustained components of Mb light responses (see preceding discussion, pages 130 – 137). This will control the timing of the excitatory drive to GCs post-synaptic to Mb BCs and mediate disinhibitory gating during ongoing stimulation (Manu and Baccus, 2011), thus introducing long-range spatial correlations that are expected to increase the information content of the population of GC spike onset latencies (Chase and Young, 2007). For instance, a large negative contrast step in one area of the retina will produce locally early GC spikes and at the same time trigger OFF L-IPSCs that will inhibit the late phase of Mb responses in distal areas of the retina. This might contribute to a latency advance of initial GC spikes in the distal areas and thus introduce positive correlations across the population latency code that would allow for the decoding of spatial information by downstream neurons in LGN or visual cortex, which may act as coincidence detectors over timescales of ~7-15 ms (Usrey et al., 2000). During high frequency contrast modulation of the surround, onset latency delay of (early) ON L-IPSCs may combine with latency advance of (late) OFF L-IPSCs (Fig 2.4, 2.8) to promote a compression of the distribution of GC spike latencies. This would allow the GC latency code to adapt to the increased temporal frequency

contrast of the image falling on the retina so that representations of discrete visual

changes do not overlap, particularly under conditions where the animal modulates the

frequency of its saccades or other active eye movements to acquire detailed information

from a rapidly changing natural scene.

REFERENCES

Abbott LF and Nelson SB (2000). Synaptic plasticity: taming the beast. Nat Neurosci 3 Suppl:1178-83.

Alshuaib WB, Mathew MV (2006). Vitamins C and E modulate neuronal potassium currents. J Membr Biol 210:193-198.

Amato A, Connolly CN, Moss SJ, Smart TG (1999). Modulation of neuronal and recombinant $GABA_A$ receptors by redox reagents. J Physiol 517 (Pt 1):35-50.

Amin J, Dickerson IM, Weiss DS (1994). The agonist binding site of the gamma-aminobutyric acid type A channel is not formed by the extracellular cysteine loop. Mol Pharmacol 45:317-323.

Angeles Luque M, Pilar Perez-Perez M, Herrero L and Torres B (2005). Involvement of the optic tectum and mesencephalic reticular formation in the generation of saccadic eye movements in goldfish. Brain Res Brain Res Rev 49(2):388-97.

Arai I, Tanaka M, Tachibana M (2010). Active roles of electrically coupled bipolar cell network in the adult retina. J Neurosci 30:9260-9270.

Artola A and Singer W (1993). Long-term depression of excitatory synaptic transmission and its relationship to long-term potentiation. Trends Neurosci 16(11):480-7.

Awatramani GB and Slaughter MM (2000). Origin of transient and sustained responses in ganglion cells of the retina. J Neurosci 20(18):7087-95.

Baccus SA, Olveczky BP, Manu M, and Meister M (2008). A retinal circuit that computes object motion. J Neurosci 28(27):6807-17.

Baden T, Esposti F, Nikolaev A and Lagnado L (2011). Spikes in retinal bipolar cells phase-lock to visual stimuli with millisecond precision. Curr Biol 21:1859-1869.

Barlow HB and Hill RM (1963). Selective sensitivity to direction of movement in ganglion cells of the rabbit retina. Science 139:412-4.

Baylor DA (1987). Photoreceptor signals and vision. Proctor lecture. Invest Ophthalmol Vis Sci 28(1):34-49.

Beenhakker MP and Huguenard JR (2010). Astrocytes as gatekeepers of GABAB receptor function. J Neurosci 30(45):15262-76.

Bi G and Poo M (2001). Synaptic modification by correlated activity: Hebb's postulate revisited. Annu Rev Neurosci 24:139-66.

Bigelow JC, Brown DS, Wightman RM (1984). Gamma-aminobutyric acid stimulates the release of endogenous ascorbic acid from rat striatal tissue. J Neurochem 42:412-419.

Bloomfield SA (1996). Effect of spike blockade on the receptive-field size of amacrine and ganglion cells in the rabbit retina. J Neurophysiol 75(5):1878-93.

Bloomfield SA, Dacheux RF (2001). Rod vision: pathways and processing in the mammalian retina. Prog Retin Eye Res 20:351-384.

Bloomfield SA, Volgyi B (2007). Response properties of a unique subtype of wide-field amacrine cell in the rabbit retina. Vis Neurosci 24:459-469.

Bouzat C, Barrantes FJ, Sigworth FJ (1991). Changes in channel properties of acetylcholine receptors during the time course of thiol chemical modifications. Pflugers Arch 418:51-61.

Brandstätter JH, Koulen P, Kuhn R, van der Putten H, Wässle H (1996). Compartmental localization of a metabotropic glutamate receptor (mGluR7): two different active sites at a retinal synapse. J Neurosci 16:4749-4756.

Buonomano DV and Merzenich MM (1998). Net interaction between different forms of short-term synaptic plasticity and slow-IPSPs in the hippocampus and auditory cortex. J Neurophysiol 80(4):1765-74.

Burkhardt DA, Fahey PK and Sikora M (1998). Responses of ganglion cells to contrast steps in the light-adapted retina of the tiger salamander. Vis Neurosci 15(2):219-29.

Burkhardt DA (2011). Contrast processing by ON and OFF bipolar cells. Vis Neurosci 28(1):69-75.

Busskamp V, Duebel J, Balya D, Fradot M, Viney TJ, Siegert S, Groner AC, Cabuy E, Forster V, Seeliger M, Biel M, Humphries P, Paques M, Mohand-Said S, Trono D, Deisseroth K, Sahel JA, Picaud S, Roska B (2010). Genetic reactivation of cone photoreceptors restores visual responses in retinitis pigmentosa. Science 329:413-417.

Calero CI, Calvo DJ (2008). Redox modulation of homomeric rho1 GABA receptors. J Neurochem 105:2367-2374.

Campanucci V, Krishnaswamy A, Cooper E (2010). Diabetes depresses synaptic transmission in sympathetic ganglia by inactivating nAChRs through a conserved intracellular cysteine residue. Neuron 66:827-834.

Castro M, Caprile T, Astuya A, Millan C, Reinicke K, Vera JC, Vasquez O, Aguayo LG, Nualart F (2001). High-affinity sodium-vitamin C co-transporters (SVCT) expression in embryonic mouse neurons. J Neurochem 78:815-823.

Cervetto L and Piccolino M (1982). Processing of visual signals in vertebrate photoreceptors. Arch Ital Biol 120(1-3):242-70.

Chase SM and Young ED (2007). First-spike latency information in single neurons increases when referenced to population onset. PNAS 104(12):5175-5180.

Chavez AE, Diamond JS (2008). Diverse mechanisms underlie glycinergic feedback transmission onto rod bipolar cells in rat retina. J Neurosci 28:7919-7928.

145

Chavez AE, Grimes WN, and Diamond JS (2010). Mechanisms underlying lateral GABAergic feedback onto rod bipolar cells in rat retina. J Neurosci 30(6):2330-9.

Chavez AE, Singer JH, and Diamond JS (2006). Fast neurotransmitter release triggered by Ca influx through AMPA-type glutamate receptors. Nature 443(7112):705-8.

Cho S, Li GL, and von Gersdorff H (2011). Recovery from short-term depression and facilitation is ultrafast and Ca^{2+} dependent at auditory hair cell synapses. J Neurosci 31(15):5682-92.

Chu XP, Close N, Saugstad JA, Xiong ZG (2006). ASIC1a-specific modulation of acid-sensing ion channels in mouse cortical neurons by redox reagents. J Neurosci 26:5329-5339.

Cook PB, McReynolds JS (1998). Lateral inhibition in the inner retina is important for spatial tuning of ganglion cells. Nat Neurosci 1:714-719.

Cook PB, Lukasiewicz PD, and McReynolds JS (1998). Action potentials are required for the lateral transmission of glycinergic transient inhibition in the amphibian retina. J Neurosci 18:2301-2308.

Cousin MA, Nicholls DG (1997). Synaptic vesicle recycling in cultured cerebellar granule cells: role of vesicular acidification and refilling. J Neurochem 69:1927-1935.

Chung S, Li X, and Nelson SB (2002). Short-term depression at thalamocortical synapses contributes to rapid adaptation of cortical sensory responses in vivo. Neuron 34(3):437-46.

Connaughton VP (2001). Organization of ON- and OFF- pathways in the zebrafish retina: neurotransmitter localization, electrophysiological responses of bipolar cells, and patterns of axon terminal stratification. Prog Brain Res 131:161-76.

Davenport CM, Detwiler PB, Dacey DM (2008). Effects of pH buffering on horizontal and ganglion cell light responses in primate retina: evidence for the proton hypothesis of surround formation. J Neurosci 28:456–464.

Deken SL, Wang D, and Quick MW (2003). Plasma membrane GABA transporters reside on distinct vesicles and undergo rapid regulated recycling. 23(5):1563-8.

Delaney KR, Qnais EY, and Hardy AB (2009). Short-term synaptic plasticity at the main and vomeronasal olfactory receptor to mitral cell synapse in frog. Eur J Neurosci 30(11):2077-88.

DeVries SH (2000). Bipolar cells use kainate and AMPA receptors to filter visual information into separate channels. Neuron 28:847-856.

DeVries SH (2001). Exocytosed protons feedback to suppress the Ca2+ current in mammalian cone photoreceptors. Neuron 32:1107-1117.

DeVries SH, Baylor DA (1995). An alternative pathway for signal flow from rod photoreceptors to ganglion cells in mammalian retina. Proc Natl Acad Sci U S A 92:10658-10662.

DeVries SH, Li W, Saszik S (2006). Parallel processing in two transmitter microenvironments at the cone photoreceptor synapse. Neuron 50:735-748.

Dixon DB, Copenhagen DR (1992). Two types of glutamate receptors differentially excite amacrine cells in the tiger salamander retina. J Physiol 449:589-606.

Dong CJ and Werblin FS (1998). Temporal contrast enhancement via GABAC feedback at bipolar terminals in the tiger salamander retina. J Neurophysiol 79(4):2171-80.

Dong CJ and Hare WA (2003). Temporal modulation of scotopic visual signals by A17 amacrine cells in mammalian retina in vivo. J Neurophysiol 89(4):2159-66.

Dowling JE, Werblin FS (1969). Organization of retina of the mudpuppy, Necturus maculosus. I. Synaptic structure. J Neurophysiol 32:315-338.

Dowling JE (1970). Organization of vertebrate retinas. Invest Ophthalmol 9(9):655-80.

Dreosti E, Esposti F, Baden T, and Lagnado L (2011). In vivo evidence that retinal bipolar cells generate spikes modulated by light. Nat Neurosci 14(8):951-2.

Duebel J, Haverkamp S, Schleich W, Feng G, Augustine GJ, Kuner T, Euler T (2006). Two-photon imaging reveals somatodendritic chloride gradient in retinal ON-type bipolar cells expressing the biosensor Clomeleon. Neuron 49:81-94.

Dyer DL, Kanai Y, Hediger MA, Rubin SA, Said HM (1994). Expression of a rabbit renal ascorbic acid transporter in Xenopus laevis oocytes. Am J Physiol 267:C301-306.

Easter SS, Johns PR and Heckenlively D (1974). Horizontal compensatory eye movements in goldfish (*Carrassius auratus*). I. The normal animal. J Comp Physiol 92:23-35.

Eggers ED, Lukasiewicz PD (2006). GABA$_A$, GABA$_C$ and glycine receptor-mediated inhibition differentially affects light-evoked signalling from mouse retinal rod bipolar cells. J Physiol 572:215-225.

Eggers ED, Lukasiewicz PD (2010). Interneuron circuits tune inhibition in retinal bipolar cells. J Neurophysiol 103:25-37.

Eggers ED and Lukasiewicz PD (2011). Multiple pathways of inhibition shape bipolar cell responses in the retina. Vis Neurosci 28(1):95-108.

Ekstrom P and Anzelius M (1998). GABA and GABA-transporter (GAT-1) immunoreactivities in the retina of the salmon (Salmo salar L). Brain Res 812(1-2):170-85.

Euler T, Masland RH (2000). Light-evoked responses of bipolar cells in a mammalian retina. J Neurophysiol 83:1817-1829.

Fahrenfort I, Klooster J, Sjoerdsma T, Kamermans M (2005). The involvement of glutamate-gated channels in negative feedback from horizontal cells to cones. Prog Brain Res 147:219-229.

Fahrenfort I, Steijaert M, Sjoerdsma T, Vickers E, Ripps H, van Asselt j, Endeman D, Klooster J, Numan R, ter Eikelder H, von Gersdorff H, Kamermans M (2009). Hemichannel-mediated and pH-based feedback from horizontal cells to cones in the vertebrate retina. *PLoS One* 4:e6090.

Famiglietti EV Jr and Kolb H (1975). A bistratified amacrine cell and synaptic circuitry in the inner plexiform layer of the retina. Brain Res 84(2):293-300.

Famiglietti EV Jr and Kolb H (1976). Structural basis for ON- and OFF- center responses in retinal ganglion cells. Science 194(4261):193-5.

Fan SF, Yazulla S (1999). Suppression of voltage-dependent K^+ currents in retinal bipolar cells by ascorbate. Vis Neurosci 16:141-148.

Feigenspan A, Bormann J (1994). Modulation of $GABA_C$ receptors in rat retinal bipolar cells by protein kinase C. J Physiol 481 (Pt 2):325-330.

Field GD and Chichilnisky EJ (2007). Information processing in the primate retina: circuitry and coding. Annu Rev Neurosci 30:1-30.

Flores-Herr N, Protti DA, Wässle H (2001). Synaptic currents generating the inhibitory surround of ganglion cells in the mammalian retina. J Neurosci 21:4852-4863.

Gauthier JL, Field GD, Sher A, Shlens J, Greschner M, Litke AM, Chichilnisky EJ (2009). Uniform signal redundancy of parasol and midget ganglion cells in primate retina. J Neurosci 29:4675-4680.

Gillis KD (2000). Admittance-based measurement of membrane capacitance using the EPC-9 patch-clamp amplifier. Pflugers Arch 439:655-664.

Gleason E, Borges S, and Wilson M (1994). Control of transmitter release from retinal amacrine cells by Ca^{2+} influx and efflux. Neuron 13:1109-17.

Gollisch T, Meister M (2008). Rapid neural coding in the retina with relative spike latencies. Science 319:1108-1111.

Gollisch T, Meister M (2010). Eye smarter than scientists believed: neural computations in circuits of the retina. Neuron 65:150-164.

Goutman JD, Escobar AL, Calvo DJ (2005). Analysis of macroscopic ionic currents mediated by GABA rho1 receptors during lanthanide modulation predicts novel states controlling channel gating. Br J Pharmacol 146:1000-1009.

Goutman JD and Glowatzki E (2011). Short-term facilitation modulates size and timing of the synaptic response at the inner hair cell ribbon synapse. J Neurosci 31(22):7974-81.

Greschner M, Thiel A, Kretzberg J and Ammermuller J (2006). Complex spike-event pattern of transient ON-OFF retinal ganglion cells. J Neurophysiol 96(6):2845-56.

Grimes WN, Zhang J, Graydon CW, Kachar B, Diamond JS (2010). Retinal parallel processors: more than 100 independent microcircuits operate within a single interneuron. Neuron 65:873-885.

Grunewald RA (1993). Ascorbic acid in the brain. Brain Res Brain Res Rev 18:123-133.

Guido W (2008). Refinement of the retinogeniculate pathway. J Physiol 586(Pt 18):4357-62.

Harrison FE, May JM (2009). Vitamin C function in the brain: vital role of the ascorbate transporter SVCT2. Free Radic Biol Med 46:719-730.

Hartveit E (1999). Reciprocal synaptic interactions between rod bipolar cells and amacrine cells in the rat retina. J Neurophysiol 81:2923-2936.

Hediger MA (2002). New view at C. Nat Med 8:445-446.

Heidelberger R, Thoreson WB, and Witkovsky P (2005). Synaptic transmission at retinal ribbon synapses. Prog Retin Eye Res 24(6):682-720.

Hirasawa H, Kaneko A (2003). pH changes in the invaginating synaptic cleft mediate feedback from horizontal cells to cone photoreceptors by modulating Ca^{2+} channels. J Gen Physiol 122:657-671.

Hosoya K, Minamizono A, Katayama K, Terasaki T, Tomi M (2004). Vitamin C transport in oxidized form across the rat blood-retinal barrier. Invest Ophthalmol Vis Sci 45:1232-1239.

Hosoya T, Baccus SA, and Meister M (2005). Dynamic predictive coding by the retina. Nature 436:71-77.

Hsueh HA, Molnar A, and Werblin FS (2008). Amacrine-to-amacrine cell inhibition in the rabbit retina. J Neurophysiol 100(4):2077-88.

Hull C, von Gersdorff H (2004). Fast endocytosis is inhibited by GABA-mediated chloride influx at a presynaptic terminal. Neuron 44:469-482.

Hull C, Li GL, and von Gersdorff H (2006a). GABA transporters regulate a standing GABAC receptor-mediated current at a retinal presynaptic terminal. J Neurosci 26(26):6979-84.

Hull C, Studholme K, Yazulla S, von Gersdorff H (2006b). Diurnal changes in exocytosis and the number of synaptic ribbons at active zones of an ON-type bipolar cell terminal. J Neurophysiol 96:2025-2033.

Ichinose T and Lukasiewicz PD (2002). GABA transporters regulate inhibition in the retina by limiting $GABA_C$ receptor activation. J Neurosci 22:3285-3292.

Ichinose T, Lukasiewicz PD (2005). Inner and outer retinal pathways both contribute to surround inhibition of salamander ganglion cells. J Physiol 565:517-535.

Ichinose T and Lukasiewicz PD (2007). Ambient light regulates sodium channel activity to dynamically control retinal signaling. J Neurosci 27:4756-64.

Jacobs AL, Werblin FS (1998). Spatiotemporal patterns at the retinal output. J Neurophysiol 80:447-451.

Jarsky T, Cembrowski M, Logan SM, Kath WL, Riecke H, Demb JB, and Singer JH (2011). A synaptic mechanism for retinal adaptation to luminance and contrast. J Neurosci 31(30):11003-15.

Jin XT, Pare JF, and Smith Y (2011). Differential localization and function of GABA transporters, GAT-1 and GAT-3, in the rat globus pallidus. Eur J Neurosci 33(8):1504-18.

Johnston GA (1996). $GABA_C$ receptors: relatively simple transmitter -gated ion channels? Trends Pharmacol Sci 17:319-323.

Jones SM, Palmer MJ (2009). Activation of the tonic $GABA_C$ receptor current in retinal bipolar cell terminals by nonvesicular GABA release. J Neurophysiol 102:691-699.

Jones SM and Palmer MJ (2011). Pharmacological analysis of the activation and receptor properties of the tonic GABA(C)R current in retinal bipolar cell terminals. PLoS One 6(9):e24892.

Joselevitch C and Kamermans M (2007). Interaction between rod and cone inputs in mixed-input bipolar cells in goldfish retina. J Neurosci Res 85(7):1579-91.

Joselevitch C and Kamermans M (2009). Retinal parallel pathways: seeing with our inner fish. Vision Res 49(9):943-59.

Kamermans M and Fahrenfort I (2004). Ephaptic interactions within a chemical synapse: hemichannel-mediated ephaptic inhibition in the retina. Curr Opin Neurobiol 14(5):531-41.

Kamermans M and Spekreijse H (1999). The feedback pathway from horizontal cells to cones. A mini review with a look ahead. Vision Res 39(15):2449-68.

Kaneko A (1973). Receptive field organization of bipolar and amacrine cells in the goldfish retina. J Physiol 235(1):133-53.

Kaneko A and Tachibana M (1985). A voltage-clamp analysis of membrane current in solitary bipolar cells dissociated from Carassius auratus. J Physiol 358:131-52.

Kastner DB and Baccus A (2011). Coordinated dynamic encoding in the retina using opposing forms of plasticity (Nat Neurosci 14:1317-22).

Kim HG and Miller RF (1993). Properties of synaptic transmission from photoreceptors to bipolar cells in the mudpuppy retina. J Neurophysiol 69(2):352-60.

Kim MH, Vickers E, and von Gersdorff H (2012). Patch-clamp capacitance measurements and Ca(2+) imaging at single nerve terminals in retinal slices. J Vis Exp 19(59):3345.

Klooster J, Nunes Cardozo B, Yazulla S and Kamermans M (2004). Postsynaptic localization of gamma-aminobutyric acid transporters and receptors in the outer plexiform layer of the goldfish retina: An ultrastructural study. J Comp Neurol 474(1):58-74.

Koizumi A, Hayashida Y, Kiuchi T, Yamada Y, Fujii A, Yagi T, and Kaneko A (2005). The interdependence and independence of amacrine cell dendrites: Patch clamp recordings and simulation studies on cultured GABAergic amacrine cells. J Int Neurosci 4:363-380.

Kolb H (1979). The inner plexiform layer in the retina of the cat: electron microscopic observations. J Neurocytol 8(3):295-329.

Kolb H and Nelson R (1983). Rod pathways in the retina of the cat. Vision Res 23(4):301-12.

Koulen P (1999). Postnatal development of GABA$_A$ receptor beta1, beta2/3, and gamma2 immunoreactivity in the rat retina. J Neurosci Res 57:185-194.

Koulen P, Brandstatter JH, Enz R, Bormann J, and Wassle H (1998). Synaptic clustering of GABA(C) receptor rho-subunits in the rat retina. Eur J Neurosci 10:115-27.

Koulen P, Malitschek B, Kuhn R, Wässle H, Brandstätter JH (1996). Group II and group III metabotropic glutamate receptors in the rat retina: distributions and developmental expression patterns. Eur J Neurosci 8:2177-2187.

Krizaj D (2000). Mesopic state: cellular mechanisms involved in pre- and post-synaptic mixing of rod and cone signals. Microsc Res Tech 50(5):347-59.

Krizaj D, Akopian A, Witkovsky P (1994). The effects of L-glutamate, AMPA, quisqualate, and kainate on retinal horizontal cells depend on adaptational state: implications for rod-cone interactions. J Neurosci 14:5661-5671.

Kuffler SW (1953). Discharge patterns and functional organization of mammalian retina. J Neurophysiol 16(1):37-68.

Kusama T, Spivak CE, Whiting P, Dawson VL, Schaeffer JC, Uhl GR (1993). Pharmacology of GABA rho 1 and GABA alpha/beta receptors expressed in Xenopus oocytes and COS cells. Br J Pharmacol 109:200-206.

Land MF (1999). Motion and vision: why animals move their eyes. J Comp Physiol A 185(4):341-52.

Le Roux N, Amar M, Moreau AW, and Fossier P (2009). Roles of nitric oxide in the homeostatic control of the excitation-inhibition balance in rat visual cortical networks. Neuroscience 163(3):942-51.

Li GL, Vigh J, and von Gersdorff H (2007). Short-term depression at the reciprocal synapses between a retinal bipolar cell terminal and amacrine cells. J Neurosci 27(28):7377-85.

Li P, Slaughter M (2007). Glycine receptor subunit composition alters the action of GABA antagonists. Vis Neurosci 1-9.

Lipton SA, Choi YB, Takahashi H, Zhang D, Li W, Godzik A, Bankston LA (2002). Cysteine regulation of protein function--as exemplified by NMDA-receptor modulation. Trends Neurosci 25:474-480.

Lukasiewicz PD, Eggers ED, Sagdullaev BT, and McCall MA (2004). GABAC receptor-mediated inhibition in the retina. Vision Res 44(28):3289-96.

Lukasiewicz PD (2005). Synaptic mechanisms that shape visual signaling at the inner retina. Prog Brain Res 147:205-18.

Lund JS (1988). Anatomical organization of macaque monkey striate visual cortex. Annu Rev Neurosci 11:253-88.

Lyubarsky AL, Falsini B, Pennesi ME, Valentini P, Pugh EN, Jr. (1999). UV- and midwave-sensitive cone-driven retinal responses of the mouse: a possible phenotype for coexpression of cone photopigments. J Neurosci 19:442-455.

Majewska MD, Bell JA, London ED (1990). Regulation of the NMDA receptor by redox phenomena: inhibitory role of ascorbate. Brain Res 537:328-332.

158

Manu M and Baccus SA (2011). Disinhibitory gating of retinal output by transmission from an amacrine cell. Proc Natl Acad Sci 108(45):18447-52.

Marc RE and Liu W (2000). Fundamental GABAergic amacrine cell circuitries in the retina: nested feedback, concatenated inhibition, and axosomatic synapses. J Comp Neurol 425(4):560-82.

Mapelli L, Rossi P, Nieus T, and D'Angelo E (2009). Tonic activation of GABAB receptors reduces release probability at inhibitory connections in the cerebellar glomerulus. J Neurophysiol 101(6):3089-99.

Masland RH, Raviola E (2000). Confronting complexity: strategies for understanding the microcircuitry of the retina. Annu Rev Neurosci 23:249-284.

Matsui K, Hasegawa J, Tachibana M (2001). Modulation of excitatory synaptic transmission by $GABA_C$ receptor-mediated feedback in the mouse inner retina. J Neurophysiol 86:2285-2298.

Matthews G, Ayoub GS, and Heielberger R (1994). Presynaptic inhibition by GABA is mediated via two distinct GABA receptors with novel pharmacology. J Neurosci 14(3 Pt 1):1079-90.

McCall MA, Lukasiewicz PD, Gregg RG, Peachey NS (2002). Elimination of the rho1 subunit abolishes $GABA_C$ receptor expression and alters visual processing in the mouse retina. J Neurosci 22:4163-4174.

McNaughton PA (1990). Light response of vertebrate photoreceptors. Physiol Rev 70(3):847-83.

Meister M, Berry MJ (1999). The neural code of the retina. Neuron 22:435-450.

Menger N, Wässle H (2000). Morphological and physiological properties of the A17 amacrine cell of the rat retina. Vis Neurosci 17:769-780.

Miledi R, Parker I, Sumikawa K (1989). Transplanting receptors from brain into oocytes. New York: Fidia Research Foundation Neuroscience Award Lecture (Smith J. J., ed.).

Moss SJ, Smart TG (2001). Constructing inhibitory synapses. Nat Rev Neurosci 2:240-250.

Molnar A, Werblin F (2007). Inhibitory feedback shapes bipolar cell responses in the rabbit retina. J Neurophysiol 98:3423-3435.

Molnar A, Hsueh A, Roska B, and Werblin FS (2009). Crossover inhibition in the retina: circuitry that compensates for nonlinear rectifying synaptic transmission. J Comput Neurosci 27(3):569-90.

Morgans CW, Zhang J, Jeffrey BG, Nelson SM, Burke NS, Duvoisin RM, and Brown RL (2009). TRPM1 is required for the depolarizing light response in retinal ON-bipolar cells. Proc Natl Acad Sci 106(45):19174-8.

Morkve SH and Hartveit E (2009). Properties of glycine receptors underlying synaptic current in presynaptic axon terminals of rod bipolar cell in the rat retina. J Physiol 587(Pt 15):3813-30.

Muller M, Goutman JD, Kochubey O, and Schneggenburger R (2010). Interaction between facilitation and depression at a large CNS synapse reveals mechanisms of short-term plasticity. J Neurosci 30(6):2007-16.

Munch TA, da Silveira RA, Siegert S, Viney TJ, Awatramani GB, and Roska B (2009). Approach sensitivity in the retina processed by a multifunctional neural circuit. Nat Neurosci 12(10):1308-16.

Naka KI (1971). Receptive field mechanism in the vertebrate retina. Science 171(972):691-3.

Nelson MT, Joksovic PM, Su P, Kang HW, Van Deusen A, Baumgart JP, David LS, Snutch TP, Barrett PQ, Lee JH, Zorumski CF, Perez-Reyes E, Todorovic SM (2007). Molecular mechanisms of subtype-specific inhibition of neuronal T-type calcium channels by ascorbate. J Neurosci 27:12577-12583.

O'Brien BJ, Caldwell JH, Ehring GR, Bumsted O'Brien KM, Luo S, and Levinson SR (2008). Tetrodotoxin-resistant voltage-gated sodium channels Na(v)1.8 and Na(v)1.9 are expressed in the retina. J Comp Neurol 508(6):940-51.

Oesch N and Diamond J (2009). A night vision neuron gets a day job. Nat Neurosci 12(10):1209-11.

Oesch NW and Diamond JS (2011). Ribbon synapses compute temporal contrast and encode luminance in retinal rod bipolar cells. Nat Neurosci 14:1555-61.

Oltedal L, Veruki ML, and Hartveit E (2009). Passive membrane properties and electrotonic signal processing in retinal rod bipolar cells. J Physiol 587:829-49.

Oltedal L and Hartveit E (2010). Transient release kinetics of rod bipolar cells revealed by capacitance measurement of exocytosis from axon terminals in rat retinal slices. J Physiol 588(Pt 9):1469-87.

Oltedal L, Morkve SH, Veruki ML, and Hartveit E (2007). Patch-clamp investigations and compartmental modeling of rod bipolar axon terminals in an in vitro thin-slice preparation of the mammalian retina. J Neurophysiol 97(2):1171-87.

Oltedal L, Veruki ML, and Hartveit E (2009). Passive membrane properties and electrotonic signal processing in retinal rod bipolar cells. J Physiol 587(Pt 4):829-49.

Olveczky BP, Baccus SA, and Meister M (2007). Retinal adaptation to object motion. Neuron 56(4):689-700.

Organisciak DT, Bicknell IR, Darrow RM (1992). The effects of L-and D-ascorbic acid administration on retinal tissue levels and light damage in rats. Curr Eye Res 11:231-241.

Overstreet LS, Jones MV, and Westbrook GL (2000). Slow desensitization regulates the availability of synaptic GABA(A) receptors. J Neurosci 20(21):7914-21.

Palacios AG, Varela FJ, Srivastava R, Goldsmith TH (1998). Spectral sensitivity of cones in the goldfish, Carassius auratus. Vision Res 38:2135-2146.

Palmer MJ (2010). Characterisation of bipolar cell synaptic transmission in goldfish retina using paired recordings. J Physiol 588:1489-1498.

Palmer MJ, Taschenberger H, Hull C, Tremere L, von Gersdorff H (2003). Synaptic activation of presynaptic glutamate transporter currents in nerve terminals. J Neurosci 23:4831-4841.

Palmer MJ (2006). Functional segregation of synaptic $GABA_A$ and $GABA_C$ receptors in goldfish bipolar cell terminals. J Physiol 577:45-53.

Pan ZH, Bahring R, Grantyn R, Lipton SA (1995). Differential modulation by sulfhydryl redox agents and glutathione of GABA- and glycine-evoked currents in rat retinal ganglion cells. J Neurosci 15:1384-1391.

Pan ZH, Zhang X, Lipton SA (2000). Redox modulation of recombinant human $GABA_A$ receptors. Neuroscience 98:333-338.

Pang JJ, Gao F, Wu SM (2007). Cross-talk between ON and OFF channels in the salamander retina: indirect bipolar cell inputs to ON-OFF ganglion cells. Vision Res 47:384-392.

Pang JJ, Gao F, Lem J, Bramblett DE, Paul DL, and Wu SM (2010). Direct rod input to cone BCs and direct cone input to rod BCs challenge the traditional view of mammalian BC circuitry. Proc Natl Acad Sci 107(1):395-400.

Papke D, Gonzalez-Gutierrez G, and Grosman C (2011). Desensitization of neurotransmitter-gated ion channels during high-frequency stimulation: a comparative study of Cys-loop, AMPA and purinergic receptors. J Physiol 589(Pt 7):1571-85.

Petrides A and Trexler EB (2008). Differential output of the high-sensitivity rod photoreceptor: AII amacrine pathway. J Comp Neurol 507(5):1653-62.

Portugal CC, Miya VS, Calaza Kda C, Santos RA, Paes-de-Carvalho R (2009). Glutamate receptors modulate sodium-dependent and calcium-independent vitamin C bidirectional transport in cultured avian retinal cells. J Neurochem 108:507-520.

Protti DA, Gerschenfeld HM, Llano I (1997). GABAergic and glycinergic IPSCs in ganglion cells of rat retinal slices. J Neurosci 17:6075-6085.

Protti DA, Llano I (1998). Calcium currents and calcium signaling in rod bipolar cells of rat retinal slices. J Neurosci 18:3715-3724.

Protti DA, Flores-Herr N, and von Gersdorff H (2000). Light evokes Ca^{2+} spikes in the axon terminal of a retinal bipolar cell. Neuron 25:215-227.

Quraishi S, Gayet J, Morgans CW, and Duvoisin RM (2007). Distribution of group-III metabotropic glutamate receptors in the retina. J Comp Neurol 501(6):931-43.

Raviola E and Dacheux RF (1987). Excitatory dyad synapse in rabbit retina. Proc Natl Acad Sci 84(20):7324-8.

Rebec GV, Pierce RC (1994). A vitamin as neuromodulator: Asc release intro extracellular fluid of the brain regulates DA and Glut transmission. Progress in Neurobiology 45:537-565.

Reich DS, Mechler F and Victor JD (2001). Temporal coding of contrast in primary visual cortex: when what, and why. J Neurophysiol 85(3):1039-50.

Reyes AD (2011). Synaptic short-term plasticity in auditory cortical circuits. Hear Res 279(1-2):60-6.

Rice ME (2000). Ascorbate regulation and its neuroprotective role in the brain. Trends Neurosci 23:209-216.

Rivera C, Wegelius K, Reeben M, Kaila K, Michael P (2000). Different sensitivities of human and rat rho(1) GABA receptors to extracellular pH. Neuropharmacology 39:977-989.

Rose RC, Bode AM (1991). Ocular ascorbate transport and metabolism. Comp Biochem Physiol A 100:273-285.

Roska B, Werblin F (2001). Vertical interactions across ten parallel, stacked representations in the mammalian retina. Nature 410:583-587.

Ruiz-Gomez A, Fernandez-Shaw C, Morato E, Marvizon JC, Vazquez J, Valdivieso F, Mayor F, Jr. (1991). Sulfhydryl groups modulate the allosteric interaction between glycine binding sites at the inhibitory glycine receptor. J Neurochem 56:1690-1697.

Ruppersberg JP, Stocker M, Pongs O, Heinemann SH, Frank R, Koenen M (1991). Regulation of fast inactivation of cloned mammalian $I_{K(A)}$ channels by cysteine oxidation. Nature 352:711-714.

Rutherford LC, Nelson SB, and Turrigiano GG (1998). BDNF has opposite effects on the quantal amplitude of pyramidal neuron and interneuron excitatory synapses. Neuron 21(3):521-30.

Sagdullaev BT, Eggers ED, Purgert R, and Lukasiewicz PD (2011). Nonlinear interactions between excitatory and inhibitory retinal synapses control visual output. J Neurosci 31(42):15102-12.

Sagdullaev BT, McCall MA, and Lukasiewicz (2006). Presynaptic inhibition modulates spillover, creating distinct dynamic response ranges of sensory output. Neuron 50(6):923-35.

Saito T, Kondo H, Toyoda J (1981). Ionic mechanisms of two types of on-center bipolar cells in the carp retina. II. The responses to annular illumination. J Gen Physiol 78:569-589.

Sakatani T and Isa T (2007). Quantitative analysis of spontaneous saccade-like rapid eye movements in C57BL/6 mice. Neurosci Res 58(3):324-31.

Sangameswaran L, Delgado SG, Fish LM, Koch BD, Jakeman LB, Stewart GR, Sze P, Hunter JC, Eglen RM, and Herman RC (1996). Structure and function of a novel voltage-gated, tetrodotoxin-resistant sodium channel specific to sensory neurons. J Biol Chem 271(11):5953-6.

Sasaki T and Kaneko A (1996). L-Glutamate-induced responses in OFF-type bipolar cells of the cat retina. Vision Res 36(6):787-95.

Sawtell NB, Williams A, Roberts PD, von der Emde G and Bell CC (2006). Effects of sensing behavior on a latency code. J Neurosci 26(32):8221-34.

Schaerer S and Kirschfeld K (2000). The role of background movement in goldfish vision. J Comp Physiol A 186(6):583-93.

Schoonheim PJ, Arrenberg AB, Del Bene F and Baier H (2010). Optogenetic localization and genetic perturbation of saccade-generating neurons in zebrafish. J Neurosci 30(20):7111-20.

Sedelnikova A, Smith CD, Zakharkin SO, Davis D, Weiss DS, Chang Y (2005). Mapping the rho1 $GABA_C$ receptor agonist binding pocket. Constructing a complete model. J Biol Chem 280:1535-1542.

Schiller PH (1992). The ON and OFF channels of the visual system. Trends Neurosci 15(3):86-92.

Schneggenburger R, Sakaba T, and Neher E (2002). Vesicle pools and short-term synaptic depression: lessons from a large synapse. Trends Neurosci 25(4):206-12.

Shen Y, Heimel JA, Kamermans M, Peachy NS, Gregg RG, and Nawy S (2009). A transient receptor potential-like channel mediates synaptic transmission in rod bipolar cells. J Neurosci 29(19):6088-93.

Shen Y, Liu XL, and Yang XL (2006). N-methyl-D-aspartate receptors in the retina. Mol Neurobiol 34(3):163-79.

Shields CR, Lukasiewicz PD (2003). Spike-dependent GABA inputs to bipolar cell axon terminals contribute to lateral inhibition of retinal ganglion cells. J Neurophysiol 89:2449-2458.

Singer JH and Diamond JS (2003). Sustained Ca^{2+} entry elicits transient postsynaptic currents at a retinal ribbon synapse. J Neurosci 23(34):10923-33.

Singer JH, Diamond JS (2006). Vesicle depletion and synaptic depression at a mammalian ribbon synapse. J Neurophysiol 95:3191-3198.

Sivyer B, Venkataramani S, Taylor WR, and Vaney DI (2011). A novel type of complex ganglion cell in rabbit retina. J Comp Neurol 519(16):3128-38.

Slaughter MM, Miller RF (1981). 2-amino-4-phosphonobutyric acid: a new pharmacological tool for retina research. Science 211:182-185.

Slaughter MM and Awatramani GB (2002). On bipolar cells: following in the footsteps of phototransduction. Adv Exp Med Biol 514:477-92.

Snellman J, Zenisek D, and Nawy S (2009). Switching between transient and sustained signaling at the rod bipolar-AII amacrine cell synapse of the mouse retina. J Physiol 587:2443-55.

Snellman J, Mehta B, Babai N, Bartoletti TM, Akmentin W, Francis A, Matthews G, Thoreson W, and Zenisek D (2011). Acute destruction of the synaptic ribbon reveals a role for the ribbon in vesicle priming. Nat Neurosci 14(9):1135-41.

Song J, Kwon O, Chen S, Daruwala R, Eck P, Park JB, and Levine M (2002). Flavonoid inhibition of sodium-dependent vitamin C transporter 1 (SVCT1) and glucose transporter isoform 2 (GLUT2), intestinal transporters for vitamin C and Glucose. J Biol Chem 277(18):15252-60.

Srinivasan MV, Laughlin SB, Dubs A (1982). Predictive coding: a fresh view of inhibition in the retina. Proc R Soc Lond B Biol Sci 216(1205):427-59.

Stadtman ER (1991). Ascorbic acid and oxidative inactivation of proteins. Am J Clin Nutr 54:1125S-1128S.

Stadtman ER (1993). Oxidation of free amino acids and amino acid residues in proteins by radiolysis and by metal-catalyzed reactions. Annu Rev Biochem 62:797-821.

Steinert JR, Robinson SW, Tong H, Haustein MD, Kopp-Scheinpflug C, and Forsythe ID (2011). Nitric oxide is an activity-dependent regulator of target neuron intrinsic excitability. Neuron 71(2):291-305.

Stell WK (1978). Inputs to bipolar cell dendrites in goldfish retina. Sens Processes 2(4):339-49.

Sterling P (2004). How retinal circuits optimize the transfer of visual information. In: The Visual Neurosciences (Chalupa LM, Werner JS ed), pp234-259. Cambridge, MA; London, England: The MIT Press.

Sterling P and Freed M (2007). How robust is a neural circuit? Vis Neurosci 24(4):563-71.

Sterling P and Matthews G (2005). Structure and function of ribbon synapses. Trends Neurosci 28(1):20-9.

Strettoi E, Raviola E, and Dacheux RF (1992). Synaptic connections of the narrow-field, bistratified rod amacrine cell (AII) in the rabbit retina. J Comp Neurol 325(2):152-68.

Sullivan JM, Traynelis SF, Chen HS, Escobar W, Heinemann SF, Lipton SA (1994). Identification of two cysteine residues that are required for redox modulation of the NMDA subtype of glutamate receptor. Neuron 13:929-936.

Szalisznyo K, Longtin A, and Maler L (2008). Effect of synaptic plasticity on sensory coding and steady-state filtering properties in the electric sense. Biosystems 92(1):16-28.

Tatsukawa T, Hirasawa H, Kaneko A, Kaneda M (2005). GABA-mediated component in the feedback response of turtle retinal cones. Vis Neurosci 22:317-324.

Taylor WR (1999). TTX attenuates surround inhibition in rabbit retinal ganglion cells. Vis Neurosci 16:285-290.

Taylor WR and Smith RG (2004). Transmission of scotopic signals from the rod to rod-bipolar cell in the mammalian retina. Vision Res 44(28):3269-76.

Thoreson WB, Babai N, Bartoletti TM (2008). Feedback from horizontal cells to rod photoreceptors in vertebrate retina. J Neurosci 28:5691-5695.

Tian M, Jarsky T, Murphy GJ, Rieke F, and Singer JH (2010). Voltage-gated Na channels in AII amacrine cells accelerate scotopic light responses mediated by the rod bipolar cell pathway. J Neurosci 30(13):4650-9.

Turrigiano GG (1999). Homeostatic plasticity in neuronal networks: the more things change, the more they stay the same. Trends Neurosci 22(5):221-7.

Usrey WM, Alonso JM and Reid RC (2000). Synaptic interactions between thalamic inputs to simple cells in cat visual cortex. J Neurosci 20(14):5461-7.

Venkataramani S and Taylor WR (2010). Orientation selectivity in rabbit retinal ganglion cells is mediated by presynaptic inhibition. J Neurosci 30(46):15664-76.

Veruki ML, Oltedal L, and Hartveit E (2008). Electrical synapses between AII amacrine cells: dynamic range and functional consequences of variation in junctional conductance. J Neurophysiol 100(6):3305-22.

Vigh J and von Gersdorff H (2005). Prolonged reciprocal signaling via NMDA and GABA receptors at a retinal ribbon synapse. J Neurosci 25(49):11412-23.

Vigh J, Li GL, Hull C, and von Gersdorff H (2005). Long-term plasticity mediated by mGluR1 at a retinal reciprocal synapse. Neuron 46(3):469-82.

Vigh J, Vickers E, and von Gersdorff H (2011). Light-evoked lateral GABAergic inhibition at single bipolar cell synaptic terminals is driven by distinct retinal microcircuits. J Neurosci 31:15884-15893.

Vigh J, Witkovsky P (2004). Neurotransmitter actions on transient amacrine and ganglion cells of the turtle retina. Vis Neurosci 21:1-11.

von Gersdorff H and Matthews G (1997). Depletion and Replenishment of Vesicle Pools at a Ribbon-Type Synaptic Terminal. J Neurosci 17:1919-1927.

von Gersdorff H, Sakaba T, Berglund K, and Tachibana M (1998). Submillisecond kinetics of glutamate release from a sensory synapse. 21(5):1177-88.

von Gersdorff H, Matthews G (1999) Electrophysiology of synaptic vesicle cycling. Annu Rev Physiol 61:725-752.

von Gersdorff H and Borst JG (2002). Short-term plasticity at the calyx of held. Nat Rev Neurosci 3(1):53-64.

Wang P and Slaughter MM (2005). Effects of GABA Receptor Antagonists on Retinal Glycine Receptors and on Homomeric Glycine Receptor Alpha Subunits. J Neurophysiol 93:3120-3126.

Wang TL, Hackam A, Guggino WB, Cutting GR (1995). A single histidine residue is essential for zinc inhibition of GABA rho 1 receptors. J Neurosci 15:7684-7691.

Wässle H, Koulen P, Brandstatter JH, Fletcher EL, Becker CM (1998). Glycine and GABA receptors in the mammalian retina. Vision Res 38:1411-1430.

Watanabe S, Koizumi A, Matsunaga S, Stocker JW, Kaneko A (2000). GABA-mediated inhibition between amacrine cells in the goldfish retina. J Neurophysiol 84:1826-1834.

Witkovsky P, Dowling JE (1969). Synaptic relationships in the plexiform layers of carp retina. Z Zellforsch Mikrosk Anat 100:60-82.

Witkovsky P, Nelson J, and Ripps H (1973). Action spectra and adaptation properties of carp photoreceptors. J Gen Physiol 61(4):401-23.

Werblin FS (2010). Six different roles for crossover inhibition in the retina: correcting the nonlinearities of synaptic transmission. Vis Neurosci 27(1-2):1-8.

Werblin FS (2011). The retinal hypercircuit: a repeating synaptic interactive motif underlying visual function. J Physiol 589(Pt 15):3691-702.

Wierda KD, Toonen RF, de Wit H, Brussaard AB, and Verhage M (2007). Interdependence of PKC-dependent and PKC-independent pathways for presynaptic plasticity. Neuron 54(2):275-90.

Witkovsky P and Dowling JE (1969). Synaptic relationships in the plexiform layers of carp retina. Z Zellforsch Mikrosk Anat 100(1):60-82.

Witkovsky P, Nelson J, and Ripps H (1973). Action spectra and adaptation properties of carp photoreceptors. J Gen Physiol 61(4):401-23.

Wong KY, Cohen ED, Dowling JE (2005). Retinal bipolar cell input mechanisms in giant danio. II. Patch-clamp analysis of ON bipolar cells. J Neurophysiol 93:94-107.

Woodward RM, Polenzani L, Miledi R (1993). Characterization of bicuculline/baclofen-insensitive (rho-like) gamma-aminobutyric acid receptors expressed in Xenopus oocytes. II. Pharmacology of gamma-aminobutyric acid A and gamma-aminobutyric acid B receptor agonists and antagonists. Mol Pharmacol 43:609-625.

Wu SM (1992). Feedback connections and operation of the outer plexiform layer of the retina. Curr Opin Neurobiol 2(4):462-8.

174

Wunk DF and Werblin FS (1979). Synaptic inputs to the ganglion cells in the tiger salamander retina. J Gen Physiol 73(3):265-86.

Yang XL (2004). Characterization of receptors for glutamate and GABA in retinal neurons. Prog Neurobiol 73(2):127-50.

Yevenes GE, Moraga-Cid G, Guzman L, Haeger S, Oliveira L, Olate J, Schmalzing G, Aguayo LG (2006). Molecular determinants for G protein betagamma modulation of ionotropic glycine receptors. J Biol Chem 281:39300-39307.

Zenisek D and Matthews G (1998). Calcium action potentials in retinal bipolar neurons. Vis Neurosci 15:69-75.

Zenisek D, Henry D, Studholme K, Yazulla S, Matthews G (2001). Voltage-dependent sodium channels are expressed in nonspiking retinal bipolar neurons. J Neurosci 21:4543-4550.

Zhang AJ, Wu SM (2009). Receptive fields of retinal bipolar cells are mediated by heterogeneous synaptic circuitry. J Neurosci 29:789-797.

Zhang D, Pan ZH, Awobuluyi M, Lipton SA (2001). Structure and function of $GABA_C$ receptors: a comparison of native versus recombinant receptors. Trends Pharmacol Sci 22:121-132.

Zhang J, Slaughter MM (1995). Preferential suppression of the ON pathway by GABA$_C$ receptors in the amphibian retina. J Neurophysiol 74:1583-1592.

Zhang J, Jung CS, Slaughter MM (1997). Serial inhibitory synapses in retina. Vis Neurosci 14:553-563.

Zhang J, Li W, Trexler EB, Massey SC (2002). Confocal analysis of reciprocal feedback at rod bipolar terminals in the rabbit retina. J Neurosci 22:10871-10882.

Zhang J, De Blas AL, Miralles CP, Yang CY (2003). Localization of GABA$_A$ receptor subunits alpha 1, alpha 3, beta 1, beta 2/3, gamma 1, and gamma 2 in the salamander retina. J Comp Neurol 459:440-453.

Zucker RS and Regehr WG (2002). Short-term synaptic plasticity. Annu Rev Physiol 64:355-405.

Circuit mechanisms of short-term plasticity of light-evoked lateral feedback inhibition at retinal bipolar cell terminals.

*The experimental methods and results presented in this Appendix are to be considered as directly supplemental to work shown in Chapter 2.

Materials and Methods

Retinal slice preparation and electrophysiology. Slices were prepared from pieces of goldfish (*Carassius auratus*; 8-14 cm) retina, as described previously (Palmer et al., 2003). For all experiments, goldfish, of either sex, were dark adapted for 1-2 hrs prior to dissection, and slicing solution contained the following (in mM): 119.0 NaCl, 2.5 KCl, 3.2 $MgCl_2$, 0.3 $CaCl_2$, 12.0 glucose, 12.0 HEPES, and 0.2 ascorbic acid. The pH was set to 7.45 with NaOH, and osmolarity was set to 260 – 265 mOsm. Dissection was performed under either dark or dim red light conditions, and recording was performed under either mesopic (1.01 x 10^3 – 5.03 x 10^3 photons $\mu m^{-2} s^{-1}$) or scotopic (5.03 x 10^1 photons $\mu m^{-2} s^{-1}$) background conditions (Krizaj, 2000). Background light levels were measured with an ILT-1700 photometer and SE033 detector from International Light Technologies (Peabody, Massachusetts). Transverse slices (250 μm thick) were cut with a Narishige ST-20 vertical slicer and transferred to a Sylgard (Dow Corning, Midland, MI) recording chamber, where they were secured in parallel lanes of petroleum jelly. The chamber and slices were then moved to an upright microscope (Zeiss Axioskop; Oberkochen, Germany), where the slices were constantly perfused with external recording solution bubbled with 95% O_2 and 5% CO_2 mixed gas at 4-5 ml/min, and viewed with infrared differential interference contrast (IR-DIC) optics through a 40x water-immersion objective (Zeiss) coupled with 2.0 pre-magnification and an IR CCD camera (XC-75, Sony). The output of the CCD camera was sent to a Hamamatsu Camera Controller C2741-62, and then to a 13" Sony B/W monitor for viewing. Axotomized bipolar cell terminals (i.e. with severed axons) were identified in the inner plexiform layer (IPL) based on: (1) Mb-shaped (bulbous) terminal morphology (Fig 2.1A), (2) single-exponential membrane time constant (not shown), and (3) the presence of an L-type Ca^{2+} current, reciprocal feedback, and ΔC_m jump (Fig 2.1B) (Palmer et al., 2003) associated with exocytosis (von Gersdorff and Matthews, 1999).

178

Axotomized bipolar cell terminals in retinal slices were voltage clamped at -60 or -70 mV (uncorrected for liquid junction potential) in the whole-cell mode using a HEKA Elektronik (Lambrecht/Pfalz, Germany) EPC-9 patch-clamp amplifier in conjunction with Pulse software running the xChart extension (Pulse version 8.53). The Sine+DC technique (Gillis, 2000) was used for real-time measurements of membrane capacitance. Briefly, a 30 mV peak-to-peak, 1-2 kHz sine wave was superimposed on the holding potential of the cells (-60 mV) and used by on-line analysis software to calculate time-resolved membrane capacitance. Standard external recording solutions contained (in mM) 100.0 NaCl, 2.5 KCl, 2.5 $CaCl_2$, 1.0 $MgCl_2$, 25.0 $NaHCO_3$, 0.2 ascorbic acid, and 12.0 glucose (pH 7.45; osmolarity, 260–265 mOsm). Patch pipettes (6-12 MΩ) were pulled, using either a vertical (Narishige, PP-830) or horizontal (Sutter Instruments, P-97) puller, from thick-walled 1.5 mm outer diameter borosilicate capillary glass from World Precision Instruments (1B150F-4; Sarasota, FL), and coated with dental wax (Cavex, West Chester, PA) to reduce pipette capacitance. Internal pipette solutions contained the following solutions (in mM): 60.0 Cs gluconate, 40.0 CsCl, 10.0 TEA-Cl, 25.0 HEPES, 3.0 Mg-ATP, 0.5 Na-GTP, and 2.0 EGTA. Some internal solutions contained 3.0 mM ascorbic acid and/or 3.0 mM reduced glutathione. All internals were set to pH 7.2 with CsOH, and osmolarity was adjusted to 250 mOsm with Cs gluconate and/or millipure H_2O. NBQX, TTX, TPMPA and gabazine (SR95531) were obtained from Tocris (Bristol, UK). All other chemicals were obtained from Sigma (St. Louis, MO).

As in Vigh et al., 2011, recordings were performed at 20-22º C during the daytime (morning/afternoon) to avoid circadian variation in glutamate release from bipolar cells (Hull et al., 2006b). Voltage-clamp series resistance (R_s) was not compensated, and liquid junction potential was not corrected. Cells with R_s > 30 MΩ or |leak| > 50 pA at a holding potential of -60 mV were excluded from analysis. Average

values for Rs and leak current at a holding potential of -60 mV were 22.0 ± 1.2 MΩ and -34.2 ± 2.6 pA, respectively (mean ± SE; n=75).

Light Stimulation. Recordings were performed under mesopic background light conditions (5.03 x 10^3 photons $\mu m^{-2}s^{-1}$; see **Chapter 2**, Fig 2.5), unless otherwise noted. Slices were stimulated with a white LED connected via soldered wire and BNC cable to a digital-to-analog output of the HEKA EPC-9 amplifier, as described previously (Vigh et al., 2011). The LED was positioned at a ~30⁰ angle above and behind the recording chamber, at a distance of 3 cm. Full field light flashes for all experiments were delivered by application of voltage steps from 0 to between 3 and 5 V, which evoked a photon flux at the slice of between 5.69 X 10^4 and 7.32 X 10^5 photons $\mu m^{-2} s^{-1}$ (unless otherwise noted), which is above the threshold for cone photoreceptor activation (~10^2 photons $\mu m^{-2} s^{-1}$; Busskamp et al., 2010). The timing and amplitude of voltage steps was controlled from within the Pulse Software (HEKA Elektronik) running the EPC-9 amplifier. Calibration of light flash timing (onset and offset) was performed with a photodiode connected to the EPC-9 amplifier through an ITHACO 4302 dual 24 dB Octave Filter. Light flash onset and offset had rise and decay time constants of 0.12 and 6.3 ms, respectively. Onset and offset times did not vary as a function of flash duration between 100 and 1000 ms, or with the presentation of paired flashes with intervals ranging between 300 and 1900 ms. Calibration of light intensity was performed with an ILT-1700 photometer and SE033 detector from International Light Technologies (Peabody, MA). Factory calibration determined the photopic illuminance response sensitivity of the detector to be 2.60 x 10^{-8} A ft^2 lm^{-1}, or 2.415 x 10^{-9} A lux^{-1}, assuming 3215 K color temperature.

Puff application of L-glutamate. Puff pipettes (7-10 MΩ) were pulled with a vertical

puller (Narishige, PP-830) using thick-walled 1.5 mm outer diameter borosilicate

capillary glass from World Precision Instruments (1B150F-4; Sarasota, FL). Pipettes

were then filled with standard external recording solution containing 1 mM L-glutamate

(Sigma). The pH of the puff solution was set to 7.45 with CsOH and HCl, and osmolarity

was set to 260 mOsm with millipure H_2O. The puff pipette was positioned at the surface

of the slice, ~50 to 80 μm upstream of the patch pipette in the OFF layer (sublamina a)

of the IPL, and the puff solution was pressure ejected at ~10 psi using a Picospritzer III

(Parker Instrumentation) driven by 100% N_2 gas. Paired puff applications were triggered

and timed with the Pulse Software (HEKA Elektronik) running the EPC-9 amplifier, and

paired pulse intervals (PPI) were set as the exact interval between the offset of the first

puff and the onset of the second puff. Puff pipettes were replaced when they became

blocked by tissue debris, and responses (i.e. puff-evoked L-IPSCs) were excluded from

analysis when they were not stable for at least three consecutive stimulations with an

inter-stimulus interval of 30 s.

Analysis of amplitude, charge and onset latency of L-IPSCs. Light responses at

each paired pulse interval (PPI) were repeated at least five times per cell and averaged,

unless otherwise stated (as previously described; see **Chapter 2**). An interval of 20 or 30

s was presented between stimulations to allow for recovery from depression in

neighboring Mb presynaptic terminals (von Gersdorff and Matthews, 1997), and

stimulation with PPIs ranging from 50 – 2300 ms were interleaved to avoid systematic

errors due to rundown of the light responses, which were generally stable during

recordings of up to 30 minutes. For PPIs shorter than 300 ms, alternating single and

double flashes were presented so that single responses could be subtracted from double

responses. This allowed for isolation of the first OFF response and second ON response

so that amplitude, charge transfer, and onset latencies could be reliably measured at short PPIs (i.e. 50 ms). In order to isolate first and second L-IPSCs during puff application of L-glutamate at a PPI of 300 ms, we subtracted first L-IPSCs taken from the 1900 ms PPI.

L-IPSC amplitude was calculated by subtracting a baseline ON and OFF current (first 20 ms following onset and offset of light flash, respectively) from the peak current amplitude during the 400 ms light flash and the 300 ms following the offset of the light flash for ON and OFF responses, respectively. Charge transfer was calculated by integrating current traces during these ON (400 ms) and OFF (300 ms) response windows following baseline subtraction.

L-IPSC onset latencies were determined using a custom IGOR procedure that detected the time at which the L-IPSC crossed a threshold current set at baseline minus 2 standard deviations (SD), where the baseline and SD were calculated from the 20 ms period at the beginning of either the ON or OFF response windows. The threshold crossing was determined by moving backwards in time from the peak of the L-IPSC, which was detected as the global minima of the current recording during the response window. Due to the uncertainty introduced to these measurements by the possibility of small, asynchronous events, latency outliers that exceeded the population mean by more than 10 SD were excluded from further analysis. Latencies calculated with a similar technique where the threshold was set at 10% of the difference between baseline and peak current were not significantly different from those calculated with the 2 SD criteria.

DIC montages. During some recordings of single axotomized Mb terminals, the internal solution contained 150-200 µM Alexa 555 hydrazide. DIC montage images were recorded in iMovie (Apple) by connecting the Hamamatsu Camera Controller to a

MacBook Pro (Apple) via a Dazzle Hollywood DV-Bridge frame-grabber. DIC images were later cropped and re-aligned to construct individual montages with ImageJ (NIH) and Photoshop (Adobe) software.

Statistical Analysis. Statistics were performed on averaged traces, unless otherwise noted, by using Prism (version 4; GraphPad Software, San Diego, CA). Two-tailed paired or unpaired Student's t-tests were used to compare data sets where appropriate, and one-sample t-tests with a hypothetical mean of 0 or 1 were used to test paired-pulse plasticity of onset latency or size, respectively, at each PPI. Welch's correction for unequal variances was used for unpaired Student's t-tests when comparing samples of disparate size or variance. Data are reported as mean ± SEM, and values of $p < 0.05$ were considered statistically significant.

Results

Temporally distinct components of GABAergic signaling regulate STP of L-IPSCs

Our previous work (Chapter 2) showed a notable difference between the temporal profiles of ON and OFF L-IPSC amplitude and charge transfer STP. In particular, charge transfer STD at short PPIs (i.e. 50 ms) tended to be more pronounced than amplitude STD (Fig 2.3). A similar comparison between L-IPSC amplitude and charge transfer STP at intermediate and long PPIs (i.e. 1100-2300 ms) revealed that, while late-phase ON STD was evident for both amplitude and charge transfer, OFF STF was primarily evident for L-IPSC amplitude. Furthermore, previous studies have shown anatomical segregation of $GABA_A$ (fast, transient) and $GABA_C$ (slow, sustained) synapses in the IPL of rat retina (Koulen et al., 1998), functional segregation of $GABA_A$ and $GABA_C$ mIPSCs (Palmer, 2006), and temporal segregation of $GABA_AR$ (fast) and $GABA_CR$ (slow) mediated reciprocal feedback IPSCs (Vigh and von Gersdorff, 2005) at both goldfish Mb

183

(Vigh and von Gersdorff, 2005) and mouse rod BC terminals (Eggers and Lukasiewicz, 2006). In addition, previous work in our lab showed a functional segregation of GAT-1 GABA transporters and signaling at Mb terminal $GABA_C Rs$ (Hull et al., 2006a). For these reasons, we directly compared the roles of temporally distinct signaling at Mb $GABA_A Rs$ and $GABA_C Rs$, as regulated by GAT-1 and GAT-2/3 transporters, in the STP of ON and OFF L-IPSC amplitude and charge transfer.

Signaling at $GABA_C Rs$ regulates STP of OFF L-IPSC amplitude

First, we tested the effect of blocking $GABA_C Rs$ (+150 μM TPMPA) on ON and OFF L-IPSC peak amplitude and onset latency STP (Fig A.1). In the presence of TPMPA, no significant STP of ON L-IPSC amplitude was seen at the 300, 1100, and 1900 ms PPIs (Fig A.1B, left). However, STD of L-IPSC amplitude was evident at the 50 ms PPI for both ON (PPR = 0.42 ± 0.06; n=6; p<0.001, one-sample t-test, null PPR = 1) and OFF L-IPSCs (Fig A.1B, right; PPR = 0.76 ± 0.04; n=5; p<0.01). Interestingly, OFF amplitude STD in the presence of TPMPA was reduced relative to control conditions at the 300 ms PPI (Control PPR = 0.82 ± 0.07, n=32; TPMPA PPR = 1.26 ± 0.14, n=6; p=0.03, unpaired Student's t-test, two tailed with Welch's correction), while OFF amplitude STF was eliminated at PPIs of both 1100 ms (Control PPR = 1.21 ± 0.10, n=32; TPMPA PPR = 0.88 ± 0.09, n=6; p=0.02) and 1900 ms (Control PPR = 1.26 ± 0.09, n=37; TPMPA PPR = 0.91 ± 0.06, n=6; p<0.01). These results supported the idea that low frequency OFF STD (i.e. PPI = 300 ms) may be driven by vesicle depletion at AC boutons that make $GABA_C$ synapses onto the Mb terminal, while low frequency OFF STF (i.e. at PPIs of 1100 or 1900 ms) may be attenuated by enhanced STD of glutamate release at neighboring BC terminals in the absence of feedback inhibition mediated by signaling at $GABA_C Rs$ (Vigh et al., 2005; Li et al., 2007; Sagdullaev et al., 2011).

GAT-1 and GAT-2/3 GABA transporters differentially regulate ON and OFF L-IPSCs

In order to test the idea that the size and timing of ON and OFF L-IPSCs may depend on

the precise, independent regulation of signaling at separate $GABA_A$ and $GABA_C$

synapses (Hull et al., 2006a; Palmer, 2006), we tested the effects of pharmacological

blockade of GAT-1 or GAT-2/3 (Fig A.2) under scotopic background conditions (5.03 x

10^1 photons $\mu m^{-2}s^{-1}$; see **Chapter 2**, Fig 2.5). These two classes of GABA transporters

(GATs) show differential spatial distribution throughout the inner and outer retina

(Ekstrom and Anzelius, 1998; Klooster et al., 2004), and have been previously shown to

exert both independent and combined influences on GABA IPSC amplitude and decay

kinetics in the thalamus (synaptic GAT-1 regulates $GABA_B$ IPSC amplitude, while

broadly distributed extrasynaptic GAT-3 regulates IPSC duration; Beenhakker and

Huguenard, 2010), globus pallidus (axonally expressed GAT-1 regulates $GABA_A$ IPSC

amplitude, and GAT-3 in glial processes regulates IPSC amplitude and decay; Jin et al.,

2011), and the retina (block of GAT-1 enhances charge transfer of $GABA_C$ IPSCs;

Ichinose and Lukasiewicz, 2002).

First, we tested the effects of GAT-1 blockade on ON and OFF L-IPSCs with a

competitive antagonist for GAT-1, SKF-89976A (SKF; Fig A.2Bi, A.2Bii). Bath application

of between 5 and 20 µM SKF caused a significant increase in ON L-IPSC charge

transfer **(**Control = -3.67 ± 0.79 pC; SKF = -5.21 ± 1.14 pC; n=8**;** p=0.04**,** paired

Student's t-test, two-tailed) and peak latency (Control = 104.50 ± 15.06 ms; SKF =

214.80 ± 43.77 ms; n=8; p=0.04) relative to control conditions. These results suggested

that GAT-1 transporters may play a critical role in the regulation of ON L-IPSCs, in

addition to their previously demonstrated role in shaping $GABA_C$R mediated standing

leak current at the Mb terminal (Hull et al., 2006a). Furthermore, the finding that block of

GAT-1 acted primarily to enhance the charge transfer and peak latency of ON L-IPSCs,

185

and not the amplitude and onset latency (data not shown), was consistent with the idea that GAT-1 functionally co-segregates with $GABA_CRs$ (Hull et al., 2006a; Palmer, 2006), which primarily drive the slow, sustained component of L-IPSCs (Fig A.4Ai). Note that L-IPSC amplitudes, especially for the OFF response, were difficult to quantify in the presence of SKF due to the large increase in standing leak current (Fig A.2Bi).

To test the idea that GAT-2/3 transporters play a functional role distinct from that of GAT-1 transporters in shaping L-IPSCs at the Mb terminal, we bath applied the specific GAT-2/3 antagonist (S)-SNAP 5114 (SNAP; Fig A.2Ai, A.2Aii). Treatment with 50 µM SNAP caused a significant increase in ON (Control = -34.62 ± 7.62 pA; SNAP = -52.80 ± 10.34 pA; n=8; p=0.02; Fig A.2Aii, upper) and OFF (Control = -28.16 ± 5.02 pA; SNAP = -49.33 ± 12.48 pA; n=8; p=0.04; Fig A.2Aii, lower) L-IPSC peak amplitude. The enhancement of OFF L-IPSC peak amplitude was reversible upon wash out (p=0.04; n=4; paired Student's t-test, two tailed; not shown). This result was consistent with the idea that GAT-2/3 may be functionally co-segregated with $GABA_ARs$ (Palmer, 2006), which contribute primarily to the fast, transient component of L-IPSCs (Fig A.4Ai). There was no significant effect of SNAP on standing leak current at the Mb terminal (Control = -32.14 ± 3.27 pA; SNAP = -37.50 ± 3.20 pA; n=8; p>0.05; not shown). This lack of an effect of SNAP on Mb standing leak current suggested that GAT-2/3 transporters, unlike GAT-1 transporters, are excluded from extrasynaptic regions of $GABA_CRs$ that mediate standing leak current (Hull et al., 2006a).

Block of GAT-2/3 transforms STP of ON L-IPSC charge and OFF L-IPSC amplitude
In order to explore the role that GABA transporter regulation of L-IPSC amplitudes and signaling at $GABA_ARs$ might play in shaping STP of ON and OFF lateral inhibitory feedback at the Mb terminal, we tested paired light flash evoked STP in the presence of 50 µM SNAP (Fig A.3) under scotopic background conditions (5.03×10^1 photons $\mu m^{-2} s^{-}$

[1]). We found that block of GAT-2/3 enhanced STD of ON L-IPSC charge transfer relative to control at the 300 ms PPI (Fig A.3B, left; Control PPR = 0.86 ± 0.09, n=34; SNAP PPR = 0.58 ± 0.10, n=8; p<0.05, unpaired Student's t-test, two tailed with Welch's correction). This result is consistent with the idea that GAT-2/3 may act to strongly buffer GABA concentration at the synaptic cleft between ON AC boutons and the Mb terminal under physiological conditions. Block of GAT-2/3 may allow for increased desensitization at $GABA_A$Rs on the Mb terminal, or may unmask strong STD due to vesicle depletion at presynaptic ON AC boutons. We also observed STD of OFF L-IPSC amplitude at a PPI of 1100 ms (Fig A.3B, right; SNAP PPR = 0.80 ± 0.08; n=8; p=0.04, one-sample t-test, null PPR = 1). This represented a significant reduction in PPR relative to the OFF L-IPSC amplitude STF observed under control conditions at the 1100 ms PPI (p<0.01, unpaired Student's t-test, two tailed with Welch's correction). Such block of STF suggests that GAT-2/3 activity may also promote $GABA_A$R desensitization at synapses from OFF ACs onto the Mb terminal.

Onset latencies of ON L-IPSCs are delayed by block of signaling at $GABA_A$Rs

In the presence of SR95531, the purely $GABA_C$ mediated component of ON and OFF L-IPSCs increased in amplitude and showed a delay (i.e. increase) in onset latency relative to the control response (Fig A.4). Summary data showed that the purely $GABA_C$ mediated component of ON L-IPSCs (+SR95531) had a significantly slower onset time than that of control responses (Fig A.4B, left; Control = 53.26 ± 2.58 ms, n=21; SR95531 = 68.32 ± 3.35 ms, n=29; p<0.01, unpaired Student's t-test, two-tailed). The purely $GABA_C$ mediated component of OFF L-IPSCs showed a non-significant trend toward onset latency delay relative to control (Fig A.4B, right; Control = 140.0 ± 12.49 ms, n=20; SR95531 = 158.8 ± 11.08 ms, n=22; p=0.27). These effects of SR95531 on ON and OFF L-IPSC onset latency were consistent with the idea that lateral $GABA_A$ and $GABA_C$

inputs arrive at the Mb via separate synapses (Palmer, 2006) with short and long latencies, respectively.

Onset latencies of OFF L-IPSCs mediated by a direct, tri-synaptic circuit are delayed by block of voltage-gated Na$^+$ channels

The large OFF L-IPSC onset latencies that we observed, both under control conditions (Fig 2.5) and when indirect, multisynaptic pathways were blocked by SR95531 (Fig A.4), suggested the involvement of wide-field OFF ACs, some of which signal via Na$^+$ action potentials (Taylor, 1999) that spread through their entire dendritic arbor (Koizumi et al., 2005). So, we further explored the AC circuitries that underlie lateral OFF pathways by testing the role of voltage-gated Na$^+$ channels in the timing of OFF L-IPSCs mediated purely by direct AC inputs.

In order to examine the possible role of AC voltage-gated Na$^+$ channels in the paired-pulse advance of OFF L-IPSCs, we examined the sensitivity of ON and OFF L-IPSC onset latency to TTX (Fig A.4). In most cells, near complete TTX block of OFF L-IPSCs prevented quantification of onset latency (Fig A.5). The subset of cells in which TTX did not completely block the OFF response showed a clear delay (increase) in onset latency (example: Fig A.4Aii; 5 µM TTX). The effect of 0.1 – 5 µM TTX on OFF L-IPSC onset latency in the presence of 25 SR was statistically significant (SR latency = 158.8 ± 11.1 ms, n=22; TTX + SR latency = 205.6 ± 17.9 ms, n=10; p<0.05, unpaired Student's t-test, two tailed; Fig A.4B, right). The involvement of voltage-gated Na$^+$ channels in the regulation of OFF L-IPSC onset latency was further supported by the finding that, at the 1900 ms PPI, addition of 0.1 - 5 µM TTX in the presence of 25 µM SR enhanced paired-pulse OFF L-IPSC onset latency advance (SR95531: 1900 ms Δ onset latency = +0.25 ± 3.0 ms, n=18; SR95531+TTX: 1900 ms Δ onset latency = -22.22 ± 7.66 ms, n=11; p<0.01, unpaired Student's t-test, two-tailed; not shown). Consistent with

188

our previous finding that voltage-gated Na$^+$ channels play a mixed or minimal role in the generation of ON L-IPSCs (Vigh et al., 2011), there was no significant effect of 0.1 – 5 µM TTX on ON L-IPSC onset latency in the presence of SR (SR latency = 68.3 ± 3.4 ms, n=29; TTX + SR latency = 74.9 ± 4.1 ms, n=23; p>0.05; Fig A.4B, left).

TTX selectively blocks OFF L-IPSCs mediated by a direct, tri-synaptic circuit

While Mb BCs lack voltage gated Na$^+$ channels, both TTX-sensitive and TTX-insensitive Na$^+$ channels have been shown to be present in some, but not all classes of ACs (Cook et al., 1998; O'Brien et al., 2008; Shields and Lukasiewicz, 2003; Tian et al., 2010). Additionally, TTX-sensitive Na$^+$ channels have been characterized in some classes of transient ON BCs in the tiger salamander retina (Ichinose et al., 2005), and ON and OFF cone BCs in the goldfish retina (Zenisek et al., 2001), and have been shown to mediate AC lateral inhibition that shapes GC center-surround receptive fields (Flores-Herr, 2001; Shields and Lukasiewicz, 2003; Taylor, 1999). Previously, we have shown that OFF L-IPSCs at the Mb terminal are partially blocked, while ON L-IPSCs are either enhanced or partially blocked, by TTX under conditions in which both direct and indirect AC connections are intact (Vigh et al., 2011).

In order to test the involvement of voltage-gated Na$^+$ channels in direct ON and OFF lateral pathways, and to pursue the identification of the involved AC classes, we bath applied TTX in the presence of 25 µM SR. Following bath application of 5 µM TTX, OFF L-IPSCs were blocked, while ON L-IPSCs, on average, remained intact (Fig A.5). Summary of data showed that mean ON L-IPSC charge transfer was not significantly affected by a range of TTX concentrations from 0.1 to 5 µM (% Δ ON charge transfer = -3.91±9.28, n=33; p>0.05, one-sample t-test, null % = 0; Fig A.5B), while OFF L-IPSC charge transfer was significantly reduced by this same range of concentrations (% Δ

189

OFF charge transfer = -54.56 ± 6.05, n=31; p<0.0001; Fig A.5B). Block of OFF L-IPSCs by TTX was significantly greater than block of ON L-IPSCs (p<0.0001, unpaired Student's t-test, two-tailed; Fig A.5B, purple brackets and asterisks).

This result was consistent with the idea that the direct OFF pathway passes through ACs that require the activation of voltage-gated Na^+ channels for signal propagation, while the direct ON pathway does not. However, the variability of the effect of TTX on ON L-IPSCs (Fig A.5B) suggested that diverse classes on ON ACs, some of which express voltage-gated Na^+ channels, might be involved in the direct pathway for ON lateral inhibition. In addition, while TTX-sensitive Na^+ channels ($K_D\sim$=5-10 nM) should be completely blocked at 0.2 μM, TTX-resistant Na^+ channels ($K_D\sim$=30 μM) should experience no block at this concentration (Sangameswaran et al., 1996). However, 5 μM TTX should produce both complete block of TTX-sensitive Na^+ channels and partial block of TTX-resistant channels. Because we observed little difference in the degree ON or OFF L-IPSC blockade between these two concentrations (% Δ ON charge transfer 0.2 µM TTX = -25.05 ± 12.18, n=7; % Δ ON charge transfer 5 µM TTX = -15.89 ± 14.76, n=10; p>0.05, unpaired Student's t-test, two-tailed; % Δ OFF charge transfer 0.2 µM TTX = -58.54 ± 17.78, n=5; % Δ OFF charge transfer 5 µM TTX = -52.54 ± 7.18%, n=12; p>0.05, unpaired Student's t-test, two-tailed), it appears unlikely that TTX-resistant Na^+ channels play a major role in lateral inhibition at the Mb terminal.

L-IPSCs evoked by direct puff application of L-glutamate in the OFF IPL exhibit STF that is enhanced by TTX

Our previous findings that light evoked OFF L-IPSCs exhibit amplitude STF (Figs 2.3, 2.8), and that direct AC depolarization evoked L-IPSCs with long latencies and sizable sustained and asynchronous components (Fig 2.7), suggested that accumulation of residual intracellular Ca^{2+} at OFF AC boutons during paired stimulation may drive paired

pulse facilitation of lateral feedback inhibition at the Mb terminal. Furthermore, this facilitation of release at AC boutons may both depend on the activation of AC voltage gated Na^+ channels (Fig A.4Aii, A.5), and interact with depression at PR ➔ BC and BC ➔ AC synapses to produce the observed biphasic temporal profiles of light evoked OFF L-IPSC STP (Fig 2.3). In order to test this hypothesis, we isolated the inner retinal component of the circuit that mediates OFF L-IPSCs (i.e. OFF AC ➔ Mb terminal) by voltage-clamping an axotomized Mb terminal and directly puffing 1 mM L-glutamate onto ACs located in the OFF IPL at a distance of ~50 to 80 µm downstream of the recorded Mb (Fig A.6A).

We found that paired glutamate puffs (10 ms duration, PPI = 300 to 2700 ms; Fig A.6B) in this configuration produced L-IPSCs at the Mb terminal that displayed charge STF at PPIs of 300 ms (Control PPR = 2.10 ± 0.37; n=13; p=0.01, one-sample t-test, null PPR = 1; Fig A.6C) and 1100 ms (PPR = 1.55 ± 0.20; n=15; p=0.01) that decayed at 1900 - 2700 ms (p>0.05). Paired glutamate puff stimulation following bath application of 1 µM TTX exhibited charge STF at PPIs of 300 ms (TTX PPR = 2.40 ± 0.35; n=8; p<0.01), 1100 ms (PPR = 2.46 ± 0.25; n=8; p<0.001), and 1900 ms (PPR = 1.74 ± 0.24; n=8; p=0.02) that decayed at 2700 ms (p>0.05). TTX enhanced STF relative to control at PPIs of 300 ms (p=0.01, unpaired Student's t-test, two tailed), 1100 ms (p<0.01), and 1900 ms (p=0.02), suggesting that activation of voltage gated Na^+ channels may promote increased release probability at synapses from OFF AC boutons onto Mb terminals under physiological conditions. We propose that this increased release probability acts to moderate a strong intrinsic tendency toward short-term facilitation at these synapses that is driven by paired pulse accumulation of residual Ca^{2+} (Zucker and Regehr, 2002).
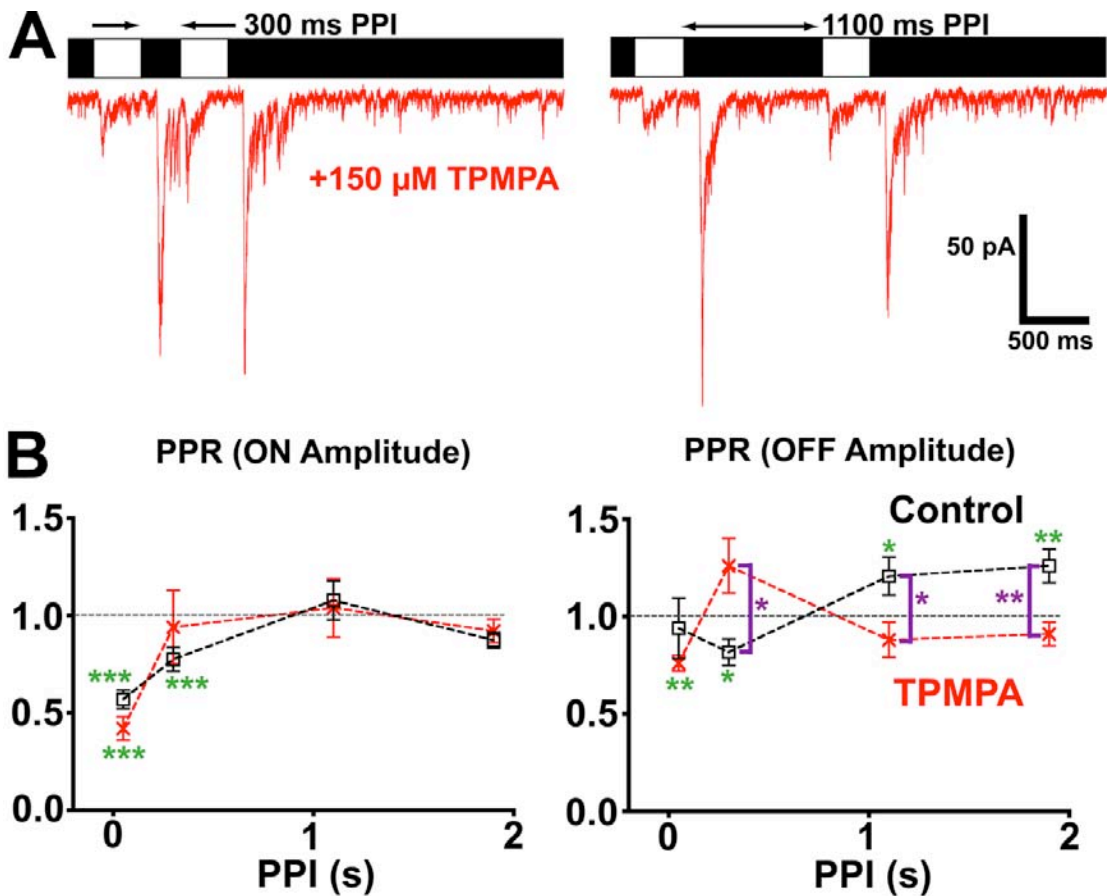
191

Figure A.1: Block of GABA$_C$Rs attenuates low frequency paired pulse depression and facilitation of OFF L-IPSC amplitudes. **(A)** Light flashes (white rectangles) with paired pulse intervals (PPIs) of 300 ms (left) or 1100 ms (right) evoked distinct ON and OFF GABAergic lateral inhibitory post-synaptic currents (L-IPSCs; red) following bath application of 150 μM TPMPA, an antagonist of GABA$_C$Rs. Traces are averages of 5 stimulations. **(B)** Summary data for temporal profile of paired pulse ratios (PPR) of ON (left) and OFF (right) L-IPSC amplitude for Control (black squares; same as Fig 2.3, left) and TPMPA (red X's) conditions. Horizontal gray dashed line indicates a PPR of one, which was the null value that each condition was tested against at each paired pulse interval (PPI; green asterisks). In addition, the two conditions were directly compared at each PPI (purple brackets, asterisks). The number of cells in each condition at each PPI

was between 5 and 7 for TPMPA, and between 6 and 39 for Control. Data shown are

mean ± SE, and represent averages of at least 5 sitmulations. *p<0.05, **p<0.01,
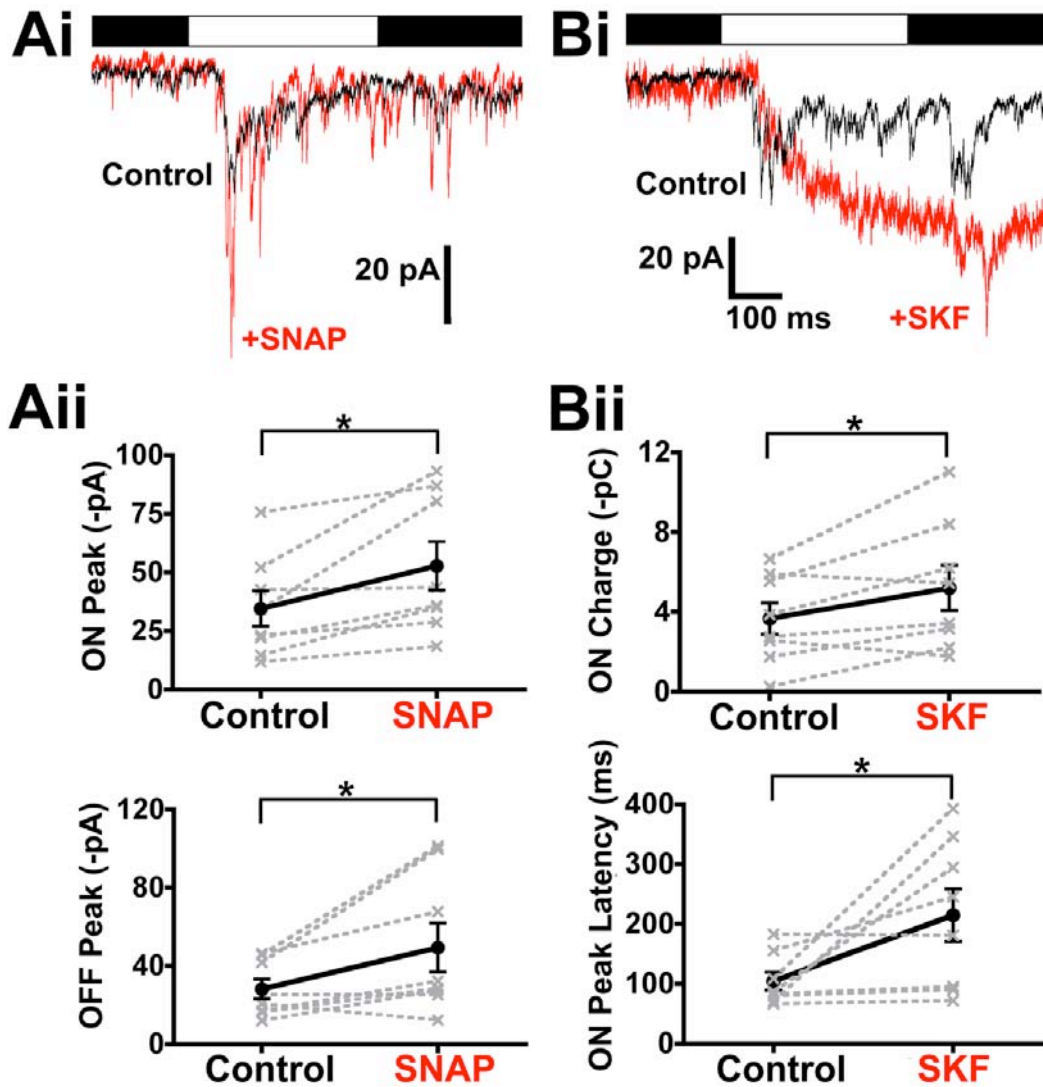
***p<0.001.

Figure A.2: Block of GAT-2/3 GABA transporters enhances ON and OFF L-IPSC amplitudes, while block of GAT-1 enhances ON L-IPSC charge transfer and delays ON L-IPSC peak latency. **(Ai)** Single light flashes (white rectangle) evoked ON and OFF GABAergic lateral inhibitory post-synaptic currents (L-IPSCs) under Control conditions (black trace; average of 18 stimulations) that exhibited increased amplitudes following bath application of 50 μM (S)-SNAP 5114 (SNAP; red trace; average of 3 stimulations), a GAT-2/3 antagonist. Traces shown are averages of n stimulations. **(Aii)** Summary data shows the effect of 50 μM SNAP (red, right) on ON (top) and OFF (bottom) L-IPSC amplitudes relative to Control (black, left). Data shown are from the same 8 cells in both

194

conditions. **(Bi)** Single light flashes evoked ON and OFF L-IPSCs under Control

conditions (black trace; average of 6 stimulations) that were transformed following bath

application of 20 μM SKF 89976 (SKF; red trace; average of 3 stimulations), a GAT-1

antagonist. **(Bii)** Summary data shows the effect of 5-20 μM SKF (red, right) on ON L-

IPSC charge transfer (top) and peak latency (bottom) relative to Control (black, left).

Data shown (gray x's and dashed lines indicate paired measurements from individual

cells; mean $\pm$ SE indicated by circles, solid black lines) are from the same 8 cells in both

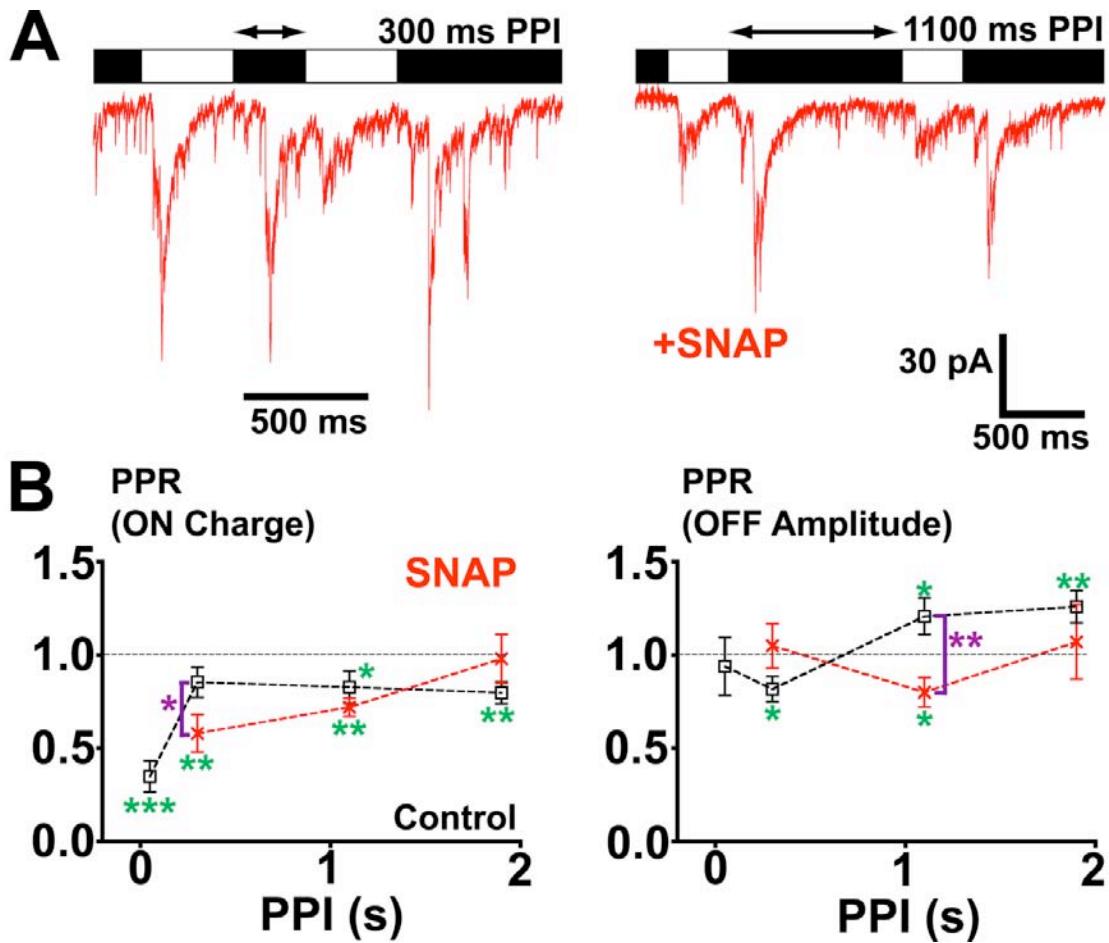conditions, and represent averages of at least 3 stimulations. *p<0.05.

Figure A.3: Block of GAT-2/3 GABA transporters increases paired pulse depression of ON L-IPSC charge and blocks facilitation of OFF L-IPSC amplitudes. **(A)** Light flashes (white rectangles) presented at paired pulse intervals (PPIs) of 300 ms (left) and 1100 ms (right) evoked ON and OFF GABAergic lateral inhibitory post-synaptic currents (L-IPSCs) following bath application of 50 μM (S)-SNAP 5114 (SNAP; red traces; average of 3-5 stimulations). **(B)** Summary data shows the effect of SNAP (red X's) on the temporal profile of paired pulse ratios (PPR) for ON L-IPSC charge transfer (left) and OFF L-IPSC amplitude (right) relative to Control conditions (black squares; same as Fig 2.3). Horizontal gray dashed line indicates a PPR of one, which was the null value that each condition was tested against at each paired pulse interval (PPI; green asterisks). In

addition, the two conditions were directly compared at each PPI (purple brackets,

asterisks). The number of cells in each condition at each PPI was 8 for SNAP, and

between 6 and 39 for Control. Data shown are mean ± SE, and represent averages of at
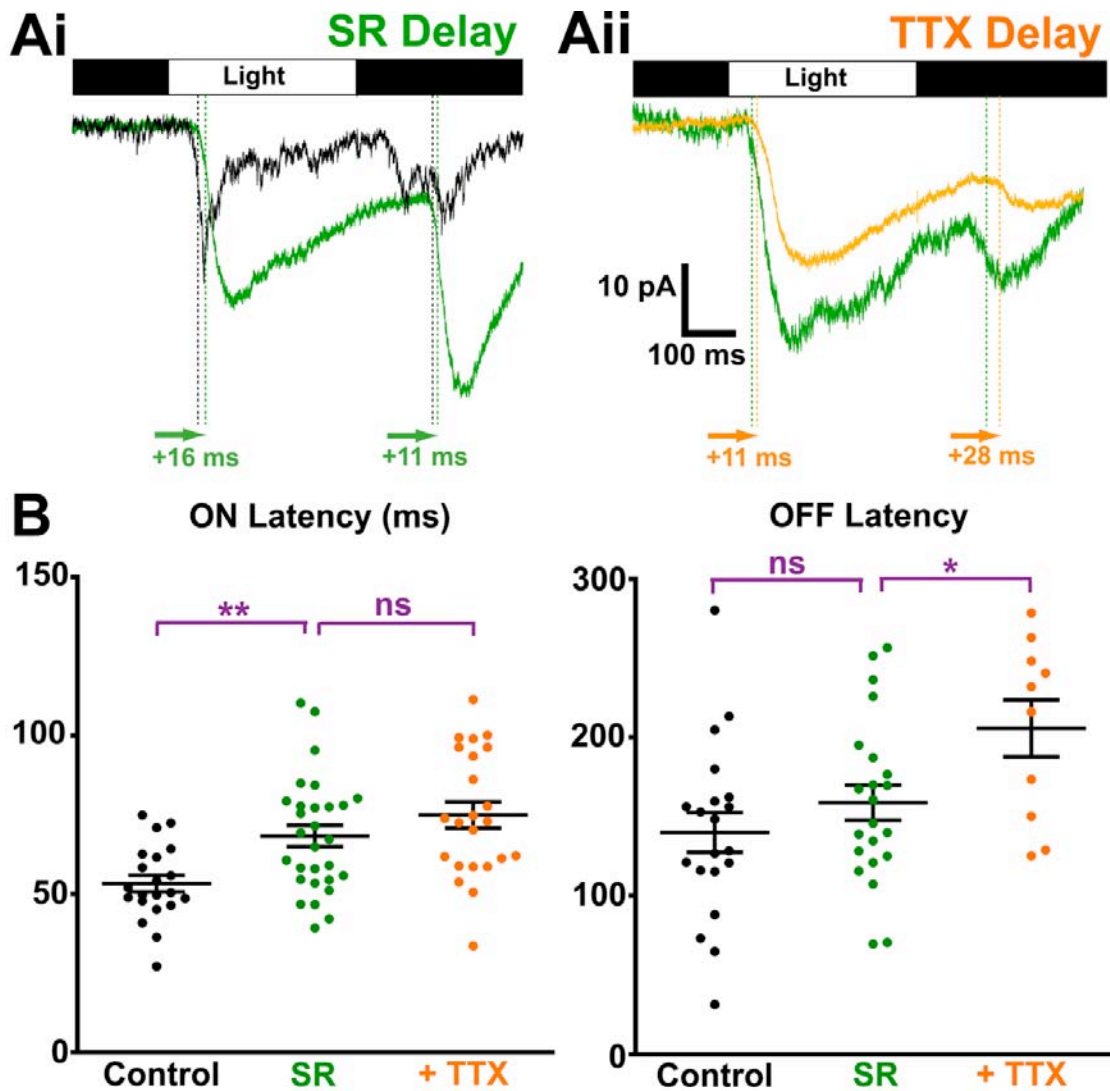
least 3 stimulations. *p<0.05, **p<0.01, ***p<0.001.

Figure A.4: Block of GABA$_A$Rs delays ON L-IPSC latencies, and subsequent block of voltage-gated Na$^+$ channels with TTX delays OFF L-IPSC latencies. **(Ai)** Single light flashes (white rectangle) evoked GABAergic ON and OFF lateral inhibitory post-synaptic currents (L-IPSCs) under Control conditions (black trace; average of 30 stimulations) that showed delayed onset latencies (green arrows) following bath application of 25 μM SR-95531 (SR; green trace; average of 16 stimulations), an antagonist of GABA$_A$Rs. **(Aii)** Single light flashes evoked ON and OFF L-IPSCs in the presence of 25 μM SR (green trace; average of 15 stimulations; different cell than in (Ai)) that exhibited delayed

onset latencies (orange arrows) following bath application of 5 μM TTX (orange trace; average of 15 stimulations). **(B)** Summary data shows the sequential effects of 12.5 to 25 μM SR (green circles; ON: 29 cells; OFF: 20 cells) and 0.1 to 5 μM TTX (orange circles; ON: 23 cells; OFF: 10 cells), relative to Control (black circles; ON: 21 cells; OFF: 20 cells) on ON (left) and OFF (right) L-IPSC onset latencies. Individual circles represent averages of at least 9 stimulations per cell, and black lines indicate mean ± SE for the population of cells in each condition. Purple brackets represent unpaired comparisons between conditions. n.s. $p > 0.05$, *$p < 0.05$, **$p < 0.01$.
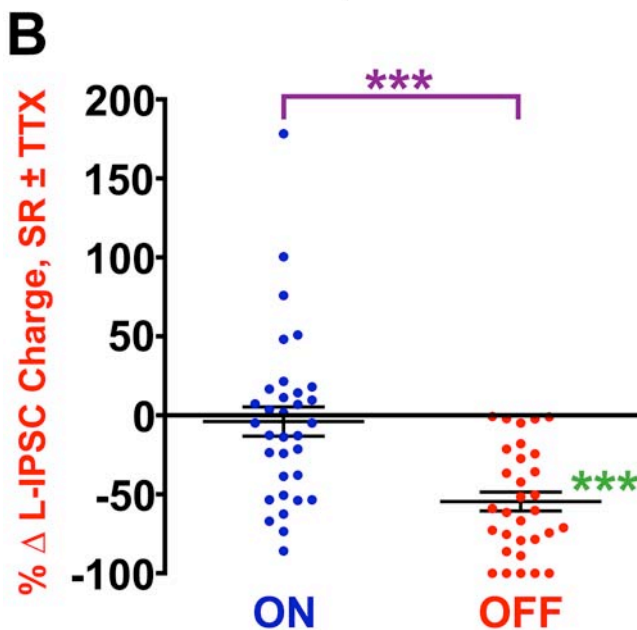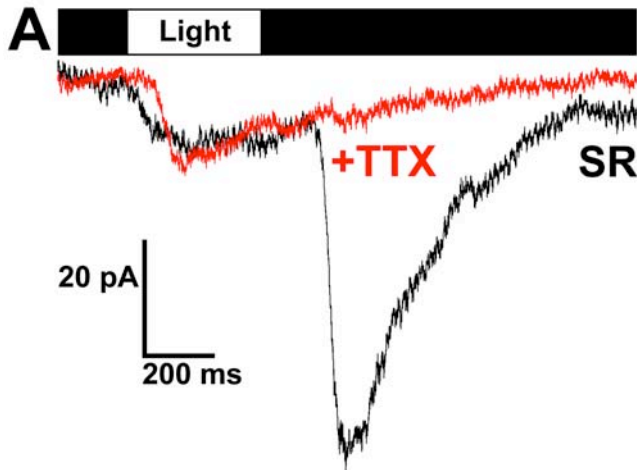
Figure A.5: Bath application of TTX in the presence of SR-95531 (SR) blocks OFF, but not ON, L-IPSCs. **(A)** Single light flashes (white rectangle) evoked ON and OFF lateral inhibitory post-synaptic currents (L-IPSCs) in the presence of 25 μM SR-95531 (SR, black trace, average of 4 stimulations). Subsequent bath application of 5 μM TTX in the same cell (red trace; average of 4 stimulations) blocked the OFF L-IPSC but left the ON L-IPSC intact. **(B)** Summary data show % change in ON (blue circles, left; 33 cells) and OFF (red circles, right; 31 cells) L-IPSC charge transfer in the presence of 25 μM SR following bath application of 0.1 to 5 μM TTX. Green asterisks indicate a comparison between normalized change in charge transfer and a null change of 0%. Purple brackets and asterisks indicate a direct comparison between ON and OFF normalized change in charge transfer. Individual circles represent averages of at least 4 stimulations per cell, and black lines indicate cell population mean ± SE for ON and OFF L-IPSCs. ***$p < 0.001$.
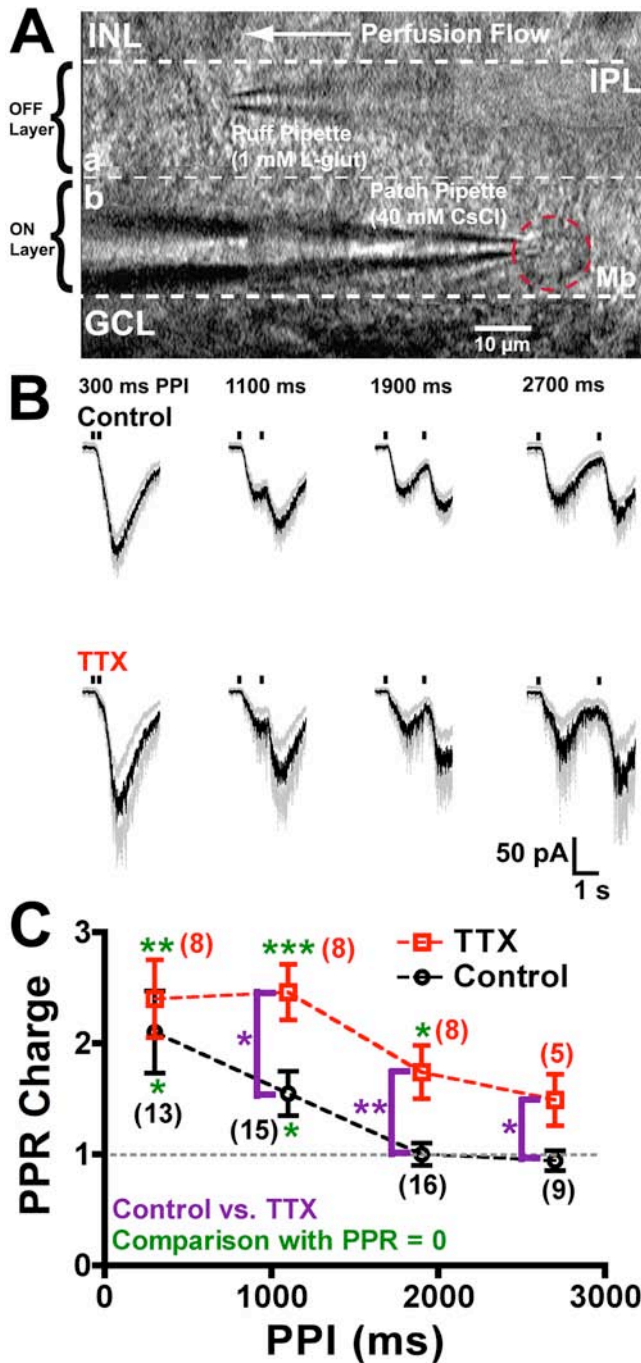
Figure A.6: Paired puff application of L-glutamate in the OFF IPL (i.e. sublamina a) reveals paired pulse facilitation of L-IPSCs that decays over 2 s and is enhanced by bath application of TTX at PPIs > 300 ms. **(A)** DIC overlay montage of paired whole-cell voltage-clamp recording of an axotomized Mb terminal (red dashed circle) in the ON layer of the inner plexiform layer (IPL; sublamina b) and puff application of 1 mM L-glutamate in the OFF IPL (sublamina a). The puff pipette was positioned ~55 μm downstream of the recorded Mb relative to the direction of bath perfusion flow. The recording pipette contained 40 mM cesium chloride (CsCl). INL = inner nuclear layer, GCL = ganglion cell layer. **(B)** Paired puff application of 1 mM L-glutamate in the OFF IPL (as shown in A) evoked paired lateral inhibitory post-synaptic currents (L-IPSCs) in the recorded Mb terminal under Control conditions at paired pulse intervals (PPI) between 300 and 2700 ms (upper panels; population mean shown in black,

201

averaged traces from individual cells shown in gray). Bath application of 1 μM TTX (lower panels) transformed paired L-IPSCs. **(C)** Summary data for temporal profile of puff-evoked L-IPSC charge transfer PPR for PPIs from 300 to 2700 ms. Control data are shown in black (open circles), and TTX data are shown in red (open squares). Number of cells in each condition is indicated for each PPI in parentheses. Green asterisks indicate a comparison between data in each condition at each PPI and a hypothetical null PPR of one (gray dashed line). Purple brackets and asterisks indicate a direct comparison between conditions at each PPI.